

The Pennsylvania State University

The Graduate School

ENZYME DYNAMICS

A Dissertation in

Chemistry

by

Xi Zhao

© 2019 Xi Zhao

Submitted in Partial Fulfillment
of the Requirements
for the Degree of

Doctor of Philosophy

December 2019

The dissertation of Xi Zhao was reviewed and approved* by the following:

Ayusman Sen
Verne M. Willaman Professor of Chemistry
Distinguished Professor of Chemistry & Chemical Engineering
Dissertation Advisor
Chair of Committee

Paul S. Cremer
J.Lloyd Huck Chair in Natural Sciences
Distinguished Professor of Chemistry & Biochemistry and Molecular Biology

Igor Aronson
Huck Chair Professor of Biomedical Engineering, Chemistry and Mathematics

Peter J. Butler
Associate Dean for Education in the College of Engineering
Professor of Biomedical Engineering

Philip C. Bevilacqua
Department Head of Chemistry
Distinguished Professor of Chemistry & Biochemistry and Molecular Biology

*Signatures are on file in the Graduate School

ABSTRACT

Enzymes are ubiquitous molecules in living systems. Apart from their primary function as catalysts, enzymes are also assumed to promote motion of other biomolecules, similar to motor proteins. Recent work shows that free swimming enzymes produce mechanical force to increase their own diffusion when they catalyze reactions. Moreover, when exposed to a gradient of reactant, enzymes move up the gradient just like cellular chemotaxis. Force generation by active enzymes has potential applications ranging from nanomachinery, nanoscale assembly, cargo transport, drug delivery, micro/nanofluidics, and chemical/biochemical sensing. By fully understanding why enzymes display enhanced diffusion and by what mechanism they assemble and move directionally, we can better monitor and manipulate the motion of enzyme powered artificial swimmers. One of the current proposed hypotheses used to explain enzyme enhanced diffusion proposes that heat released during enzyme catalyzed reactions causes the increase in diffusion. To further investigate the mechanisms driving this phenomenon, aldolase, an endothermic enzyme, was studied initially. By applying Fluorescence Correlation Spectroscopy (FCS), the results demonstrate that aldolase shows enhanced diffusion in the presence of substrate even in a heat absorbing environment. To further explore the mechanism, aldolase's substrate was substituted for a competitive inhibitor that periodically binds and unbinds to the active site of aldolase without promoting a catalytic reaction. Even in this case, the diffusion of aldolase increases and therefore, we propose that enzyme periodical conformational changes lead to enzyme force generation. To confirm our hypothesis, hexokinase was also studied. Hexokinase is unique because it only binds and unbinds to its substrate, D-glucose without its cofactors (adenosine triphosphate and magnesium chloride). Fluorescence correlation spectroscopy (FCS) was done to show that the diffusion of hexokinase increases in the presence of only D-glucose, further proving our hypothesis that conformational changes lead to the enhanced diffusion of enzymes.

Another goal of this work was to understand the chemotaxis of enzymes and their potential impact on cellular activities. Enzymes that are part of a reaction cascade have been shown to assemble through sequential chemotaxis; each enzyme follows its own specific substrate gradient, which in turn is produced by the preceding enzymatic reaction. Thus, the sequential chemotaxis in catalyst cascades allows for the time-dependent, self-assembly of specific catalyst particles participating in the cascade. This is an example of how information can arise from chemical gradients and it is tempting to suggest that a similar mechanism underlies the organization of living systems.

The impulsive force generated by enzyme catalysis can also be transmitted to the surrounding fluid and inert particles, resulting in fluid pumping and enhanced particle diffusion. When attached to bigger particles, enzymes act as “engines”, imparting motility to the particles and moving them directionally in a substrate gradient.

Based on what we observed with the physical activity of free enzymes, we hypothesize that, *in vivo*, enzymes may be responsible for the stochastic motion of the cytoplasm, the organization of metabolons and signaling complexes, and the convective transport of fluid in cells.

TABLE OF CONTENTS

LIST OF FIGURES	vii
LIST OF TABLES	xv
ACKNOWLEDGEMENTS	xvi
Chapter 1 Introduction	1
1.1 Enzyme Enhanced Diffusion.....	1
1.2 Enzyme Chemotaxis and its hypothesized contribution to metabolon	6
1.3 Transduction energy to surroundings.....	7
1.4 Applications of mechanical force generated by enzyme.....	8
1.5 Research goals.....	16
1.6 References	18
Chapter 2 Enhanced Diffusion of Enzyme with or without Catalysis	22
2.1 Introduction	22
2.2 Experimental Results and Discussion	24
2.2.1 Enhanced Diffusion of Aldolase	24
2.2.2 Enhanced Diffusion of Aldolase in the presence of inhibitors.....	25
2.2.3 Enhanced Diffusion of Hexokinase.....	29
2.3 Numerical Results Summary.....	32
2.4 Conclusion.....	38
2.5 Experimental Details	39
2.5.1 Fluorescent Labeling of HK and Ald	39
2.5.2. Diffusion Measurement using FCS	40
2.6 Acknowledgements	44
2.7 References	44
Chapter 3 Enzyme Chemotaxis.....	47
3.1 Introduction	47
3.2 Results and discussion.....	48
3.2.1 Hexokinase Chemotaxis	49
3.2.2 Aldolase Chemotaxis.....	55
3.2.3 Chemotaxis as a Factor in Metabolon Formation	58
3.2.4 Chemotactic Co-localization of Hexokinase and Aldolase.....	64
3.3 Numerical Results Summary.....	66
3.4 Conclusion.....	69
3.5 Experimental Details	70
3.5.1 Fluorescent Labeling of Hexokinase and Aldolase.....	70
3.5.2 Enzyme activity assays.....	70
3.5.3 Progress Curve Simulation	71
3.5.4 Microfluidic Device Fabrication	72
3.5.5 Confocal Microscope Imaging	73
3.6 Acknowledgements	73

3.7 References	73
Chapter 4 Enhanced Diffusion of Passive Tracers in Active Enzyme Solutions.....	77
4.1 Introduction	77
4.2 Results and discussion.....	78
4.3 Conclusion.....	94
4.4 Experimental Details	94
4.4.1 Urease Activity Assay	94
4.4.2 Fluorescence Correlation Spectroscopy (FCS) Measurements	95
4.4.3 Coating Tracer Particle Surface with Bovine Serum Albumin	97
4.4.4 DLS measurements.....	100
4.5 Acknowledgements	101
4.6 References	101
Chapter 5 Micromotors Powered by Enzyme Catalysis in the Microfluidic Channel.....	105
5.1 Introduction	105
5.2 Results and Discussion.....	106
5.3 Conclusion.....	111
5.4 Experimental Details	111
5.4.1 Coating of Streptavidin-functionalized Polystyrene Microspheres with Biotinylated Enzymes.....	111
5.4.2 Microfluidic Channel Fabrication	113
5.4.3 Confocal Set-up.....	114
5.5 Acknowledgements	114
5.6 References	115
Concluding Remarks.....	117
Appendix Supporting Information for Chapter 3:.....	119
Enzyme Chemotaxis	119
Computational modeling of cross-diffusion.....	119
Analysis of HK and Ald Aggregates Trajectories.....	123
References	125

LIST OF FIGURES

- Figure 1-1.** (A) Illustration of the motion of the urease functionalized Janus hollow microsphere that is self-propelled by the decomposition of urea to its products. (B) The diffusion of the urease powered microspheres in the presence of increasing concentrations of urease, protecting agent or without inhibitor. Reprinted from *ACS Nano* **2016**, *10*, 3597–3605, Copyright 2016. 10
- B) 11
- Figure 1-2.** (A) Diffusion coefficients nanobots using DLS (green) and optical tracking (blue) without urea and in the presence of 100 mM urea in either PBS buffer or water. (B) The intensity of Dox inside the human epithelial cervix adenocarcinoma (HeLa) cells over time without urea (black) and in the presence of 10 mM urea (gray). (C) The percentage of cells that are viable with nanobots (black) and with Dox containing nanobots (green) in the presence of increasing urea concentrations. Reprinted from *Advanced Functional Materials*. **2017**, 1705086, Copyright 2017. 12
- Figure 1-3.** Illustration of the experimental setup for the enzyme powered micropumps. Glass slides were coated with PEG and gold was patterned using electron beam evaporation. A quaternary ammonium thiol was added to the gold patch so that it self-assembled into a monolayer on the gold. The enzymes can then selectively bind to the thiol group through electrostatic attractions [44]. Reprinted from *Nat. Chem.* **2014**, *6*, 415–422., Copyright 2014. 13
- Figure 1-4.** Demonstration of the solutal buoyancy mechanism. In the inward pump, the reactants that are produced are less dense than the products, so the local fluid rises and then due to convective flows, comes back down and moves towards the patch on the glass slide. In the outward pump, the enzyme products produced are denser than the reactants, causing the fluid to locally become denser and slide down and away from the patch [44,47, 48]. Reprinted from *Acc. Chem. Res.* **2018**, *51*, 2373-2381, Copyright 2018. 16
- Figure 2-1.** A) The diffusion of tagged aldolase was measured in FCS at different substrate concentrations. The diffusive motion of aldolase increased with increasing reaction rate. The error bars represent standard deviations calculated for 15 different measurements, under identical conditions. B) The enhanced diffusion of aldolase in the presence of substrate returns to the base value (observed in the absence of the substrate) when the substrate is consumed. All values are significantly different with $p < 0.05$ Reprinted from *Nano Lett.* **2017**, *17* (7), 4415–4420. Copyright 2017. 25
- Figure 2-2.** Diffusion of aldolase enhances with increasing pyrophosphate (PPi) concentration (the dashed line corresponds to the base value in the absence of substrate). PPi is a competitive inhibitor of aldolase. Reprinted from *Nano Lett.* **2017**, *17* (7), 4415–4420. Copyright 2017. 26

- Figure 2-3. (A-C)** The diffusion of aldolase in the various concentrations of AMP, ADP and ATP shows in an inhibitor concentration dependent manner. The increase in aldolase diffusion is less than aldolase in the presence of its substrate solution. Aldolase diffusion increases to a plateau in the presence of AMP, ADP and ATP at different concentrations. The error bars represent the standard deviation of 10 different measurements..... 28
- Figure 2-4. A)** The diffusion of fluorescently labeled hexokinase was measured in FCS in various solutions with or without cofactor and substrate. Hexokinase showed crucial amplification when binding and unbinding substrate without catalysis ($30.69 \pm 5.44 \%$), although diffusion of the enzyme increased the most during the turnover reaction ($46.22 \pm 4.49 \%$). **B)** We also demonstrated that the diffusion of hexokinase enhances in a substrate- dependent manner either without catalysis or with catalysis. The diffusion of hexokinase was measured in different glucose concentrations in either the absence or presence of 1mM ATP and 1mM $MgCl_2$. The error bars represent the standard deviation calculated for 10 different measurements, under identical conditions. 31
- Figure 2-5. (A)** Substrate binding and unbinding drives a stochastic two-state process. The enzyme switches randomly between two equilibrium states, where it is either free or bound. **(B)** Structure of an aldolase monomer (Protein Data Bank ID: 1ADO, subunit A), generated with VMD.23 The residue colored in red indicates the location of the active site.22 **(C)** Aldolase enzyme modeled as a dumbbell. R is the position of the center of mass of the enzyme, x represents its elongation. The grey sphere symbolizes the whole enzyme, whose typical size is denoted by a. Reprinted from *Nano Lett.* **2017**, *17* (7), 4415–4420. Copyright 2017. 33
- Figure 2-6.** Relative increase of the diffusion coefficient of aldolase molecules measured in FCS experiments (symbols) in the presence of: **(A)** FBP as a substrate, **(B)** pyrophosphate (PPi) as a competitive inhibitor and compared to the fitting function (solid line), with A and K as free parameters. The relatively large error bars for the experiments performed with PPi originate from the error on the measurement of D_0 , which affects the standard deviation for the quantity $\Delta D=D_0$. Reprinted from *Nano Lett.* **2017**, *17* (7), 4415–4420. Copyright 2017. 35
- Figure 2-7.** Representative intensity fluctuation curves and corresponding autocorrelation fits obtained for fluorescently tagged aldolase dispersed in 0 mM and 0.1 mM FBP solutions respectively. Reprinted from *Nano Lett.* **2017**, *17* (7), 4415–4420. Copyright 2017. 44
- Figure 3-1. (A)** The first four steps of glycolysis and their associated enzymes: hexokinase (HK), phosphoglucose isomerase (Iso), phosphofructokinase (PFK), and aldolase (Ald). **(B)** Photo-lithographically fabricated flow-based microfluidic channel for studying enzyme chemotaxis. The channel is 40 mm in length, 360 μm in width, and 100 μm in depth. Due to laminar flow, the effective width of each flow channel is 120 μm . Fluorescence intensities were analyzed along the black line shown in the figure, leaving off 20 μm next to the sidewalls. Reprinted from *Nat. Chem.* **2018**, *10* (3), 311–317. Copyright 2018. 48

- Figure 3-2.** Linear relationships between fluorescence intensity (arbitrary units) and concentration for both HK and Ald. This enables directly correlating fluorescence intensity to the concentration of enzyme. Reprinted from *Nat. Chem.* **2018**, *10* (3), 311–317. Copyright 2018. 49
- Figure 3-3.** **A)** The chemotactic migrations of hexokinase within the channel with glucose only and within the channel with glucose, ATP and cofactor were measured at the end of microfluidic channel. The fluorescent intensity profile was smoothed by Gaussianamp fitting in Origin. **B)** an enlarged portion of **Figure 3-3A**. When a gradient of only glucose was imposed, enzyme migrated more than in the buffer and slightly less than the migration observed during the full catalysis gradient. 51
- Table 3- 1 Distance from the start of the microfluidic channel converted into time spent inside the channel for specified channel geometry. Reprinted from *Nat. Chem.* **2018**, *10* (3), 311–317. Copyright 2018. 52
- Figure 3-4.** Catalysis induced enzyme focusing. A starting equilibrium distribution of HK (200 nM), D-glucose (50 mM), and MgCl₂ (100 mM) shows focusing towards the middle channel when ATP (50 mM) is introduced into it. Note that catalysis does not occur in the absence of ATP (control). Experimental conditions: Flow rate, 30 μl/h; distance, 38 mm; interaction time, 55 s. The general concave shape of the curves is indicative of the wall effect. **(A)** N.F.I. (Normalized fluorescence intensity) as a function of distance from the center of the channel. Fluorescence intensities are normalized across all channels such that the total fluorescence intensity across all channels is fixed for all experiments, and rescaled such that the central channel for the D-Glucose control experiment sums to 100. Side channels are shaded in gray. Data points are locally fitted to a second degree polynomial. **(B)** Integrated N.F.I. per channel. Error bars are 95% confidence intervals obtained from 500 bootstrap iterations of the fitting process. A pairwise t-test with Holm adjustment was conducted to test for significant differences in the intensities across channels. ***: p<0.001, n.s.: not significant. Reprinted from *Nat. Chem.* **2018**, *10* (3), 311–317. Copyright 2018. 54
- Figure 3-5.** Catalysis induced enzyme focusing as a function of interaction time in the microchannel. A starting equilibrium distribution of HK (200 nM), D-glucose (50 mM), and MgCl₂ (100 mM) shows focusing towards the middle channel when ATP (50 mM) is introduced into it. Percent Excess enzyme in the middle channel = amount of enzyme in the middle channel in the experiment minus the amount of enzyme in the middle channel in the control (no ATP) divided by the total amount of enzyme in all three channels. The error bar represents the standard deviation of three identical measurements. Reprinted from *Nat. Chem.* **2018**, *10* (3), 311–317. Copyright 2018. 54
- Figure 3-6.** **(A)** Chemotactic migration of aldolase within the substrate side, measured at 38 mm from the start of the microchannel. We measured a shift of (5.61 ± 0.51) μm in fluorescent intensity profile at this position when the FBP concentration at the inlet was 10 mM. The intensity profiles were smoothed by B-spline fitting in Origin. **(B)** Magnitude of aldolase chemotaxis as a function of the interaction time with the substrate. The errors bars represent standard deviations calculated for three independent measurements carried out under identical conditions..... 56

- Figure 3-7.** Aldolase migrated more towards where it changes conformations. The easier it is to bind with the inhibitor (with lower disassociation constant), the more chemotactic shift aldolase shows..... 57
- Figure 3-8.** Fluorescence intensity measured across the channels are plotted against the width of the channels for center and right channels. The grey background represents the approximate right channel. When compared to the movement of Ald towards buffer, the enzyme shows enhanced migration into the channel that generates Fructose-1,6- biphosphate in situ. Reprinted from *Nat. Chem.* **2018**, *10* (3), 311–317. Copyright 2018. 58
- Figure 3-9. (A)** While Ald chemotaxes towards its substrate gradient, HK flowing along with its substrate in its own channel shows no movement into the adjacent channel. **(B)** Control experiments performed for studying the chemotactic response of Ald towards its substrate precursors. Ald shows no movement towards the channel containing an incomplete mixture of the enzyme cascade. Reprinted from *Nat. Chem.* **2018**, *10* (3), 311–317. Copyright 2018..... 60
- Figure 3-10** The simulated substrate and product progression curves through the first four enzymes in the glycolytic cascade. Reprinted from *Nat. Chem.* **2018**, *10* (3), 311–317. Copyright 2018. 61
- Figure 3-11 (A)** Ald shows a chemotactic response compared to HK as expected based on the sequence of reactions. When 10 mM mannose is introduced along with 10 mM D-glucose, HK shows a reduced chemotaxis corresponding to the slower rate of mannose phosphorylation by HK. **(B)** D-glucose gradient-driven sequential movement of HK and Ald for the entire enzymatic reaction cascade was also observed in the presence of Ficoll PM 70 (20% w/v), an induced crowded environment mimicking cytosolic crowding conditions in a cell. Ald (blue bars) shows a chemotactic migration towards substrate channel compared to HK (red bars) corresponding to the cascade reaction sequence. Reprinted from *Nat. Chem.* **2018**, *10* (3), 311–317. Copyright 2018. 63
- Figure 3-12.** HK, Iso, PFK, Ald, D-glucose, MgCl₂ and ATP were mixed and injected into a sealed hybridization chamber. The depth of the chamber is 0.9 mm and the diameter of the chamber well is 20 mm. Conditions; 200 nM HK labeled with amine-reactive (ex/em: 493/518) Dylight dye, 200 nM Iso, 200 nM FPK, 200 nM Ald conjugated with thiol-reactive (ex/em: 638/658) Dylight dye, 10 mM ATP, 20 mM MgCl₂, and 10 mM D-glucose in 20% w/v 70 M Ficoll was mixed and injected into a hybridization chamber, which was sealed on the surface of a glass slide. Controls were also performed either with D-glucose but no Iso and PFK present, or substituting D-glucose with L-glucose, or no glucose. Reprinted from *Nat. Chem.* **2018**, *10* (3), 311–317. Copyright 2018 64
- Figure 3-13.** HK trajectories from three separate experiments in which D-glucose was present for which the corresponding Ald trajectory was highly correlated. Experimental conditions: 200 nM HK labeled with amine-reactive (ex/em: 493/518) Dylight dye, 200 nM Iso, 200 nM FPK, 200 nM Ald conjugated with thiol-reactive (ex/em: 638/658) Dylight dye, 10 mM ATP, 20 mM MgCl₂, and 10 mM D-glucose in 20% w/v 70 M Ficoll mixed and injected into a sealed

hybridization chamber (Scheme S1). A pixel is $0.46 \times 0.46 \mu\text{m}$ and the frame rate is 1 frame every 1.29 s. The trajectories are recorded for 10 frames, ~ 13 s. Reprinted from *Nat. Chem.* **2018**, *10* (3), 311–317. Copyright 2018..... 65

- Figure 3-14.** Computed profiles of the total enzyme concentration replicating experimental conditions from Figure 2 applied to catalysis-induced enzyme focusing **(A)** Modeled chemotactic response of HK in the presence of ATP. The parameters are chosen to replicate the conditions of the experiment described in Figure 2A. **(B)** Integrated N.F.I. of the enzyme in the central channel for experimental (left) and modeled (right) enzyme focusing. The experimental figure is the average of three experimental trials. Reprinted from *Nat. Chem.* **2018**, *10* (3), 311–317. Copyright 2018. 69
- Figure 4-1.** Diffusion of **(A)** RhB, **(B)** 50 nm and **(C)** 100 nm fluorescent polystyrene particles measured in active urease solutions (10 nM) at different concentrations of urea. The error bars represent standard deviations calculated for 20 different measurements, under identical conditions. With increasing reaction rate, the diffusion of tracers in each case was enhanced, suggesting transfer of *momentum* from the catalysts to these particles. **(D)** Correlation between the diffusion of 50 nm fluorescent particles and total reaction rates at various concentrations of urea. The reaction rates are calculated based on Michaelis-Menten kinetics, for 10 nM urease. Reprinted from *Nano Lett.* **2017**, *17*, 4807–4812 Copyright 2017. 80
- Figure 4-2.** Diffusion of **(A)** RhB, **(B)** 50 nm and **(C)** 100 nm fluorescent polystyrene particles measured in active aldolase solutions at different concentrations of FBP. The error bars represent standard deviations calculated for 20 different measurements, under identical conditions. With increasing reaction rate, the diffusion of tracers in each case was found to enhance, suggesting transfer of *momentum* from the catalysts to these particles. **(D)** Correlation between the diffusion of 50 nm fluorescent particles and total reaction rates at various concentrations of FBP. The reaction rates are calculated based on Michaelis-Menten kinetics, for 10 nM aldolase. Reprinted from *Nano Lett.* **2017**, *17*, 4807–4812 Copyright 2017. 82
- Figure 4-3.** Diffusion of 50 nm fluorescent polystyrene beads measured in active hexokinase at different concentration of glucose without cofactors. The error bars represent standard deviations calculated for 10 different measurements, under identical conditions..... 82
- Figure 4-4.** **(A)** Time dependent shifts in diffusion of $2 \mu\text{m}$ BSA-coated polystyrene sulfate microspheres, dispersed in 10 nM urease and 0.5 mM urea, estimated using dynamic light scattering particle size analysis. As the reaction goes to completion, the peak for the diffusion coefficient distribution profile gradually returns to the zero substrate value (from black to blue). All the curves are smoothed with B-spline fitting in Origin. **(B)** Tracer diffusion as a function of substrate concentration, measured using DLS. For each substrate concentration, 3 separate measurements were taken at time zero (which corresponded to the maximum changes in tracer diffusion at that substrate concentration). ***: $p < 0.001$; *: $p < 0.05$. Reprinted from *Nano Lett.* **2017**, *17*, 4807–4812 Copyright 2017. 84

- Figure 4-5.** (A) Diffusion coefficient distribution of 2 μm polystyrene sulfate tracers, coated with BSA, dispersed in (A) DI Water and (B) 10 mM Urea, recorded in DLS. The measurements were taken successively at three different times. The measured diffusion of the tracers is $0.23 \pm 0.01 \mu\text{m}^2/\text{s}$ in DI water and $0.24 \pm 0.01 \mu\text{m}^2/\text{s}$ in 10 mM urea. Reprinted from *Nano Lett.* **2017**, *17*, 4807–4812 Copyright 2017. 84
- Figure 4-6.** (A) Absorption spectra of urease inhibited with pyrocatechol. (B) Diffusion profile of 2 μm sulfate tracers in inhibited urease solution in the presence of substrate. Reprinted from *Nano Lett.* **2017**, *17*, 4807–4812 Copyright 2017. 86
- Figure 4-7.** (A) Time dependent shifts in diffusion of 2 μm BSA- coated polystyrene sulfate tracers, dispersed in 10 nM aldolase and 0.01 mM FBP. As the reaction proceeds to completion, peak of the diffusion coefficient distribution profile gradually returns to the zero substrate value (from black to blue). The plots are smoothed with B-spline fitting in Origin. (B) Tracer diffusion as a function of substrate concentration, measured using DLS. For each substrate concentration, 3 separate measurements were taken at time zero (which corresponded to the maximum changes in tracer diffusion at that substrate concentration). ***: $p < 0.001$; *: $p < 0.05$. Reprinted from *Nano Lett.* **2017**, *17*, 4807–4812 Copyright 2017. 87
- Figure 4-8.** Diffusion coefficient distribution of 2 μm polystyrene sulfate tracers, coated with BSA, dispersed in 1 mM FBP only, and recorded in DLS. The measurements were taken successively at three different times. The measured diffusion of the tracers is $0.24 \pm 0.01 \mu\text{m}^2/\text{s}$. Reprinted from *Nano Lett.* **2017**, *17*, 4807–4812 Copyright 2017. 87
- Figure 4-10.** (A-D) Time dependent shifts in diffusion of 2 μm polystyrene sulfate tracers, coated with BSA, dispersed in 200 nM catalase and (0-1) mM H_2O_2 solutions. As the reaction proceeds to completion at each substrate concentration, the peak of the diffusion coefficient distribution profile gradually returns to the zero substrate value (from black to blue). The plots are smoothed with B-spline fitting in Origin. (E) Tracer diffusion in active catalase solution as a function of H_2O_2 concentration. For each substrate concentration, 3 separate measurements were taken at time zero (which corresponded to the maximum changes in tracer diffusion at that substrate concentration). ***: $p < 0.001$. Reprinted from *Nano Lett.* **2017**, *17*, 4807–4812 Copyright 2017. 89
- Figure 4-11.** Diffusion coefficient of 2 μm polystyrene sulfate tracers, coated with BSA, in 1 mM H_2O_2 , showing no significant enhancement in diffusion. Reprinted from *Nano Lett.* **2017**, *17*, 4807–4812 Copyright 2017. 90
- Figure 4-12.** Enhanced diffusion of 50 nm polystyrene fluorescent tracers during urea hydrolysis and (C-D) FBP splitting, measured using dynamic light scattering particle size analyzer. During catalysis, the particles' diffusion in urea and urease solution increased by nearly $20.1 \pm 2.1\%$, which is consistent with the increase measured in FCS ($19.6 \pm 5.8\%$). The diffusion of the same tracer particles in FBP and aldolase solutions, measured by DLS increased by $20.4 \pm 2.4\%$, which is close to the enhancement recorded in FCS ($18.8 \pm 4.0\%$). Reprinted from *Nano Lett.* **2017**, *17*, 4807–4812 Copyright 2017. 91

- Figure 4-13.** The change in tracer diffusion as a function of inverse tracer radius at the same enzyme and substrate concentrations (and therefore, at the same reaction rates). (A) For urease, the variation was measured for 10 nM enzyme and 10 mM urea concentration, (B) while for aldolase the enzyme and substrate concentrations were 10 nM and 1 mM respectively. Reprinted from *Nano Lett.* **2017**, *17*, 4807–4812 Copyright 2017. 93
- Figure 4-14.** Colorimetric activity assay of urease. From the rate of change of absorbance with time, activity of the enzyme was estimated following the reference curve reported in Ref. (S1). The measured turnover number of Jack bean urease was 625/s. Reprinted from *Nano Lett.* **2017**, *17*, 4807–4812 Copyright 2017. 95
- Figure 4-15. (A-B)** Fluorescence images of 2 μm polystyrene sulfate tracers (A) without and (B) with BSA coatings, after treating them with DyLight 550 Maleimide dye tagged urease solution for 10 min. Images (C-D) shows similar experiments carried out with catalase tagged with Alexa Fluor 594 dyes. BSA coating significantly minimized adsorption of enzymes on the particle surface. Reprinted from *Nano Lett.* **2017**, *17*, 4807–4812 Copyright 2017. 99
- Figure 4-16. (A-B)** Fluorescence images of 2 μm polystyrene sulfate tracers (A) without and (B) with BSA coatings, after treating them with DyLight 550 Maleimide dye tagged urease solution for 10 min. Images (C-D) shows similar experiments carried out with catalase tagged with Alexa Fluor 594 dyes. BSA coating significantly minimized adsorption of enzymes on the particle surface. Reprinted from *Nano Lett.* **2017**, *17*, 4807–4812 Copyright 2017. 99
- Figure 4-17.** Diffusion coefficient distribution of 2 μm polystyrene sulfate tracers, coated with BSA, dispersed in (A) DI Water and (B) 10 mM Urea, recorded in DLS. The measurements were taken successively at three different times. The measured diffusion of the tracers is $0.23 \pm 0.01 \mu\text{m}^2/\text{s}$ in DI water and $0.24 \pm 0.01 \mu\text{m}^2/\text{s}$ in 10 mM urea. Reprinted from *Nano Lett.* **2017**, *17*, 4807–4812 Copyright 2017. 100
- Figure 5-1. (A)** Schematic of the three-inlet microfluidic set up used to observe chemotaxis of enzyme coated particles towards higher substrate concentrations. The excess migration of the functionalized particles towards the substrate side was quantified by measuring the fluorescence intensity of the polymer spheres along a straight line across the channel (shown in red) at a distance of 38 mm from the start. The figure also shows chemotactic migration of (B, D) urease and (C, E) catalase coated fluorescent microspheres in presence of imposed substrate concentration gradients, observed within three-inlet microfluidic channels. The enzyme functionalized particles are flown through the middle channel of the device, while through the side channels, either buffer alone or buffered solution of appropriate substrates are introduced at the same flow rate. Reprinted from *Nano Lett.* **2015**, *15* (12), 8311–8315. Copyright 2015. 108
- Figure 5-2.** Chemotactic migrations of urease coated microparticles measured at different times (at different positions of the microfluidic channel along its length, from the start) at (A) 10 mM and (B) 100 mM urea. The error bars represent standard

deviations for six independent measurements. Reprinted from *Nano Lett.* **2015**, *15* (12), 8311–8315. Copyright 2015. 110

Figure 5-3. Fluorescence and optical microscopy images of **(A)** 2 μm streptavidin-functionalized polystyrene particles coated with tagged biotinylated catalase and **(B)** uncoated 2 μm streptavidin-functionalized polystyrene particles. Reprinted from *Nano Lett.* **2015**, *15* (12), 8311–8315. Copyright 2015..... 112

Figure A-1. Modeling results for the simplified enzyme cross diffusion. **(A)** Total enzyme concentration in central channel. With catalysis we observe significant enzyme focusing. Without catalysis, focusing is not noticeable. **(B)** The sum of product concentration and enzyme complex concentration is used to estimate the number of forward binding events. The number of binding events in the case with catalysis is several orders of magnitude greater than in the case with no catalysis due to turnover. Insert: close up of data at beginning of the reaction. **(C)** Enzyme concentration in central channel over time. Without catalysis, the enzyme-complex equilibrium shifts almost immediately towards the complex ES, and $[E]$ drops to zero. With catalysis, ES is turned over and the equilibrium shifts towards E. **(D)** Enzyme-Substrate complex concentration in the central channel over time. Reprinted from *Nat. Chem.* **2018**, *10* (3), 311–317. Copyright 2018..... 122

Figure A-2. Results from a confocal imaging experiment where D-Glucose and all four enzymes were present: All sample HK trajectories (red) found in the image stack, and all Ald trajectories (blue) which are identified as possible candidates for trajectories originating from the same HK-Ald aggregate. Reprinted from *Nat. Chem.* **2018**, *10* (3), 311–317. Copyright 2018. 124

LIST OF TABLES

Table 2- 1. Tabulation of the dissociation constants of AMP, ADP, ATP and PPi binding towards aldolase parameters and diffusion enhancements [12, 13]. <i>Nano Lett.</i> 2017, 17 (7), 4415–4420. Copyright 2017.	29
Table 2- 2 Typical Calibration parameters obtained in FCS experiments. <i>Nano Lett.</i> 2017, 17 (7), 4415–4420. Copyright 2017.	41
Table 2- 3 Typical Experiment parameters obtained in FCS experiments with FBP from 0 to 0.05 mM. <i>Nano Lett.</i> 2017, 17 (7), 4415–4420. Copyright 2017.	42
Table 2- 4 Typical Experiment parameters obtained in FCS with FBP from 0.1 mM to 1 mM. <i>Nano Lett.</i> 2017, 17 (7), 4415–4420. Copyright 2017.	42
Table 3- 2 Amount of enzyme (HK or Ald) migrated into the central channel (containing either buffer only or 10 mM D-glucose and buffer) at specified time periods (see Figure 6B). The starting concentration of both enzymes is 200 nM. Reprinted from <i>Nat. Chem.</i> 2018, 10 (3), 311–317. Copyright 2018.	63
Table 3- 3 Total number of detected hexokinase (HK) trajectories and total number of HK trajectories found to be correlated with an aldolase (Ald) trajectory (correlation >95%). Reprinted from <i>Nat. Chem.</i> 2018, 10 (3), 311–317. Copyright 2018.	65
Table A-1 Kinetics parameters of HK. Reprinted from <i>Nat. Chem.</i> 2018, 10 (3), 311–317. Copyright 2018.	119
Table A-2 Kinetics parameters and reaction of HK. Reprinted from <i>Nat. Chem.</i> 2018, 10 (3), 311–317. Copyright 2018.	120
Table A-3 Glucose binding and unbinding parameters of HK. Reprinted from <i>Nat. Chem.</i> 2018, 10 (3), 311–317. Copyright 2018.	121
Table A-4 Parameters used in the computational analysis. A pixel is 0.46×0.46 μm and the frame rate is 1 frame every 1.29 s. Reprinted from <i>Nat. Chem.</i> 2018, 10 (3), 311–317. Copyright 2018.	125

ACKNOWLEDGEMENTS

I would like to start by thanking my advisor, Professor Ayusman Sen, for his guidance and inspiration during these past 6 years. He has always been there when I needed help and at the same time, he gave me enough freedom to develop and learn as an independent researcher. He showed me how to be a better scientist through his patience in research and collaborations. I am grateful for his perseverance through both bureaucratic and financial difficulties, so that I would be allowed to start an internship at a big pharma company to help me with my career.

Next, I would like to thank my committee members, Professor Peter Butler, Professor Paul Cremer and Professor Igor Aronson. Dr. Butler taught me how to use the very delicate fluorescence correlation spectroscopy (FCS) instrument that I used to develop the projects that I will present in this dissertation. I sincerely appreciate all the time and effort he spent with me making sure the instrument worked successfully. I would also like to thank Professor Paul Cremer who has been very generous in exposing me to research regarding lipids and liposomes. Because of his guidance, I started to gain interest in the field of formulation science and decided that was where I wanted to start my career. I am grateful that Professor Igor Aronson provided me with valuable suggestions and feedback on my research.

I have had the pleasure of working with wonderful scientists and I would like to thank all of my collaborators: Prof. Stephen Benkovic, Prof. Ramin Golestanian, Prof. Henry Hess, Prof. Peter Butler, Prof. Ubaldo Córdova, Dr. Krishna Kanti Dey, Dr. Michelle Spiering, Dr. Vinita Yadav, Dr. Pierre Illien, Dr. Henri Palacci, Dr. Farzad Mohajerani, Selva Jeganathan and Ben Tansi, my accomplishments are proof of the great work that we have done together. A special thanks to my mentor, Dr. Krishna Kanti Dey, who was an inspiration to everyone around him and helped me gain confidence in the work I was doing. I would also like to thank Grace Òlan Garcia, my summer REU student, for doing great work and for helping me understand how to be a good mentor.

I would like to give a very special thanks to all of the Sen lab; thank you to Wentao, Hua, Chandrani, Frances, Vinita, Flory and Scott for welcoming me with kindness, Ghida for tolerating my pranks, Isa for helping me stay organized and always responsive to my jokes, Raj for always supporting my black-hole-like job searching, regardless of whether or not I graduated, Maiti for being an expert at being a great postdoc while also enjoying life to the fullest. Many thanks to Lyanne, who accompanied me with the warmest smiles and open arms through grad school.

Now to thank my current lab family; Kayla, Josh, Alicia, Matt, Ben, Ambika, Farzad, Allan, Subhadip, Ashlesha and Angus. Thank you all for offering support and care in your own way. I truly enjoyed all the time we spent together. I am so grateful to all of you provide me with favors and suggestions when I was hunting jobs. Many thanks to Kayla and Allan, for being my personal proofreaders. Thanks Josh and Ambika for being my mental support.

I want to highlight all the friendships I have sustained and built during my PhD. Thank you to the friends I made at Penn State: Simou, Kaixi, Pengtao, Xuefei, Yifan, Xiang, Ally, Lyanne, and Emily, for all the memories, the encouragement, and support. A special thanks to Simou and Kaixi for being an amazing support system. Finally, thank you to my family; my mom, Bailing Qi and my dad Lishan Zhao. Thank you for always tolerating my bad mood, for pushing me forward when I just wanted to give up, for loving me unconditionally and for all the sacrifices you have made for me. I am super proud and grateful that you are my parents.

I feel like it was just yesterday that I failed in the teaching assistant English qualification exam and was very anxious about which group that I should put myself in. Just like a blink, 6 years have flown past, and I have come so far from where I started. It has been a tough journey, filled with struggles, but overall it was very rewarding. I could not have gotten to where I am now without the support of my parents, my friends and my great lab mates. Sometimes life is like a black hole, no matter what you do, you will not get any response, but if you keep working hanging in there, you will get the brightest light.

Chapter 1

Introduction

This chapter is an adapted reproduction from *Acc. Chem. Res.* **2018**, *51*, 2373-2381 with permission from American Chemistry Society.

1.1 Enzyme Enhanced Diffusion

Through converting chemical energy to mechanical force, biological motors in living systems are able to perform precise tasks both spatially and temporally. Processive motors like kinesin and dynein transport cargo along microtubules and nonprocessive motors like myosin II muscle contract actin filament. Various types of motors perform activities in the cytoplasm and these forces have a great impact on cells' activities, such as signaling protein, individually, or cells dividing, collectively. Interestingly, motor proteins are not the only proteins that can have a mechanical force. It has been demonstrated that active enzymes, besides primarily functioning as catalysts, diffuse more when they convert substrate to product and this diffusion increases in a substrate concentration dependent manner [1-7]. Inactive enzymes showed much less effective diffusive motion in the presence of enzyme substrate. The diffusion coefficients of fluorescently labeled enzymes are usually measured with a fluorescence correlation spectrometer (FCS), a precise instrument customized with time- correlated single-photon counting (TCSPC) instrumentation. As the fluorescent molecules diffuse in and out of the diffraction- limited observation volume (1-2 fl) [8-9], it will induce the fluorescence fluctuation. The recorded fluorescence swing is then auto-correlated and fit to a 3D multi- component model to determine the diffusion coefficient of the fluorescent labeled enzymes and free dye molecules. The auto correlation of the intensity signal is defined by Eq (1-1) as

$$G(\tau) = \sum_{i=1}^n \frac{1}{N_i} \left[1 + \left(\frac{\tau}{\tau_D^i} \right) \right]^{-1} \left[1 + \left(\frac{1}{w} \right)^2 \left(\frac{\tau}{\tau_D^i} \right) \right]^{-\frac{1}{2}} \quad (1-1)$$

where

$$\tau_D^i = \frac{r^2}{4D_i} \quad (1-2)$$

Here, N_i is the average number of fluorophores of the i^{th} species in the observation volume, τ is the auto-correlation time, w is the structure factor, which is defined as the ratio of height to width of the illumination profile, and τ_D^i is the characteristic diffusion time of the i^{th} fluorescent particle with diffusion coefficient D_i crossing a circular area with radius r .

Muddana et al. used Langevin dynamic simulations to estimate the force accounting for the single enzyme diffusion enhancement in each turnover [1]. Enzymes are in the low Reynold's number regime and therefore, the viscous forces are more significant than the inertial effects. Therefore,

$$\frac{dy}{dx} = \frac{1}{\gamma} F(r) + \eta(t) \quad (1-3)$$

where γ is the drag coefficient, F is the force acting on the particles, and $\eta(t)$ is the stochastic force. Equation 3 can be numerically integrated using the following equation [10]

$$r(t + \Delta t) = r(t) + \frac{\Delta t}{\gamma} F(t) + \left(\sqrt{2k_B T \frac{\Delta t}{\gamma}} \right) \gamma^G \quad (1-4)$$

where γ is the Stokes- Einstein drag coefficient for a spherical particle, k_B is the Boltzmann's constant, γ^G is the Gaussian distributed set of random numbers with mean=0 and standard deviation=1, and Δt is the integration time step (10 ns). Using the turnover number (the number of substrate molecules that can be converted to product per second) of enzymes, we can calculate the impulse time as the force working on particles in each catalytic reaction per active site. The force is then adjusted to the Langevin dynamics simulation until the increased diffusion coefficient matches the observed

diffusion coefficient in experiments. The forces produced during the urease and catalase catalytic reactions have been simulated as 12 pN and 9 pN per turnover, respectively, which are close to the force measured for motor proteins in the cells like kinesin and myosin [11, 12].

Possible mechanisms behind energy transduction by enzymes remain an open question, although several hypotheses have been put forward to account for the experimental observations – including pH changes and phoresis, local and global thermophoretic effects and reaction induced conformational changes in enzymes during catalytic conversion of substrate to products.

pH- effect and Phoresis: Initially, the change of local pH was considered as one possible explanation for the enhanced diffusion of enzymes. To test the instantaneous pH change in the local medium during enzyme catalysis, a pH sensitive dye molecule, SNARF-1, was applied to label urease fluorescently. The lifetime of SNARF-1 changed significantly from 0.8 ns in the 0.01 M urea solution to 1.15 ns in the 0.1 M urea solution, while the diffusion coefficient of urease barely increased. Thus, local pH changes as reasoning for enhanced enzyme movement are ruled out. An alternative explanation for enhanced diffusion of enzymes is hypothesized as the result of self-electrophoresis. Due to the diffusive motion of the two types of ions produced through urea conversion, an electric field is built up in the local area of enzymes over a short time interval. The self-generated electric field could propel the negatively charged urease until the ions diffuse away. The force, responsible for the boosted diffusion, is 12 pN estimated by Langevin dynamics simulation which is close to the electrophoretic force (20 pN) between an anion 2nm away from the center of urease in the water. However, the diffusion of catalase (an enzyme that converts hydrogen peroxide to water and oxygen [2]) was also investigated and was found to show faster motion during catalysis. This indicated that the electrophoretic force could not be the universal reason for accelerating the diffusion of enzymes, as water and oxygen are nonionic products. Golestanian presented that in the cases of conversion involving non-ionic chemicals, the diffusion of enzymes is increased by the asymmetric dispersion

of products in the vicinity of enzymes during the catalysis reactions [13]. The motion is owed to slip velocity that is induced by the depletion of products close to the enzyme active sites. Note that the rotational diffusion is a very important factor for products generation. The time scale of rotational diffusion is

$$T_R = 8\pi\eta R^3 / (k_B T) \quad (1-5)$$

where R is the radius of spherical colloids (enzymes). When the radius of spherical colloids is 2 μm the rotational diffusion time is 50 s. However, the radius of enzymes usually ranges from 3-7 nm, which implies the rotational diffusion time of enzymes are as small as something on the order of 10^{-8} s. Within 10 ns the enzyme can rotate to any other direction and forgetting the memory of product gradient generated 10 ns before. Therefore, there is some evidence against the plausibility that the enhancement of enzyme diffusion is due to a self-generated phoretic effect.

Local and global thermophoretic effect: Inspired by the green fluorescent protein blinking with external temperature excitation, Riedel et al. [4] performed a series of experiments and proposed that heat released during catalytic turnover as a chemoacoustic effect is the origin of the enhancement of enzymes during catalytic turnover. They measured the diffusion of exothermic enzymes with enthalpies ranging from -43.5kJ/mol to -100 kJ/mol (alkaline phosphatase, urease, and catalase) and one enzyme (triose phosphate isomerase) with what is considered to be a neutral enthalpy enzyme ($\Delta H = -3$ kJ/mol [14]) and found that the diffusion of exothermic enzymes in the presence of their substrates increases not only in a substrate concentration dependent manner but also increases relatively with reaction rate. However, no enhancement of diffusion was observed through FCS while triose phosphate isomerase catalyzed D- glyceraldehyde 3-phosphate. Based on the above observations, it was concluded that the released thermal energy formed asymmetric pressure waves that pressed enzymes towards the solvent. In Newton's law, the solvent molecules act with the same force as they go back to the enzyme molecules, therefore the enzymes gain momentum and display

higher motility. However, even assuming the heat generated during enzyme catalysis is completely transferred to solution and raises the local temperature, the temperature difference, ΔT , was only calculated to be a few micro Kelvin. The diffusion coefficient change caused by ΔT is only $10^{-14} \mu\text{m}^2/\text{s}$, which is significantly less than the diffusion difference of $8.0 \mu\text{m}^2/\text{s}$ in the case of urease. Moreover, Golestanian [15] argued that the randomization of the heat translating to the surroundings cannot be neglected, therefore increasing the temperature of the whole system. In practice, the energy will behave like a wave, travelling through the whole system and vanishing at the container boundaries. A collective heating model was built as well to quantify the biological observations with the predicted change of diffusion, ΔD , in the same magnitude as the experimental data. Nevertheless, only 0.2 K increment of temperature with 1 μM urease and 1 M urea in 10 mM PBS/D₂O during catalysis was observed using a thermocouple and NMR spectroscopy with a methanol thermometer, not as high of a temperature as what is predicted in the literature [15. 16]. The experimental temperature difference is not even close to reaching the value in the model.

Conformational change: Another possible mechanism to explain the enhancement behavior of enzyme diffusion is the hydrodynamic force caused by conformational changes during catalysis. According to Purcell's scallop theorem, at low Reynold's numbers, the movement of objects is dominated by the drag force and small objects need to undergo nonreciprocal actuations to prompt a net displacement. Bearing this principle in mind, Kapral and others [17] proposed that the molecular machines can use irreversible wavelike deformations of their bodies to induce fluid flow and to facilitate the motion. The hydrodynamic force can be detected by a conformational-dependent mobility tensor that they developed. When the mobility of molecules is diagonal, the hydrodynamic interaction is absent in the system and no propulsion will take place. Nevertheless, taking the noisy environment into consideration, Lauga [18] demonstrated that the reciprocal change can also lead to a net displacement, as their rotational diffusion is orders of magnitude higher than their translational

diffusion. Starting with a simulation of a spherical swimmer, they took both rotation and instantaneous velocity into account, seeing that the diffusivity of the swimmer is significantly higher than pure Brownian motion even without net motion. Diffusivity increments with reversal change can also be used to explain the biased motion when the swimmers are placed in an external potential gradient. The mathematical estimation of enzyme enhancement induced by the hydrodynamic force was also investigated [15, 19], where the mechanochemical cycle of enzyme catalysis was simplified into two steps: the enzyme goes from its free state to its reaction state and then goes back from its reaction state to its native state. With the simplifications, the alternation of diffusion coefficient is written as, $\Delta D \approx \kappa R^2$, where κ is the turnover rate and R is the radius of enzyme. For urease, the ΔD is $0.8 \mu\text{m}^2/\text{s}$, which hardly reaches the order of magnitude that we observed experimentally. In previous cases, people only discussed the possibility of the contribution of enzymes' conformational change to enzyme effective diffusivity, no one has observed this experimentally. Hexokinase and aldolase were studied in Chapter 2 and a Krebs cycle enzyme was also studied by Minter [20], in which both cases, the diffusion of the enzyme increases in the presence of substrate without co-factor to progress to full catalysis.

1.2 Enzyme Chemotaxis and its hypothesized contribution to metabolon

Given that enzymes can generate sufficient mechanical energy to cause movement, another question that arises is whether it can perform directional movement in the presence of a substrate concentration gradient, paralleling cellular chemotaxis. Yu et al. firstly observed that complexes of DNA template associated with RNA polymerase in the free solution displayed biased movements when it encountered a gradient of its substrate NTP [5]. We also carried out several experiments to explore the motility of non-bound enzymes imposed in their corresponding substrate gradients. A

two-inlet-one-outlet microfluidic channel was fabricated to use for building up a gradient across the interface by flowing fluorescent enzyme from one inlet and substrate solution through another one. When the enzymes are allowed to flow with substrate, enzymes exhibit chemotactic shifts towards substrate gradient as compared to buffer solution [2].

To explain the theoretical aspect of enzyme chemotaxis, several studies were performed. A theory for chemotaxis was established by Schurr et al [21]; it was originally developed for non-reactive and binding-driven systems, however, it has also shed light on the possible thermodynamic origin of enzyme chemotaxis as substrates are principally ligands for these biocatalysts. It explains the thermodynamic tendency of probe macromolecules to climb up the concentration gradient of binding ligands in solution. They derived an expression for the chemotactic/directional movement of the macromolecules in the ligand gradient which increases monotonically as macromolecule-ligand binding becomes stronger. Later, Guha et al. applied a slightly modified version of this expression to their experimental results and showed that the model is in qualitative and quantitative agreement with the chemotaxis of small dye molecules towards a high concentration of various interacting polymers in solutions [22]. In another theoretical work followed by experimental verification, Sitt et al. predicted that when there is a gradient of a binding site on a surface, interacting molecules would again directionally move toward the region with a high density of binding sites along the surface [23,24]. So, in both of the theories mentioned, binding was identified as the origin of molecular chemotaxis.

1.3 Transduction energy to surroundings

The work done by Miño et al. which states that active matter in solution can transduce energy to tracers in the solution with increasing effective diffusion [25], encourages us to study the influence of enzyme catalysis on inert particles in the low Reynolds number regime. We hypothesize that

enzymes might play a crucial role in the dynamic environment of the cytoplasm, as an explanation for one of the phenomenon observed by the Weitz group [26]. When they track the motion of injected submicron sized tracer particles in living cells, the diffusive motion of tracers, calculated as the ensemble-averaged mean-square displacement (MSD) relative to interval time (s). It has been well known that the cytoplasm is a forceful environment with the activity of molecular motors such as kinesin, dynein and myosin II [27]. The motion of tracers was measured to be higher than Brownian motion, considered as a reflection of the fluctuating cytoplasm. To characterize the effect of each type of protein motor, the authors inhibited the myosin II initially with blebbistatin and observed an obvious dropped slope on MSD vs t. Then the cells were treated with ATP depletion, sodium azide and 2-dexoyglucose, to prevent all ATP dependent activities. However, the diffusion of tracers in the cytoplasm was measured still higher than the Brownian motion induced purely by thermal energy. Therefore, the molecular motors and other ATP dependent processes contribute a significant portion to the fluctuating cytoplasm but are not the whole reason for the force. Another metabolism-dependent motion was observed by Parry et al [28]. In the cytoplasm of a bacteria, the driving force was neither from molecular motors nor DNA related activities. Therefore, we proposed that the impulsive force by the free enzymes during catalysis in the cytoplasm is another source of the cytoplasm dynamism. The force quantified in Guo et al.'s study is 10 pN, similar to the enzyme mechanical force simulated by us. Also, the time scale of the force study was from 0.01s-1s which is also on the time scale of enzymatic reactions.

1.4 Applications of mechanical force generated by enzyme

Thus far, we have discussed enzymes' wide assortment of capabilities, ranging from force generation to chemotactic motion when exposed to substrate concentration gradients. Because of these properties, scientists have begun to explore new avenues of enzyme research by conjugating

enzymes to other materials. In these systems, the enzyme can act as an “engine” for an inactive or immobile particle and propel them forward using the energy harnessed from substrate turnover [29]. One early example of this induced motion is the conjugation of enzymes to polystyrene beads [16,30].

Ma et al. [31] demonstrate that enzymes can be conjugated to more complex particles with different functionalities to achieve new properties. In this work, the authors are able to synthesize a stimuli-responsive, self-propelling hollow microsphere that was able to act as a drug delivery vehicle. To do so, they bound urease to the silica side of a hollow Janus nanoparticle and coated the other side in iron. When urea was added to the system, the particle was able to propel itself forward in solution while also allowing for magnetic steering control that is provided by the iron hemisphere. The authors were also able to incorporate a remote “on/off” switch using enzyme inhibitors and protecting agents. It was determined that when inhibitors, such as Ag^+ and Hg^{2+} , were added to the system, urease did not function properly, and the velocity of the particle was significantly lowered or stopped, depending on the inhibitor concentration. The motion could be recovered however, after the addition of a thiol protecting agent (DTT) as this compound binds to the inhibitors more readily than it binds to the urease. This is illustrated in **Figure 1-1**. [31] There are multiple examples of enzymes being attached on various other materials, such as enzyme functionalized polymersomes [32], stomatocytes [33], carbon nanotubes [34], gold nanorods [35, 36] macroscale carbon fibers [37] and more [38-42].

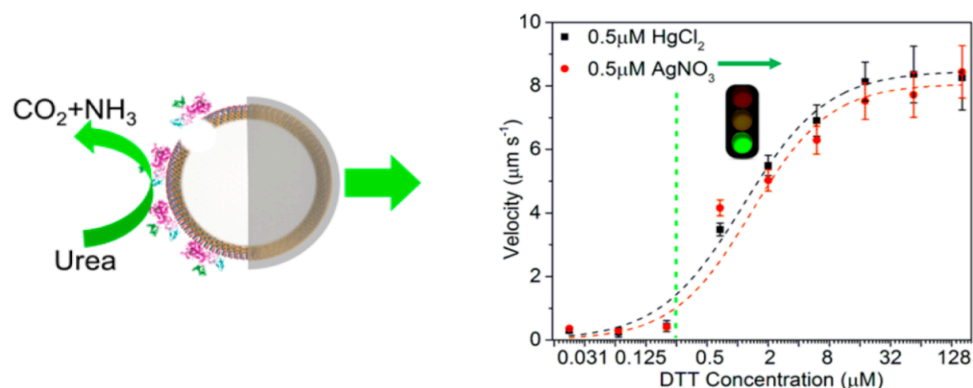
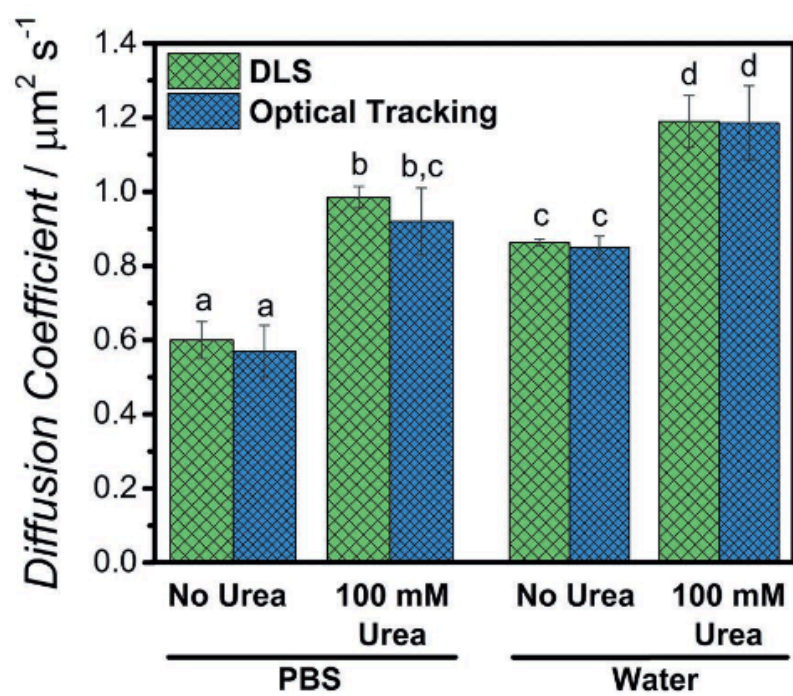


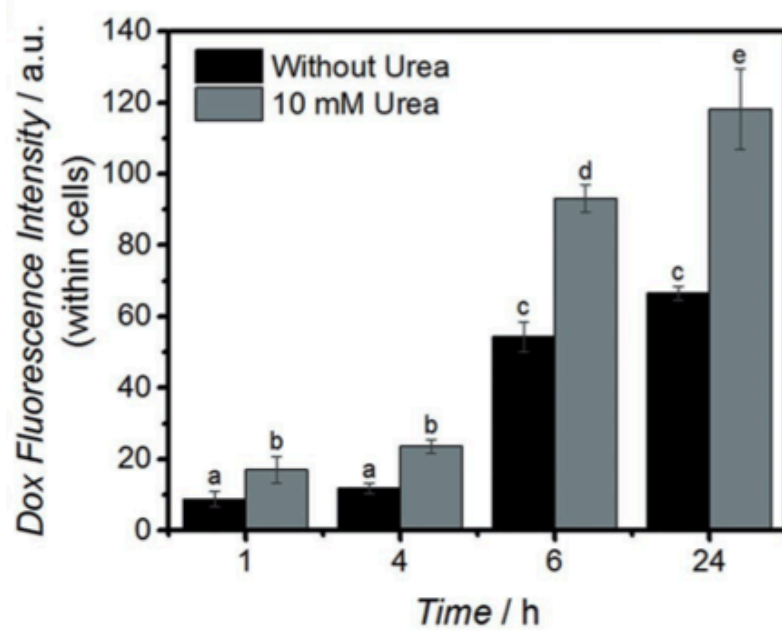
Figure 1-1. (A) Illustration of the motion of the urease functionalized Janus hollow microsphere that is self-propelled by the decomposition of urea to its products. (B) The diffusion of the urease powered microspheres in the presence of increasing concentrations of urease, protecting agent or without inhibitor. Reprinted from *ACS Nano* **2016**, *10*, 3597–3605, Copyright 2016.

The aforementioned studies have all had success in *in vitro* systems, but there is a lack of enzyme powered motors that have been shown to function *in vivo*. A recent study by Hortelão et al, was one of the first to probe the success of urease powered doxorubicin (an anticancer hydrophilic drug) loaded core shell silica spheres, termed nanobots, inside cancer cells [43]. Here, the urease driven decomposition of urea serves multiple purposes, the first being the nanobot's ability to propel itself, the second being the faster release rates of Dox from the bot and the third being the improved anticancer efficiency of the particle. The active nanobot (in the presence of urea) was assessed against the passive system (without urea) and the active particle was more successful on all three accounts, as seen in **Figure 1-2** below [43]. Although this study just assessed the effectiveness of one enzyme powered motor, its success could lead to the continued development and production of these autonomous systems that can be applied for drug delivery and other biomedical applications.

A



B



C

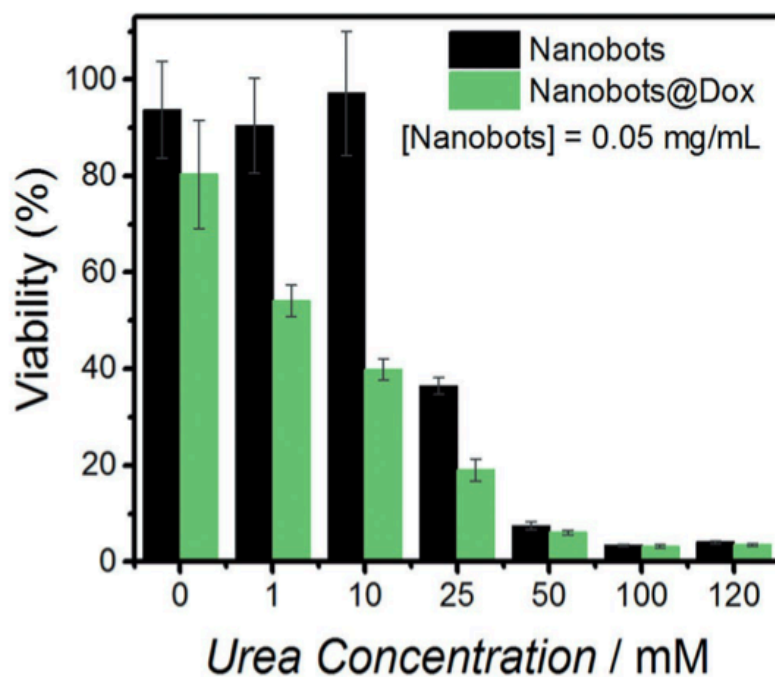


Figure 1-2. (A) Diffusion coefficients nanobots using DLS (green) and optical tracking (blue) without urea and in the presence of 100 mM urea in either PBS buffer or water. (B) The intensity of Dox inside the human epithelial cervix adenocarcinoma (HeLa) cells over time without urea (black) and in the presence of 10 mM urea (gray). (C) The percentage of cells that are viable with nanobots (black) and with Dox containing nanobots (green) in the presence of increasing urea concentrations. Reprinted from *Advanced Functional Materials*. 2017, 1705086, Copyright 2017.

Furthermore, when immobilized onto a surface, enzymes are able to transfer that force to the surrounding fluid and induce pumping of the fluid and any particles that are suspended in the fluid [44]. Sengupta et al. were the first to synthesize and characterize these pumps. In their study, enzymes such as glucose oxidase, catalase, lipase and urease, were attached to a gold patch via a thiol monolayer attachment (**Figure 1-3**) [44].

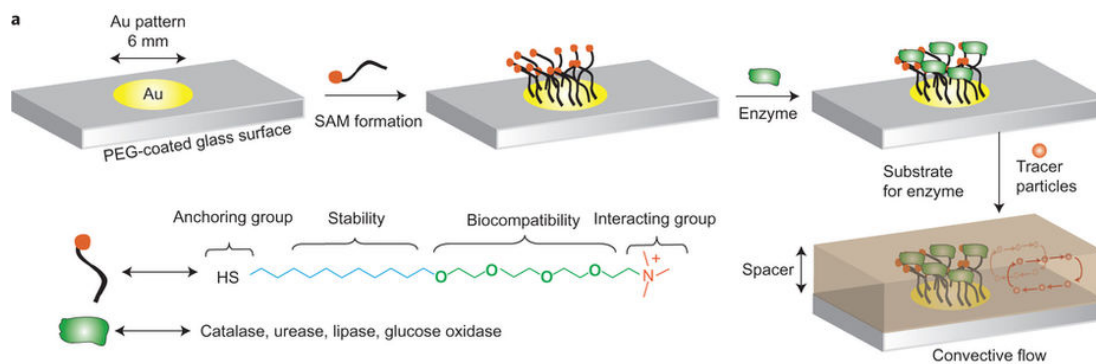


Figure 1-3. Illustration of the experimental setup for the enzyme powered micropumps. Glass slides were coated with PEG and gold was patterned using electron beam evaporation. A quaternary ammonium thiol was added to the gold patch so that it self-assembled into a monolayer on the gold. The enzymes can then selectively bind to the thiol group through electrostatic attractions [44]. Reprinted from *Nat. Chem.* **2014**, 6, 415–422., Copyright 2014.

When the substrate solution was introduced into the closed system, pumping was induced and was found to be dependent on the substrate concentration. Additionally, they determined that the flow direction could be changed depending on the enzyme that was used in the system. For example, glucose oxidase, catalase and lipase pumped fluid inward (towards the gold patch) when in the presence of their respective substrates. However, when urease was introduced into the system with urea, fluid was pumped outward (away from the gold patch) [44]. This behavior was further studied by Ortiz-Rivera et al [45]. In this work, they determined that at high coverage of urease enzyme, significant outward pumping was seen. However, as the coverage of the enzyme was decreased, they saw that the pumping direction could switch to inward, depending on the distance away from the pump and the time of observation. Theoretical and modeling studies were also done, and they were found to agree with the experimental observations. Additionally, it was determined that the speed and direction of flow could change based on the ratios of the reactant diffusivities and expansion coefficients to product diffusivities and expansion coefficients. With this information, the group was

able to better understand the pumping system and they used this knowledge in order to have better control over the pumping speed and direction.

As stated before, the applications for these pumps are numerous. Proof of concept experiments were done in the Sen group to highlight some of the ways that these pumps can be used. First, glucose oxidase was immobilized in a hydrogel with the small molecule, insulin. Over time, insulin will leak from the gel, but when glucose was added, the leaching rate was found to be significantly faster. This demonstrated that delivery of a drug could be induced when coupled with an enzyme pumping system. In another key study, urease enzyme was immobilized onto gold stripes along the surface of a microchannel. A urea concentration gradient was applied over the stripes and they saw fluid continually pump in one direction. Therefore, after some time, the originally evenly distributed passive particles were now mostly sedimented at the far end of the channel. In this way, they were able to induce directional pumping of passive particles down a microchannel, a valuable asset for microfluidic systems, bioassays and complex synthesis [46]. These enzyme-powered pumps have also been shown to act as sensors for toxins, such as mercury, cadmium, nickel, and cyanide. As these substances are inhibitors for the enzyme, flow speeds are significantly reduced or stopped when exposed to different concentrations of the inhibitors. This allows for the quantitative detection of the toxin concentration. In practice, these sensors were able to detect concentrations that were significantly below the limit set by the EPA, making them excellent sensors for use in remote locations, where external power sources are difficult to find [47].

Although multiple applications and benefits of the self-pumping enzyme systems have been explored, the mechanism behind the pumping was not fully understood. As a result, Valdez et al. further probed the enzyme pumping system to determine the driving force behind the pumping [48]. Multiple mechanisms, such as diffusiophoresis, osmophoresis and self-electrophoresis, were originally proposed to explain this behavior, as these have all been used to explain the behavior of

catalytic particles attached to a surface. Diffusiophoresis results in a concentration gradient being produced as reactants are being converted to products. Electrophoresis was thought to apply if charged products were being produced, which was the case for many of the enzyme pumps, including glucose oxidase and lipase. However, for any of these pump systems, when the pump system was inverted so that the immobilized enzyme was now at the top of the chamber instead of the bottom, the directionality of pumping reversed. This ruled out any of the previously proposed mechanisms, as direction should not change in diffusiophoretic or electrolytic mechanisms. Because of the reversal of direction when the pump was inverted, it was inferred that the mechanism must be due to some sort of buoyancy effect. The research group then tried to determine if thermal buoyancy, in which heat is being produced and changing the density of the fluid, or solutal buoyancy, in which the reaction products have different densities than the reactants, was the dominant mechanism. Using theory and experiments, it was determined that solutal buoyancy was the driving force, as the heat produced from the reaction was not sufficient enough to account for the experimentally observed speed of pumping, but the differences in density were. It was found that when the products were denser than the reactants, the fluid settled and slid down and away from the micropump. Conversely, when the products were less dense than the reactants, the fluid would rise up and away from the pump and then flow along the glass slide toward the pump (**Figure 1-4**) [44,47,48]. Determining the mechanism behind these pumps can allow for enhanced spatio-temporal control over the micropumps so that new architectures can be explored for these pumps.

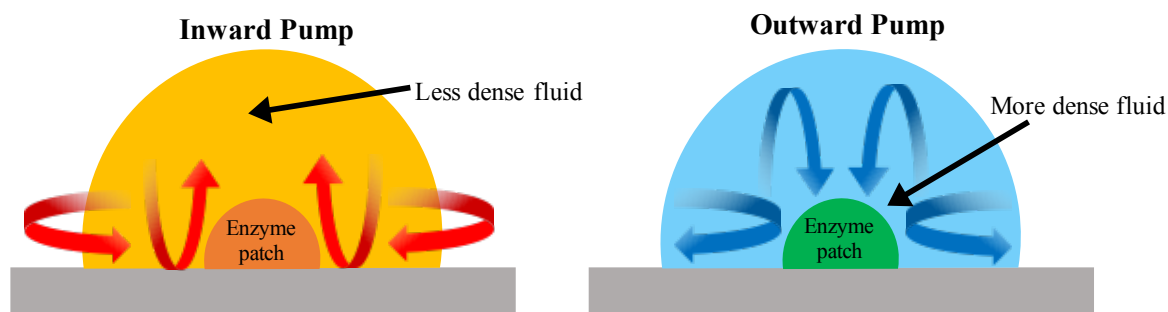


Figure 1-4. Demonstration of the solutal buoyancy mechanism. In the inward pump, the reactants that are produced are less dense than the products, so the local fluid rises and then due to convective flows, comes back down and moves towards the patch on the glass slide. In the outward pump, the enzyme products produced are denser than the reactants, causing the fluid to locally become denser and slide down and away from the patch [44,47, 48]. Reprinted from *Acc. Chem. Res.* 2018, 51, 2373-2381, Copyright 2018.

1.5 Research goals

In this work, I sought to achieve 4 goals: (1) understanding of the mechanisms that lead to enhanced diffusion of enzymes, (2) understanding of single enzyme chemotaxis and sequential chemotaxis in catalyst cascades that is similar to the organization of living systems, (3) exploring how the impulsive force generated by enzyme catalysis can be transmitted to the surroundings, (4) developing enzymes as tiny engines. From a fundamental viewpoint, I aim to understand the underlying science involved in the force generation by free enzymes and their potential contributions to cell signaling and organization in the cytoplasm. At the same time, learning more about enzymes as force generated swimmers will make an impact in the field of nanotechnology for the design of highly controlled and sensitive artificial swimmers while increasing the efficiency and biocompatibility of such systems.

In Chapter 2, two different enzymes were investigated to understand how heat and enzyme conformational changes impact enzyme movement. First, we observed significant reaction rate-

dependent increase in the diffusion of aldolase, which catalyzes an *endothermic* reaction. Then we measured the diffusion of aldolase in the presence of competitive inhibitors (a species that competes with substrate binding on the active site and induces enzyme shape changes without undergoing a catalytic reaction) and the diffusion of hexokinase in the substrate only solution (without cofactor Mg^{2+} to promote the reaction, hexokinase only binds and unbinds to its substrate). Both enzymes show an increase in diffusion. This suggests that conformational changes alone are the reason for diffusion enhancement, and heat produced during reactions may not be necessary. Based on these observations, a new model is also proposed that uses conformational fluctuations induced by binding and unbinding events to explain the motion.

In Chapter 3, to further explain enzyme chemotaxis, both aldolase and hexokinase were studied. Both hexokinase and aldolase move up gradients of species where they only bind and unbind ligands and do not catalyze reactions. Moreover, by studying sequential chemotaxis in a four-enzyme cascade reaction, it is demonstrated that each enzyme independently follows its own specific substrate gradient, which is produced by the preceding enzymatic reaction. The extent of enzyme migration is proportional to the time the enzyme is exposed to the substrate gradient. Significantly, the chemotactic migration of enzymes is fairly rapid even under conditions that mimic cytosolic crowding. The observed rate was very similar to the reported rate of enzyme diffusion in living cells.

In Chapter 4, urease and aldolase were used in the study to understand whether nanoscale active particles like enzymes transfer their momentum to the surroundings, resulting in enhanced diffusion of suspended tracers. It was determined that passive tracers (in the presence of enzymes and substrate) with sizes ranging from nanometers to microns showed enhanced diffusion in an activity dependent manner. Furthermore, when the catalytic reaction rate was the same, tracer diffusion enhancement was found to be inversely correlated to the size of the tracer particles. This is similar to observations made in other active microscopic systems.

In Chapter 5, because of enzymes' ability to generate force during catalysis, enzymes can act as “engines” for inactive particles and propel them. One early example of this induced motion involves conjugation of enzymes to polystyrene beads. The enzyme coated particle also chemotaxed directionally in a substrate gradient. Finally, I conclude this dissertation with remarks on what has been done with force generation by free enzymes and the future directions of this study, highlighting the goals that we aim to explore further.

1.6 References

- [1] Muddana, H. S.; Sengupta, S.; Mallouk, T. E.; Sen, A.; Butler, P. J. Substrate Catalysis Enhances Single Enzyme Diffusion. *J. Am. Chem. Soc.* **2010**, *132*, 2110–2111.
- [2] Sengupta, S.; Dey, K. K.; Muddana, H. S.; Tabouillot, T.; Ibele, M. E.; Butler, P. J.; Sen, A. Enzyme Molecules as Nanomotors. *J. Am. Chem. Soc.* **2013**, *135* (4), 1406–1414.
- [3] Sengupta, S.; Spiering, M. M.; Dey, K. K.; Duan, W.; Patra, D.; Butler, P. J.; Astumian, R. D.; Benkovic, S. J.; Sen, A. DNA Polymerase as a Molecular Motor and Pump. **2014**, *8* (3), 2410–2418.
- [4] Riedel, C.; Gabizon, R.; Wilson, C. A. M.; Hamadani, K.; Tsekouras, K.; Marqusee, S.; Pressé, S.; Bustamante, C. The Heat Released during Catalytic Turnover Enhances the Diffusion of an Enzyme. *Nature* **2015**, *517* (7533), 227–230.
- [5] Yu, H.; Jo, K.; Kounovsky, K. L.; Pablo, J. J. de; Schwartz, D. C. Molecular Propulsion: Chemical Sensing and Chemotaxis of DNA Driven by RNA Polymerase. *J. Am. Chem. Soc.* **2009**, *131* (16), 5722–5723.
- [6] Illien, P.; Zhao, X.; Dey, K. K.; Butler, P. J.; Sen, A.; Golestanian, R. Exothermicity Is Not a Necessary Condition for Enhanced Diffusion of Enzymes. *Nano Lett.* **2017**, *17* (7), 4415–4420.
- [7] Zhao, X.; Palacci, H.; Yadav, V.; Spiering, M. M.; Gilson, M. K.; Butler, P. J.; Hess, H.; Benkovic, S. J.; Sen, A. Substrate-Driven Chemotactic Assembly in an Enzyme Cascade. *Nat. Chem.* **2017**, *10* (3), 311–317.
- [8] Elson, E. L.; Magde, D. Fluorescence Correlation Spectroscopy. I. Conceptual Basis and Theory. *Biopolymers* **1974**, *13* (1), 1–27.

- [9] Magde, D.; Elson, E. L.; Webb, W. W. Fluorescence Correlation Spectroscopy. II. An Experimental Realization. *Biopolymers* **1974**, *13* (1), 29–61.
- [10] Butler, P. J.; Dey, K. K.; Sen, A. Impulsive Enzymes: A New Force in Mechanobiology. *Cell. Mol. Bioeng.* **2015**, *8* (1), 106–118.
- [11] Kojima, H.; Muto, E.; Higuchi, H.; Yanagida, T. Mechanics of Single Kinesin Molecules Measured by Optical Trapping Nanometry. *Biophys. J.* **1997**, *73* (4), 2012–2022.
- [12] Mehta, A. D.; Rief, M.; Spudich, J. A.; Smith, D. A.; Simmons, R. M. Single-Molecule Biomechanics with Optical Methods. *Science*, **1999**, *283* (5408), 1689–1695.
- [13] Golestanian, R. Anomalous Diffusion of Symmetric and Asymmetric Active Colloids. *Phys. Rev. Lett.* **2009**, *102*, 188305.
- [14] Goldberg, R. N.; Tewari, Y. B.; Bhat, T. N. Thermodynamics of Enzyme-Catalyzed Reactions--a Database for Quantitative Biochemistry. *Bioinformatics* **2004**, *20* (16), 2874–2877.
- [15] Golestanian, R. Enhanced Diffusion of Enzymes That Catalyze Exothermic Reactions. *Phys. Rev. Lett.* **2015**, *115* (10), 108102.
- [16] Dey, K. K.; Zhao, X.; Tansi, B. M.; Méndez-Ortiz, W. J.; Córdova-Figueroa, U. M.; Golestanian, R.; Sen, A. Micromotors Powered by Enzyme Catalysis. *Nano Lett.* **2015**, *15* (12), 8311–8315.
- [17] Sakaue, T.; Kapral, R.; Mikhailov, A. S. Nanoscale Swimmers: Hydrodynamic Interactions and Propulsion of Molecular Machines. *Eur. Phys. J. B* **2010**, *75* (3), 381–387.
- [18] Lauga, E. Enhanced Diffusion by Reciprocal Swimming. *Phys. Rev. Lett.* **2011**, *106* (17), 178101.
- [19] Bai, X.; Wolynes, P. G. On the Hydrodynamics of Swimming Enzymes. *J. Chem. Phys.* **2015**, *143* (16), 165101.
- [20] Wu, F.; Pelster, L. N.; Minter, S. D. Krebs Cycle Metabolite Formation: Metabolite Concentration Gradient Enhanced Compartmentation of Sequential Enzymes. *Chem. Commun.* **2015**, *51* (7), 1244–1247.
- [21] Schurr, J. M.; Fujimoto, B. S.; Huynh, L.; Chiu, D. T. A Theory of Macromolecular Chemotaxis. *J. Phys. Chem. B* **2013**, *117* (25), 7626–7652.
- [22] Guha, R.; Mohajerani, F.; Collins, M.; Ghosh, S.; Sen, A.; Velegol, D. Chemotaxis of Molecular Dyes in Polymer Gradients in Solution. *J. Am. Chem. Soc.* **2017**, *139* (44).
- [23] Sitt, A.; Hess, H. Directed Transport by Surface Chemical Potential Gradients for Enhancing Analyte Collection in Nanoscale Sensors. *Nano Lett.* **2015**, *15* (5), 3341–3350.

- [24] Zhang, C.; Sitt, A.; Koo, H. J.; Waynant, K. V.; Hess, H.; Pate, B. D.; Braun, P. V. Autonomic Molecular Transport by Polymer Films Containing Programmed Chemical Potential Gradients. *J. Am. Chem. Soc.* **2015**, *137* (15), 5066–5073.
- [25] Miño, G.; Mallouk, T. E.; Darnige, T.; Hoyos, M.; Dauchet, J.; Dunstan, J.; Soto, R.; Wang, Y.; Rousselet, A.; Clement, E. Enhanced Diffusion Due to Active Swimmers at a Solid Surface. *Phys. Rev. Lett.* **2011**, *106* (4), 048102.
- [26] Guo, M.; Ehrlicher, A. J.; Jensen, M. H.; Renz, M.; Moore, J. R.; Goldman, R. D.; Lippincott-Schwartz, J.; Mackintosh, F. C.; Weitz, D. A. Probing the Stochastic, Motor-Driven Properties of the Cytoplasm Using Force Spectrum Microscopy. *Cell* **2014**, *158* (4), 822–832.
- [27] Vale, R. D. The Way Things Move: Looking Under the Hood of Molecular Motor Proteins. *Science* (80-.). **2000**, *288* (5463), 88–95.
- [28] Parry, B. R.; Surovtsev, I. V.; Cabeen, M. T.; O’Hern, C. S.; Dufresne, E. R.; Jacobs-Wagner, C. The Bacterial Cytoplasm Has Glass-like Properties and Is Fluidized by Metabolic Activity. *Cell* **2014**, *156* (1–2), 183–194.
- [29] Ma, X.; Hortelão, A. C.; Patiño, T.; Sánchez, S. Enzyme Catalysis To Power Micro/Nanomachines. *ACS Nano* **2016**, *10*, 9111–9122.
- [30] Gáspár, S. Enzymatically Induced Motion at Nano- and Micro-Scales. *Nanoscale* **2014**, *6* (14), 7757–7763.
- [31] Ma, X.; Wang, X.; Hahn, K.; Sánchez, S. Motion Control of Urea-Powered Biocompatible Hollow Microcapsules. *ACS Nano* **2016**, *10* (3), 3597–3605.
- [32] Joseph, A.; Contini, C.; Cecchin, D.; Nyberg, S.; Ruiz-Perez, L.; Gaitzsch, J.; Fullstone, G.; Tian, X.; Azizi, J.; Preston, J.; et al. Chemotactic Synthetic Vesicles: Design and Applications in Blood-Brain Barrier Crossing. *Sci. Adv.* **2017**, *3*, 1700362.
- [33] Abdelmohsen, L. K. E. A.; Nijemeisland, M.; Pawar, G. M.; Janssen, G.-J. A.; Nolte, R. J. M.; van Hest, J. C. M.; Wilson, D. A. Dynamic Loading and Unloading of Proteins in Polymeric Stomatocytes: Formation of an Enzyme-Loaded Supramolecular Nanomotor. *ACS Nano* **2016**, *10*, 2652–2660.
- [34] Pantarotto, D.; Browne, W. R.; Feringa, B. L. Autonomous Propulsion of Carbon Nanotubes Powered by a Multienzyme Ensemble. *Chem. Commun.* **2008**, *0*, 1533–1535.
- [35] Pavel, I.-A.; Bunea, A.-I.; David, S.; Gáspár, S. Nanorods with Biocatalytically Induced Self-Electrophoresis. *ChemCatChem* **2014**, *6*, 866–872.
- [36] Bunea, A.-I.; Pavel, I.-A.; David, S.; Gáspár, S. Modification with Hemeproteins Increases the Diffusive Movement of Nanorods in Dilute Hydrogen Peroxide Solutions. *Chem. Commun.* **2013**, *49*, 8803.

- [37] Mano, N.; Heller, A. Bioelectrochemical Propulsion. *J. Am. Chem. Soc.* **2005**, *127*, 11574–11575.
- [38] Orozco, J.; García-Gradilla, V.; D’Agostino, M.; Gao, W.; Cortés, A.; Wang, J. Artificial Enzyme-Powered Microfish for Water-Quality Testing. *ACS Nano* **2013**, *7*, 818–824.
- [39] Wu, Z.; Lin, X.; Zou, X.; Sun, J.; He, Q. Biodegradable Protein-Based Rockets for Drug Transportation and Light-Triggered Release. *ACS Appl. Mater. Interfaces* **2015**, *7*, 250–255.
- [40] Singh, V. V.; Kaufmann, K.; Esteban-Fernández de Ávila, B.; Uygun, M.; Wang, J. Nanomotors Responsive to Nerve-Agent Vapor Plumes. *Chem. Commun.* **2016**, *52*, 3360–3363.
- [41] Sattayasamitsathit, S.; Kaufmann, K.; Galarnyk, M.; Vazquez-Duhalt, R.; Wang, J. Dual-Enzyme Natural Motors Incorporating Decontamination and Propulsion Capabilities. *RSC Adv.* **2014**, *4*, 27565–27570.
- [42] Sanchez, S.; Solovev, A. A.; Mei, Y.; Schmidt, O. G. Dynamics of Biocatalytic Microengines Mediated by Variable Friction Control. *J. Am. Chem. Soc.* **2010**, *132*, 13144–13145.
- [43] Hortelão, A. C.; Patiño, T.; Perez-Jiménez, A.; Blanco, À.; Sánchez, S. Enzyme-Powered Nanobots Enhance Anticancer Drug Delivery. *Adv. Funct. Mater.* **2017**, 1705086.
- [44] Sengupta, S.; Patra, D.; Ortiz-Rivera, I.; Agrawal, A.; Shklyaev, S.; Dey, K. K.; Córdova-Figueroa, U.; Mallouk, T. E.; Sen, A. Self-Powered Enzyme Micropumps. *Nat. Chem.* **2014**, *6* (5), 415–422.
- [45] Ortiz-Rivera, I.; Shum, H.; Agrawal, A.; Sen, A.; Balazs, A. C. Convective Flow Reversal in Self-Powered Enzyme Micropumps. *Proc. Natl. Acad. Sci. U. S. A.* **2016**, *113* (10), 2585–2590.
- [46] Das, S.; Shklyaev, O. E.; Altemose, A.; Shum, H.; Ortiz-Rivera, I.; Valdez, L.; Mallouk, T. E.; Balazs, A. C.; Sen, A. Harnessing Catalytic Pumps for Directional Delivery of Microparticles in Microchambers. *Nat. Commun.* **2017**, *8*, 14384.
- [47] Ortiz-Rivera, I.; Courtney, T. M.; Sen, A. Enzyme Micropump-Based Inhibitor Assays. *Adv. Funct. Mater.* **2016**, *26* (13), 2135–2142.
- [48] Valdez, L.; Shum, H.; Ortiz-Rivera, I.; Balazs, A. C.; Sen, A. Solutal and Thermal Buoyancy Effects in Self-Powered Phosphatase Micropumps. *Soft Matter* **2017**, *13* (15), 2800–2807.

Chapter 2

Enhanced Diffusion of Enzyme with or without Catalysis

A part of this chapter is an adapted reproduction from *Nano Lett.* **2017**, *17*, 4415–4420. with permission from American Chemistry Society.

2.1 Introduction

The observation of force generation by catalytic molecules during chemical transformations has opened up a new area of mechanochemistry [1]. Enzyme molecules, in addition to their primary function as catalysts in biochemical reactions, have recently been proposed to act as force generators during substrate turnover. In a series of experiments, Sen et al. first demonstrated that the diffusive movement of urease, catalase and DNA polymerase, increased with increasing substrate concentration, which suggests that the role of catalysis is important in the transduction of chemical energy into mechanical motion [2-4]. The possible mechanisms behind enhanced enzyme diffusion remains an open question although several proposals have been put forward. Self-propulsion through diffusiophoresis has been suggested for molecules like urease, which generate ionic products [5]. Motility resulting from reaction-induced conformational changes has also been proposed as a possibility [6-8]. Bustamante et al. attributed enhanced diffusion of enzymes to the exothermicity of the chemical reactions involved, where motion is induced via a local thermophoretic effect [9]. According to this proposal, the instantaneous heat released during substrate turnover generates an asymmetric pressure wave that is responsible for the transient displacement of the center of mass of the enzyme molecule and enhancing its diffusion. More recently, Golestanian has estimated the magnitude of diffusion enhancement originating from different possible mechanisms - self-thermophoresis, stochastic swimming, and global temperature increases during enzymatic turnover

of substrates [10]. The results suggest that stochastic swimming due to collective heating and conformational changes are more likely to account for the experimentally measured diffusion enhancement of the enzymes studied so far. Herein, we show that aldolase, which catalyzes an endothermic reaction with the $\Delta H \sim 30\text{-}60 \text{ kJ mol}^{-1}$ [11-12], is also capable of generating enough mechanical force during substrate turnover to significantly enhance its diffusion and that of inert molecules and tracer particles dispersed in solution.

More interestingly, in order to understand the importance of the catalytic step in the mechanochemical cycle, the diffusion of aldolase in the presence of inhibitors was also measured. A competitive inhibitor of aldolase was used that binds at the same place that the substrate binds [13,14]. In the presence of the aldolase competitive inhibitor, the diffusion of aldolase shows significant enhancement, demonstrating that the catalytic step is not necessary. These findings are consistent with experiments performed with Krebs cycle enzymes [15], the diffusion coefficient of enzymes are enhanced in the presence of their substrates even in the absence of their cofactor, and that binding/unbinding with conformational changes of enzymes is sufficient to lead to enhanced diffusion of enzymes. To confirm the mechanism related to conformational change, we investigated the diffusion of hexokinase, which has a two lobe structure and only periodically associates and disassociates with substrate when there is no Mg^{2+} as a cofactor to promote catalysis. [16-18] We firstly demonstrated that the diffusion of enzymes in solution can be enhanced significantly even without any chemical reaction and simply by inducing periodic conformational changes in those molecules. Moreover, the conformational changes of enzymes can produce enough energy to also move passive tracers in the solution.

2.2 Experimental Results and Discussion

2.2.1 Enhanced Diffusion of Aldolase

Diffusion experiments were performed in FCS with samples containing 10 nM labeled aldolase in the presence of varied concentrations of fructose-1,6-bisphosphate (FBP, 0-1 mM). The diffusion of aldolase was found to increase in a substrate concentration dependent manner, implying the role of catalytic turnover in enhancing diffusion. Also, the result clearly suggests that reaction exothermicity is not a prerequisite for reaction-induced diffusion enhancement. Surprisingly, even with a very low turnover rate ($k_{cat} \sim 5 \text{ s}^{-1}$ at physiological pH) [13], diffusion of aldolases enhances by nearly 31.04%. Aldolase diffusion and the total rate of reaction in the system at various concentrations of FBP are shown in **Figure 2-1A**. As can be seen, the diffusion values correlate well with the total reaction rate of the system. To rule out the possibility of deagglomeration causing the enhancement diffusion of aldolase, we also compared the diffusion of aldolase before, during, and at the completion of the reaction. As shown in **Figure 2-1B**, while the diffusivity of aldolase increases during turnover, it returns to the base value after the substrate is consumed.

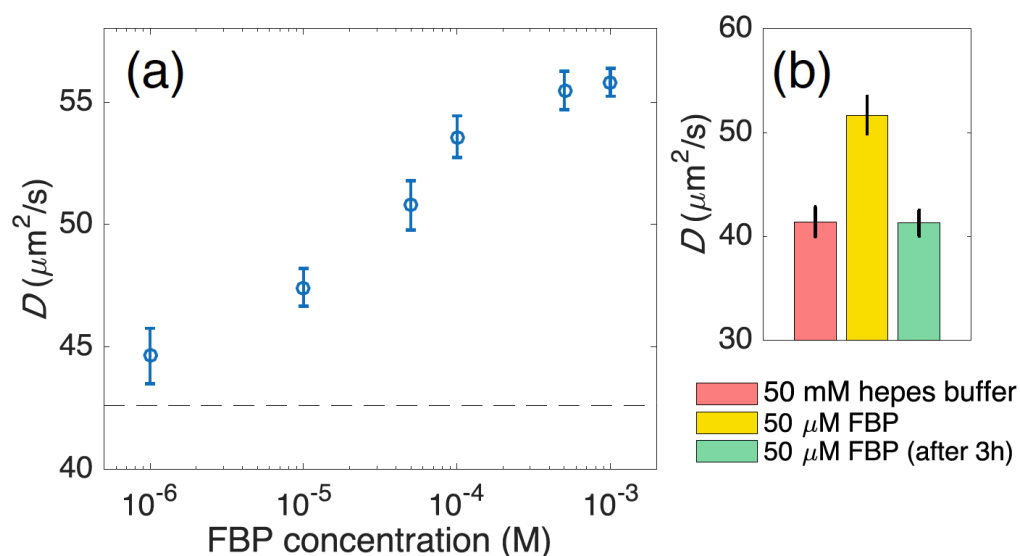


Figure 2-1. A) The diffusion of tagged aldolase was measured in FCS at different substrate concentrations. The diffusive motion of aldolase increased with increasing reaction rate. The error bars represent standard deviations calculated for 15 different measurements, under identical conditions. **B)** The enhanced diffusion of aldolase in the presence of substrate returns to the base value (observed in the absence of the substrate) when the substrate is consumed. All values are significantly different with $p < 0.05$. Reprinted from *Nano Lett.* **2017**, 17 (7), 4415–4420. Copyright 2017.

2.2.2 Enhanced Diffusion of Aldolase in the presence of inhibitors

The observed enhanced diffusion of aldolase with similar relative magnitudes to the significantly faster enzymes and the same characteristic Michaelis-Menten dependence on the substrate concentration poses an apparent paradox: the enhanced diffusion cannot be controlled by the magnitude of the reaction rate, but it exhibits the same dependence on the substrate concentration. Moreover, given the thermodynamic properties of aldolase, the non-equilibrium mechanisms relying on the exothermicity of the catalytic reaction cannot be extended to the present case. Therefore, our experimental observations lead us to reconsider the theoretical paradigm around this physical

phenomenon. In order to probe the importance of the catalytic step of the mechanochemical cycle, we also measured the performances of enzymes in the presence of the reversible inhibitor, PPi, which is a competitive inhibitor of aldolase and binds at the same active sites as FBP [13,14]. In the presence of PPi alone, diffusion of aldolase shows significant enhancement **Figure 2-2**, demonstrating that the catalytic step of the reaction scheme is not necessary to lead to enhanced diffusion. These findings are consistent with recent experiments performed on citrate synthase and malate dehydrogenase, which suggest that the diffusion coefficients of the enzymes are enhanced in the presence of their substrates even in the absence of their cofactors, and that binding/unbinding is sufficient to lead to enhanced diffusion of enzymes.

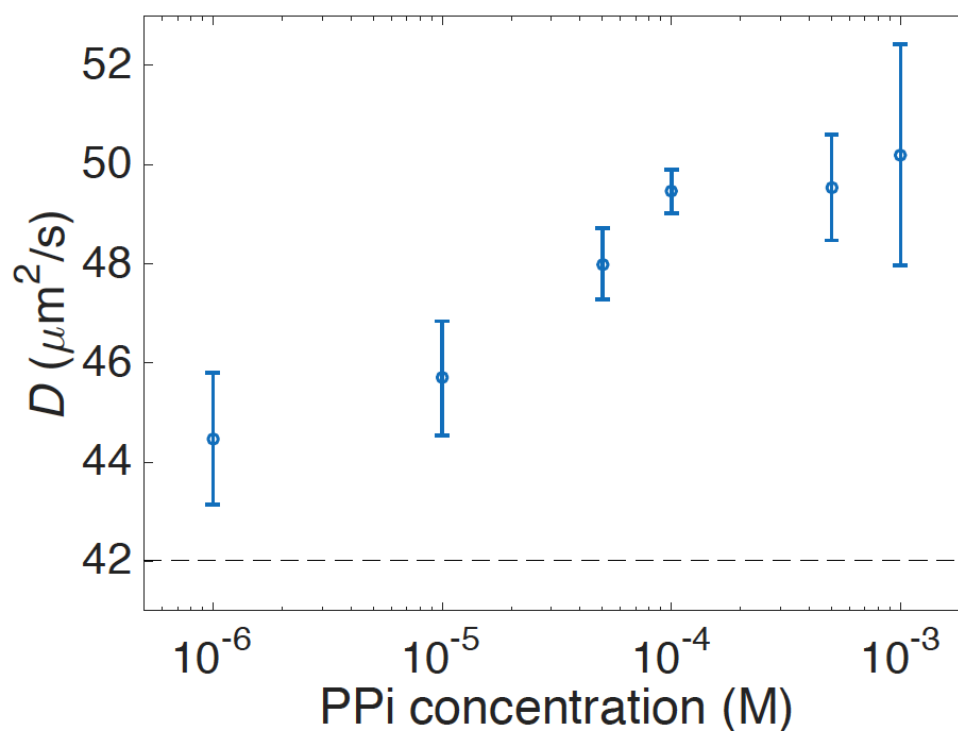
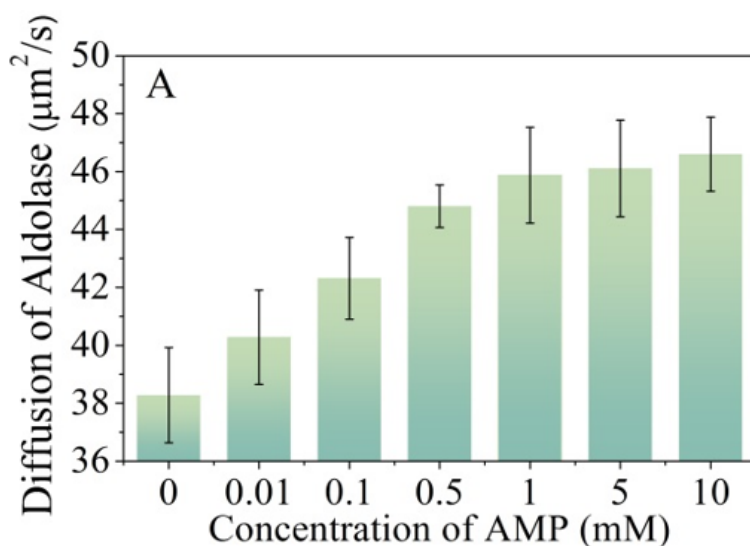


Figure 2-2. Diffusion of aldolase enhances with increasing pyrophosphate (PPi) concentration (the dashed line corresponds to the base value in the absence of substrate). PPi is a competitive inhibitor of aldolase. Reprinted from *Nano Lett.* **2017**, *17* (7), 4415–4420. Copyright 2017.

In addition to PPI, we also investigate aldolase in the presence of its other competitive inhibitors, AMP, ADP and ATP. The diffusion of aldolase increases significantly in all three inhibitor solutions as compared to the buffer. However, the diffusion enhancement in reversible inhibitor solutions is less than when the enzyme undergoes full catalysis. The increase of aldolase diffusion was initially considered to be related with the binding affinity between inhibitors and aldolase. Binding affinity is typically measured and reported by the equilibrium dissociation constant (K_D), $K_D = \frac{K_{off}}{K_{on}} = \frac{[A][B]}{[AB]}$, which is used to evaluate strengths of bimolecular interactions. The smaller the K_D value, the greater the binding affinity of the ligand for its target. Note that the dissociation constant can only indicate the amount of enzyme-inhibitor complex in the solution instead of association and dissociation rate. The dissociation constant can be found in previous literature and the percentages of aldolase diffusion enhancement are summarized in **Table 2-1**.



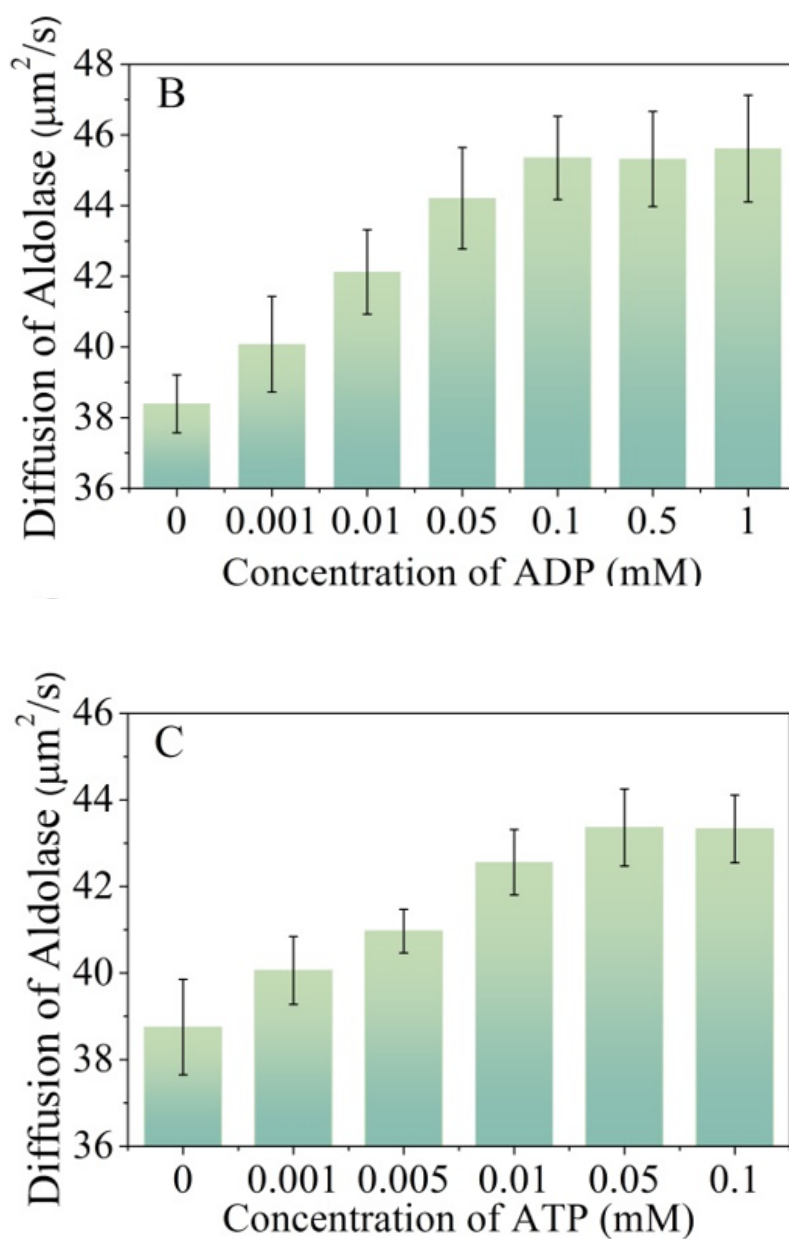


Figure 2-3. (A-C) The diffusion of aldolase in the various concentrations of AMP, ADP and ATP shows in an inhibitor concentration dependent manner. The increase in aldolase diffusion is less than aldolase in the presence of its substrate solution. Aldolase diffusion increases to a plateau in the presence of AMP, ADP and ATP at different concentrations. The error bars represent the standard deviation of 10 different measurements.

Table 2- 1. Tabulation of the dissociation constants of AMP, ADP, ATP and PPi binding towards aldolase parameters and diffusion enhancements [12, 13]. *Nano Lett.* **2017**, *17* (7), 4415–4420. Copyright 2017.

	K_D / mM	$\Delta D/D_0$	ΔG
AMP	3.70 ± 0.40	21.03%	- 13.88
ADP	0.30 ± 0.03	16.7%	- 20.11
ATP	0.034 ± 0.004	11.89%	- 25.51
PPi	0.046 ± 0.010	20.39%	- 24.76

2.2.3 Enhanced Diffusion of Hexokinase

Hexokinase is an ATP dependent enzyme which can convert glucose to glucose- 6-phosphatase with Mg^{2+} as an activator. In aqueous solution, Mg^{2+} binds the negatively charged phosphate oxygen of ATP, promoting the catalysis by transferring the electrons in the MgATP^{2-} complex and helping the reaction between the phosphate on ATP and the hydroxyl group of glucose. When glucose binds to hexokinase, it induces a conformational change of the enzyme to exclude water molecules and make the hydroxyl oxygen closer to the phosphate on ATP [16]. The structure of hexokinase can be defined as two lobes. Generally, the two lobes of hexokinase keep open. When the enzymes bind to glucose, the two lobes will be in a closed state leading to a modified structure [17]. Hexokinase will only undergo a conformational change by associating and disassociating with glucose, when there is no ATP and Mg^{2+} to promote catalysis. The rate of associating and disassociating are comparable [18]. According to this, we measured the diffusion of hexokinase in different solutions to see how it changes in the presence of catalysis and absence of catalysis. The

measurements of hexokinase diffusion were carried out using 20 nM fluorescently labeled enzymes in various solutions. (**Figure 2-4A.**) The diffusion of hexokinase in buffer solution was measured as $72.44 \pm 2.15 \mu\text{m/s}^2$, which was close to the theoretical value calculated through the Stokes- Einstein equation with a known radius of hexokinase. When ATP, MgCl_2 and the MgATP^{2-} complex were added into the enzyme solution, respectively, the diffusion showed increases in all three cases. We speculate that this is due to the slight changes in the hexokinase structure when ATP, MgCl_2 or the MgATP^{2-} complex binds to hexokinase in a place other than the active site. Surprisingly, the hexokinase diffusion only increased by $30.69 \pm 5.44 \%$ in the presence of substrate. The diffusion of hexokinase was also measured in the presence of only glucose with various concentrations, comparing the diffusion of hexokinase with full catalysis with various glucose concentrations (**Figure 2-4B.**) The diffusion of hexokinase in the presence of glucose only is always smaller than the diffusion of hexokinase when it undergoes full catalysis. However, when only binding and unbinding exist between enzymes and substrate, the diffusion of enzymes increased while the substrate concentration was higher and reached a plateau at a substrate concentration smaller than the concentration at which enzyme diffusion reached a plateau with full catalysis. This is mainly because the amount of active binding sites is saturated. When compared to the enzyme diffusion that occurs during the catalytic reaction, the contribution of conformational changes of enzyme are a major component. Some other factors during the catalysis reaction may help increase the diffusion more.

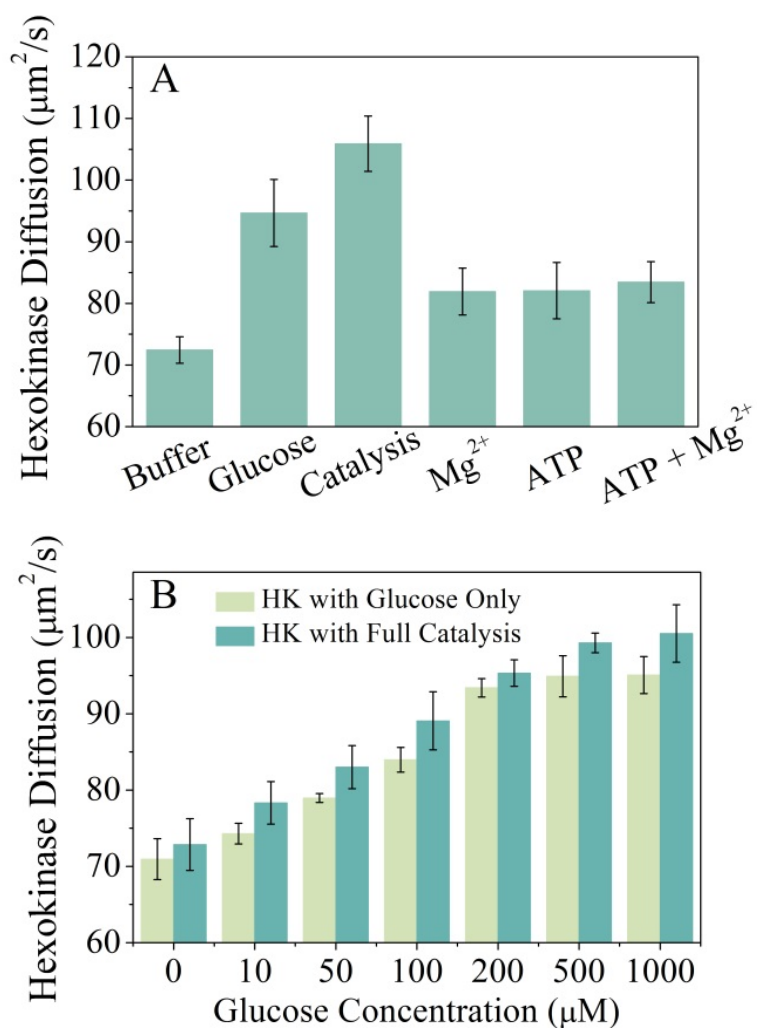


Figure 2-4. **A)** The diffusion of fluorescently labeled hexokinase was measured in FCS in various solutions with or without cofactor and substrate. Hexokinase showed crucial amplification when binding and unbinding substrate without catalysis ($30.69 \pm 5.44\%$), although diffusion of the enzyme increased the most during the turnover reaction ($46.22 \pm 4.49\%$). **B)** We also demonstrated that the diffusion of hexokinase enhances in a substrate- dependent manner either without catalysis or with catalysis. The diffusion of hexokinase was measured in different glucose concentrations in either the absence or presence of 1mM ATP and 1mM MgCl_2 . The error bars represent the standard deviation calculated for 10 different measurements, under identical conditions.

2.3 Numerical Results Summary

To completely assess the effects that were probed experimentally, a theoretical model was developed that assumed that the protein exists in two different states, namely a free state and a bound state, in which a substrate molecule is present in the active site (see **Figure 2-5A**). Note that this simplified picture is an equilibrium description of the problem, which does not involve the chemical or catalytic step of the process and is therefore independent of the degree of exothermicity of the overall reaction. Relying on this simplified stochastic picture, we then aim to describe the effect of changes on conformational fluctuations induced by the binding and unbinding events. We first consider the simple case where the enzyme is always free (in the absence of substrate molecules). The state of the enzyme is then completely described by the position of its center of mass R and a vector C , that describes the conformation of the enzyme, and whose dimensions corresponds to the number of internal degrees of freedom. Given the complexity of the real structure of biomolecules (see **Figure 2-5B** for a representation of aldolase), C is a high dimensional vector that does not need to be specified for now. The mobility coefficient μ of the enzyme depends on its geometrical properties, and therefore on its conformational state C . The overall diffusion coefficient of the enzyme as measured in the FCS experiments is an average of the conformations explored by the enzyme and can be related to the mobility through the fluctuation-dissipation theorem [19,20] as

$$D = k_B \mu \int dC \mu(C) p(C) \equiv k_B T \langle \mu \rangle, \quad (3-1)$$

where $p(C)$ is the probability to find the enzyme in a given conformation C . This expression is valid as long as the timescale on which conformational changes occur, which is comparable to the rotational diffusion time, is smaller than any other timescale.

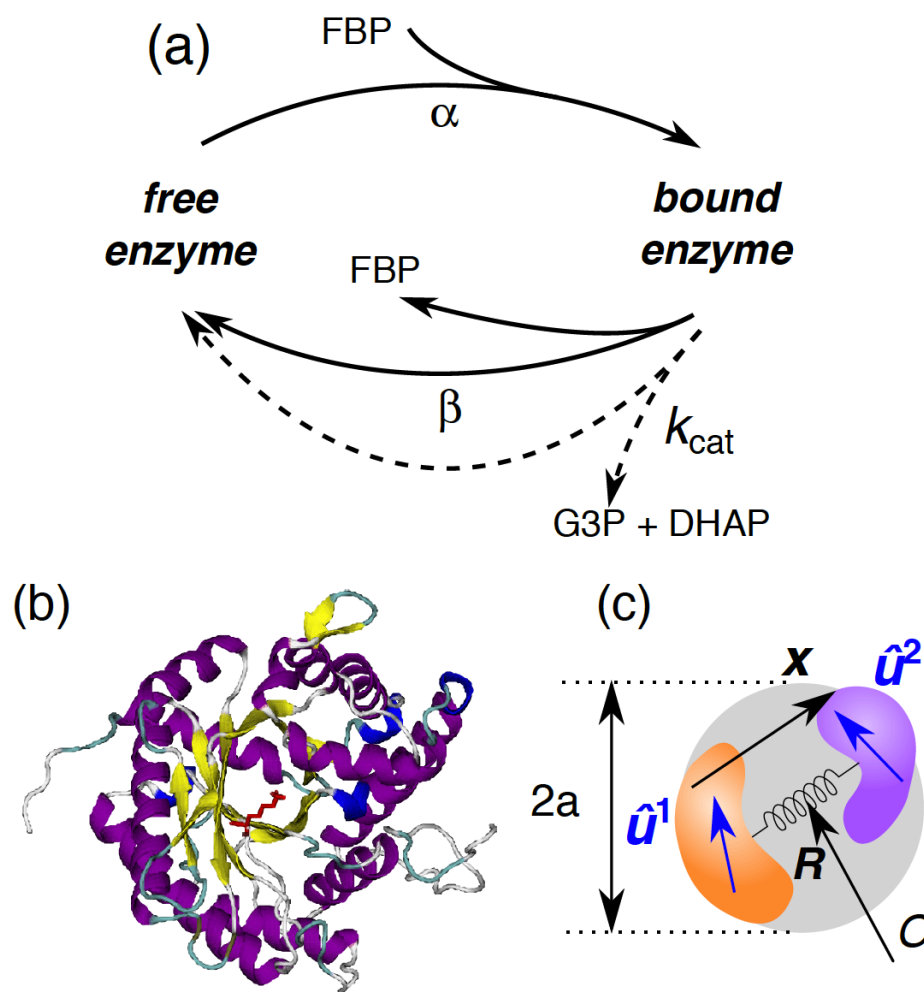


Figure 2-5. (A) Substrate binding and unbinding drives a stochastic two-state process. The enzyme switches randomly between two equilibrium states, where it is either free or bound. (B) Structure of an aldolase monomer (Protein Data Bank ID: 1ADO, subunit A), generated with VMD.²³ The residue colored in red indicates the location of the active site.²² (C) Aldolase enzyme modeled as a dumbbell. R is the position of the center of mass of the enzyme, x represents its elongation. The grey sphere symbolizes the whole enzyme, whose typical size is denoted by a . Reprinted from *Nano Lett.* **2017**, *17* (7), 4415–4420. Copyright 2017.

In the presence of the substrate, the enzyme switches randomly between a free state and another state where it is bound to a substrate molecule. The binding rate α is expected to be proportional to the substrate concentration S . Noticing that the distribution of the conformation

coordinate C is different in the two states (free and bound), we expect the rates α and β to depend on this coordinate. The detailed balance condition takes the form $\alpha\rho_f(C) = \beta\rho_b(C)$, where ρ_f (resp. ρ_b) is the distribution of C knowing that the enzyme is in the free (resp. bound) state. Writing $\rho_f \propto e^{-U_f(C)/k_B T}$ and $\rho_b \propto e^{-U_b(C)/k_B T}$ where U_f and U_b are the effective potential corresponding to given conformations, we get

$$\frac{\alpha}{\beta} \propto \frac{S}{K} e^{-[U_b(C) - U_f(C)]/k_B T}, \quad (3-2)$$

where K_0 is the bare equilibrium constant. The transitions of the enzyme between two equilibrium states therefore modify the effective distribution of the conformational variable. Assuming that the binding and unbinding rates α and β are very large compared to the intrinsic timescales of the enzyme, one can establish the effective distribution of C as

$$p(C) \simeq \frac{1}{Z} \left[1 + \frac{S}{K} e^{-\frac{U_b(C) - U_f(C)}{k_B T}} \right] e^{-U_f(C)/k_B T}, \quad (3-3)$$

where Z is a normalization constant. It follows that the average of any conformation- dependent quantity $\Phi(C)$ can be written as

$$\langle \Phi \rangle = \langle \Phi \rangle_f + [\langle \Phi \rangle_b - \langle \Phi \rangle_f] \frac{S}{S+K}, \quad (3-4)$$

where the averages are defined using the corresponding Boltzmann weights, and where we define the equilibrium constant $K = K_0 \frac{\int dC e^{-U_f(C)/k_B T}}{\int dC e^{-U_b(C)/k_B T}}$. Within this picture, the relative diffusion enhancement writes

$$\frac{\Delta D}{D_0} = \frac{\langle \mu \rangle_b - \langle \mu \rangle_f}{\langle \mu \rangle_f} \frac{S}{S+K} \equiv A \frac{S}{S+K}, \quad (3-5)$$

This result shows that even if the catalytic step of the chemical cycle is neglected, in such a way that the modifications of the diffusion coefficient cannot be related to the rate of product formation, the relative change in diffusion still exhibits a Michaelis-Menten-like dependence over the substrate concentration, and is independent of the catalytic rate of the whole chemical reaction. The dimensionless coefficient A is a complex quantity, that depends on the shape of the interaction

potentials $U_f(C)$ and $U_b(C)$, and that includes contributions from all the internal degrees of freedom of the enzyme that are affected by binding and unbinding. This simple Equation 3-5, which contains the minimal ingredients of our new physical paradigm, can be used to fit the experimental data obtained for aldolase in the presence of the substrate FBP or in the presence of the competitive inhibitor PPI with A and K as free parameters. For the experiments with FBP, we find $A = 0.3$ and $K = 2.16 \cdot 10^{-5} \text{ M}$, which is comparable to the Michaelis constant reported for aldolase in the presence of FBP at physiological pH [13] ($1.28 \cdot 10^{-5} \text{ M}$), **Figure 2-6A**. In the presence of the inhibitor PPI **Figure 2-6B**, we find $A = 0.19$ and $K = 9.4 \cdot 10^{-6} \text{ M}$, the dissociation constant given in the literature being $4.6 \cdot 10^{-5} \text{ M}$ [21].

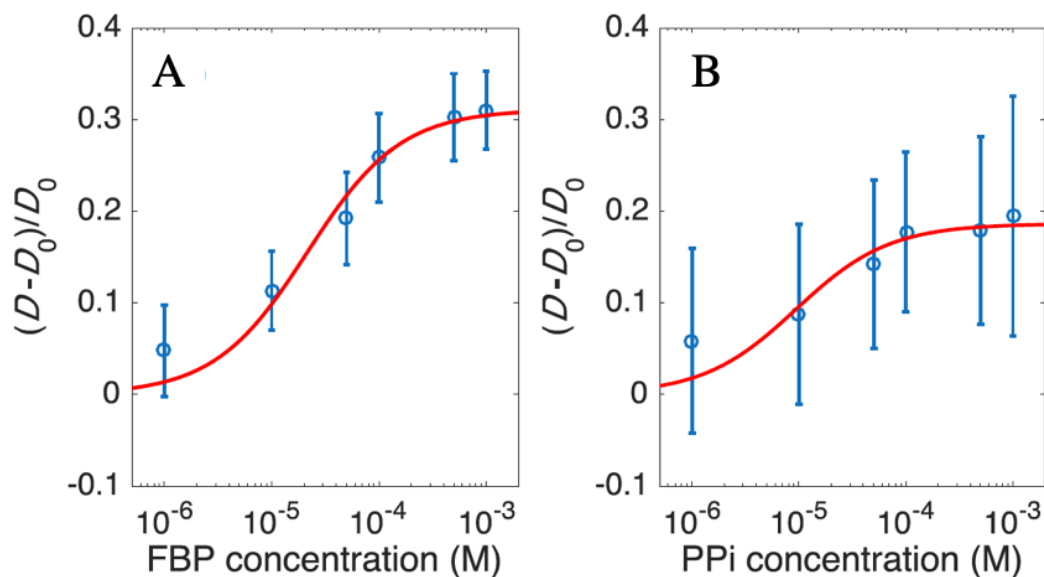


Figure 2-6. Relative increase of the diffusion coefficient of aldolase molecules measured in FCS experiments (symbols) in the presence of: **(A)** FBP as a substrate, **(B)** pyrophosphate (PPI) as a competitive inhibitor and compared to the fitting function (solid line), with A and K as free parameters. The relatively large error bars for the experiments performed with PPI originate from the error on the measurement of D_0 , which affects the standard deviation for the quantity $\Delta D = D - D_0$. Reprinted from *Nano Lett.* **2017**, 17 (7), 4415–4420. Copyright 2017.

In order to get a more quantitative description of the changes in the average mobility coefficients, we need to consider in greater details the modifications of the conformational fluctuations induced by binding and unbinding. The simplest way to describe the conformational state of the enzyme is to reduce the conformational state C to a single parameter R that describes the hydrodynamic radius of the enzyme. Structural studies of aldolase have recently shown that the effect of FBP binding was to bring residues near the active site closer one to another, therefore effectively reducing the hydrodynamic radius of the molecule. The mobility coefficient of the molecule goes as the inverse of the hydrodynamic radius, so that the contribution to A coming from this effective size reduction can be estimated as $A1 \sim |\delta R|/R$, in a way that deformations of the order of a few Å can have a significant impact on the measured diffusion coefficient. Then, in order to go further in the description of the internal degrees of freedom of the molecule and to take into account the effect of binding/unbinding on its elastic properties, we use a minimal dumbbell model (**Figure 2-5C**), where the structure of the enzyme is reduced to two hydrodynamically coupled subunits interacting via a harmonic potential that we recently studied in detail [22]. The conformational state C now reduces to a vector x that represents the elongation of the dumbbell. In the particular case where the dumbbell is symmetric, and in the limit where the subunits are far one from another, one can show that the averaged mobility coefficient is given by [22]

$$\langle \mu \rangle = \frac{1}{12\pi\eta} \left(\frac{1}{a_0} + \left\langle \frac{1}{x} \right\rangle \right), \quad (3-6)$$

where η is the viscosity of water, a_0 is the typical size of the subunits and x is the length of the dumbbell. Binding of a substrate molecule to the enzyme will generally hinder the fluctuations of internal degrees of freedom, and therefore make the protein stiffer. The contribution $A2$ to the dimensionless coefficient $[\langle \mu \rangle_b - \langle \mu \rangle_f] / \langle \mu \rangle_f$ can be calculated explicitly by assuming that the potential energies associated with the internal variable x are of the form $U_f = \frac{1}{2}k_f(x - a)^2$ and $U_b =$

$\frac{1}{2}k_b(x - a)^2$ with $k_b > k_f$ and where a is the typical size of the enzyme. In the limit of very large k_f and k_b with a finite difference $\delta k \equiv k_b - k_f$, we find $A_2 \propto \frac{k_B T}{k_f a^2} \frac{\delta k}{k_f}$ up to a dimensionless prefactor of order 1. The dimensionless number $\frac{k_B T}{k_f a^2}$ represents the relative amplitude of the length fluctuations of the dumbbell, and is bounded by unity, such that increased stiffness can significantly increase the enzyme diffusion coefficient. This contribution can be related to the concept of entropic allostery [22] which suggests that ligand binding to a macromolecule can change its vibrational entropy, in addition to affecting its static structure. Finally, this model can be refined by assuming that the subunits have more complex shapes and undergo orientational fluctuations (**Fig. 2-5C**). The conformation state of the enzyme is then described by the vector $C = (x, \hat{u}^1, \hat{u}^2)$ where \hat{u}^1 and \hat{u}^2 are unit vectors characterizing the orientations of the subunits. These additional degrees of freedom will affect the overall diffusion coefficient of the dumbbell. We recently employed a Fokker-Planck description of the stochastic dynamics of the dumbbell and a careful treatment of the coupling between the internal and external degrees of freedom induced by hydrodynamic interactions to show that the internal fluctuations can contribute negatively to the effective diffusion coefficient of the position of the dumbbell [23]. It is beyond the scope of this thesis to present the details of this calculation, and we simply give the following simplified and generic form for the effective diffusion coefficient:

$$D = D_{ave} - \delta D_{fluc}, \quad (3-7)$$

where the first term corresponds to the average contribution from the translational modes of the dumbbell, and the second term represents fluctuation-induced corrections arising from the internal degrees of freedom. The latter is controlled by the asymmetry of the dumbbell and the anisotropy of the individual subunits, and is typically a fraction of D_{ave} , depending on the precise geometrical properties of the dumbbell. Its negative sign is a generic feature of fluctuation-induced interactions

[24]. In particular, this analysis indicates how hindering the orientational fluctuations of freely-rotating parts of the molecule can enhance its overall diffusion. Therefore, these contributions, that originate from a reduction of the hydrodynamic radius of the enzyme, an increased stiffness, or hindering of the internal modes fluctuations of the enzyme can yield significant diffusion enhancements, which are of the order of a fraction of the bare diffusion coefficient of the enzyme. Although this extended dumbbell model is an idealized representation of the enzyme that greatly simplifies its structure, it contains, with very few internal degrees of freedom, the minimal ingredients to represent the compressional and orientational fluctuation modes that prevail inside a real macromolecule, and should therefore accurately predict the main features observed with FCS experiments.

2.4 Conclusion

In summary, by employing aldolase, a slow enzyme that catalyzes an endothermic reaction, we demonstrated experimentally that exothermicity is not a necessary condition for the observation of enhanced diffusion in the presence of substrate molecules. These results challenge previous physical scenarios that were proposed to account for this phenomenon. By exploring the diffusion of aldolase in the presence of reversible inhibitors and the diffusion of hexokinase in the absence of cofactors, where ligands only bind and unbind to the active sites of enzymes, it is demonstrated that periodical conformational changes significantly affect the mobility coefficient of enzymes. Guided by these experimental results and by structural studies of aldolase, we proposed a new physical paradigm, in which the enzyme stochastically switches between two equilibrium states, in which it is either free or bound. Using simple physical arguments and a more subtle analysis of the fluctuation-induced effects mediated by hydrodynamic interactions, we generically show how substrate binding can modify the mobility and eventually enhance the diffusion of the enzyme. While

we have obtained this result using the assumption that the binding and unbinding rates are considerably higher than the catalytic reaction rate, it is natural to expect that for faster enzymes these rates could be comparable, in which case we will obtain a combination of the above effect and the stochastic swimming that is controlled by the (fast) reaction rate. Finally, we emphasize the generality of this mechanism; since substrate binding-unbinding is universal for enzymes, the proposed mechanism for enhanced diffusion should be universally present for all enzymes and should be observable provided the changes in the conformational fluctuations are sufficiently large in relative terms. While our main aim has been to propose a new generic physical mechanism, more detailed studies of the molecular structure of the enzymes, for example using molecular dynamics simulation [25], could help determine the precise characteristics that would allow enhanced diffusion of enzymes upon substrate binding and unbinding.

2.5 Experimental Details

2.5.1 Fluorescent Labeling of HK and Ald

Hexokinase (from *Saccharomyces cerevisiae*, Sigma Aldrich) was tagged with Alexa Fluor 532 dye (ex/em: 532/ 553; Thermo Fisher Scientific) by using an Alexa Fluor 532 protein labeling kit. The number of dye molecules per HK enzyme molecule was ~ 0.4 , as quantified using UV-vis spectroscopy. All solutions for experiments were prepared in 50 mM HEPES, pH 7.4 buffer. Aldolase (from rabbit muscle; Sigma-Aldrich) was labeled with a thiol-reactive dye, Dylight 550 (ex/em: 562/576; Thermo Fisher Scientific). Labeling of Aldolase was carried out with four folds

excess of the fluorescent dye and 1 mM EDTA on a rotator at 4°C for 2–3 h in 50 mM HEPES buffer (pH 7.4). The number of dye molecules per Aldolase enzyme molecule was ~ 1 .

2.5.2. Diffusion Measurement using FCS

Autocorrelation curves were fit to Eq. (8) using Levenberg–Marquardt non-linear least squares regression algorithm with Origin software. Quality of the fitted curves was assessed based on chi-square (χ^2) values. Diffusion coefficients of the fluorescent tracers were measured in the presence of enzymatic catalysis using TCSPC instrumentation. Fluctuations in fluorescence intensity arising from the diffusion of the tracer particles were auto-correlated and fitted to a multi-component 3D diffusion model to determine their diffusion coefficient in solution. The experimental solutions were prepared in deionized water instead of phosphate buffer, since in the presence of free ions the tracer particles were found to agglomerate resulting in distortions in the recorded signal. Using the oscilloscope in the SPC-630 module from Becker and Hickl, the laser was focused to be within the solution, where multiple measurements were taken using the FIFO mode.

FCS was performed on a custom-built microscope based optical setup. Excitation light from a PicoTRAIN 532 nm, 80 MHz, 5.4 ps pulsed laser (High-Q Laser) was guided through an IX-71 microscope (Olympus), with an Olympus 60 \times /1.2-NA water-immersion objective. Emitted fluorescent light from the sample was passed through a dichroic beam splitter (Z520RDC-SP-POL, Chroma Technology) and focused onto a 50 μ m, 0.22-NA optical fiber (Thorlabs), which acted as a confocal pinhole. The signal from the photomultiplier tube was routed to a preamplifier (HFAC-26) and then to a time-correlated single-photon counting (TCSPC) board (SPC-630, Becker and Hickl). The sample was positioned with a high-resolution 3-D piezoelectric stage (NanoView, Mad City Laboratories). The measurements were performed with 26.5 μ W and 30.2 μ W excitation power for tagged enzyme and tracers, respectively, and the optical system was calibrated before each

experiment using free 50 nm fluorescent particles in double distilled water. Fluorescent molecules moving in and out of the diffraction-limited observation volume induce bursts in fluorescence collected in first-in, first-out (FIFO) mode by the TCSPC board, which was incorporated in the instrument. Fluctuations in fluorescence intensity from the diffusion of molecules were auto-correlated and fit by a multicomponent 3D model to determine the diffusion coefficients of individual species. The autocorrelation of the intensity signal is defined by Eq. (3-8).

$$G(\tau) = \sum_{i=1}^n \frac{1}{N_i} \left[1 + \left(\frac{\tau}{\tau_D^i} \right) \right]^{-1} \left[1 + \left(\frac{1}{w} \right)^2 \left(\frac{\tau}{\tau_D^i} \right) \right]^{-\frac{1}{2}} \quad (3-8)$$

Where
$$\tau_D^i = \frac{r^2}{4D_i} \quad (3-9)$$

Here, N_i is the average number of fluorophores of the i^{th} species in the observation volume, τ is the auto-correlation time, w is the structure factor, which is defined as the ratio of height to width of the illumination profile, and τ_D^i is the characteristic diffusion time of the i^{th} fluorescent particle with diffusion coefficient D_i crossing a circular area with radius r .

Table 2- 2 Typical Calibration parameters obtained in FCS experiments. *Nano Lett.* **2017**, 17 (7), 4415–4420. Copyright 2017.

Calibration				
τ_D (μs)	N	Confocal Radius/ nm	w (radius of confocal volume over its half height)	Chi Square
7138.25	0.89	505.8	7.5	0.00018
7648.94	0.85	523.58	8.35	0.00022

7741.99	0.91	526.76	10.42	0.00028
6676.06	1.05	489.15	6.03	0.00005
7244.59	1.11	509.55	5.65	0.00006
		Average: 510.97	Average: 7.59	Average: 0.00016

Table 2- 3 Typical Experiment parameters obtained in FCS experiments with FBP from 0 to 0.05 mM. *Nano Lett.* **2017**, *17* (7), 4415–4420. Copyright 2017.

Experiment								
FBP concentration	0 mM		0.001 mM		0.01 mM		0.05 mM	
	τD	N						
	1574.37	6.38	1569.76	7.3	1364.61	5.83	1304.24	7.19
	1608.66	5.38	1440.32	5.63	1348.07	5.19	1297.88	6.86
	1529.10	6.53	1443.54	6.12	1431.66	4.6	1236.82	8.13
	1552.88	5.18	1480.51	6.1	1379.26	5.5	1303.69	7.59
	1547.65	7.49	1489.36	7.06	1366.80	5.09	1299.18	11.5

we show typical values of τD obtained for tagged aldolase dispersed in different concentrations of FBP. Each experiment comprises of 5 independent measurements, carried out under identical conditions.

Table 2- 4 Typical Experiment parameters obtained in FCS with FBP from 0.1 mM to 1 mM. *Nano Lett.* **2017**, *17* (7), 4415–4420. Copyright 2017.

Experiment

FBP concentration	0.1 mM		0.5 mM		1 mM	
	τD	N	τD	N	τD	N
	1219.51	6.72	1167.97	8.1	1175.07	6.7
	1278.62	7.66	1200.14	4.89	1181.49	4.34
	1202.28	7.97	1166.14	4.21	1164.99	4.76
	1225.02	9	1186.99	6.21	1176.45	3.93
	1205.04	8.96	1194.38	5.3	1170.87	4.75

The quality of the fitted curves was assessed by chi-square (χ^2) analysis. Typical values of w and r obtained during one calibration (comprising of 5 independent measurements, carried out under identical conditions) is shown in **Table 2-2**. Next, fluctuations in fluorescence intensity arising from the diffusion of fluorescently tagged enzyme molecules within the confocal volume in the presence and absence of substrate FBP, were auto-correlated to Eq. 1 to determine the characteristic diffusion time, and thereby the translational diffusion constant D of the molecule, using the values of w and r measured during calibration, **Table 2-3&4**. The quality of the fitted curves was again assessed by chi-square (χ^2) analysis. **Figure 2-7** shows representative intensity fluctuation curves and corresponding autocorrelation fits obtained for fluorescently tagged aldolase dispersed in 0 mM and 0.1 mM FBP solutions respectively.

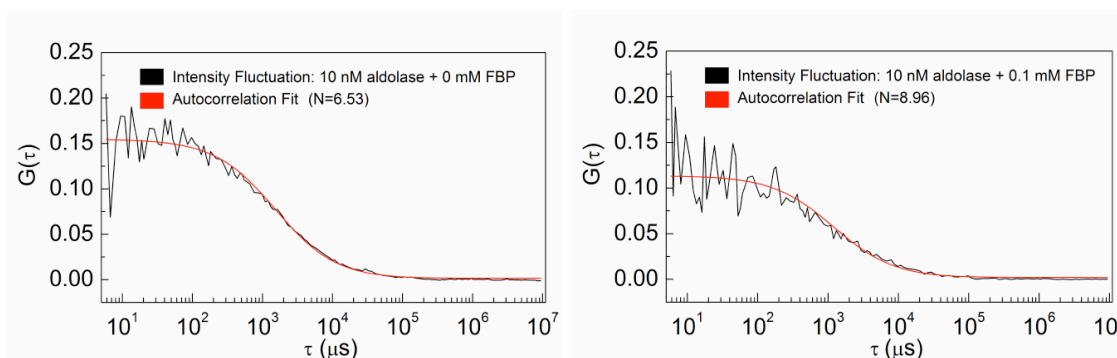


Figure 2-7. Representative intensity fluctuation curves and corresponding autocorrelation fits obtained for fluorescently tagged aldolase dispersed in 0 mM and 0.1 mM FBP solutions respectively. Reprinted from *Nano Lett.* **2017**, *17* (7), 4415–4420. Copyright 2017.

2.6 Acknowledgements

This work was supported by Penn State MRSEC funded by the National Science Foundation (DMR-1420620). Xi Zhao acknowledges Dr. Pierre Illien and Prof. Ramin Golestanian for theoretical calculations and modeling. The author thanks Prof. Peter J. Butler and Dr. Krishna Kanti Dey for assistance with enzyme diffusion measurement.

2.7 References

- [1] Butler, P. J.; Dey, K. K.; Sen, A. Impulsive Enzymes: A New Force in Mechanobiology *Cell Mol. Bioeng.*, **2015**, *8*(1), 106-118.
- [2] Muddana, H. S.; Sengupta, S.; Mallouk, T. E.; Sen, A.; Butler, P. J. Substrate Catalysis Enhances Single-Enzyme Diffusion. *J. Am. Chem. Soc.* **2010**, *132*, 2110–2111.
- [3] Sengupta, S.; Dey, K. K.; Muddana, H. S.; Tabouillot, T.; Ibele, M. E.; Butler, P. J.; Sen, A. Enzyme Molecules as Nanomotors. *J. Am. Chem. Soc.* **2013**, *135*, 1406–1414.
- [4] Sengupta, S.; Spiering, M. M.; Dey, K. K.; Duan, W.; Patra, D.; Butler, P. J.; Astumian, R. D.; Benkovic, S. J.; Sen, A. DNA Polymerase as Molecular Motor and Pump *ACS Nano* **2014**, *8*(3), 2410-2418.

- [5] Colberg, P.H.; Kapral, R. Angström-scale Chemically Powered Motors *Europhys. Lett.* **2014**, *106*, 30004.
- [6] Sakaue, T.; Kapral, R.; Mikhailov, A. S. Nanoscale Swimmers: Hydrodynamic Interactions and Propulsion of Molecular Machines *Eur. Phys. J. B* **2010**, *75*, 381-387.
- [7] Cressman, A.; Togashi, Y.; Mikhailov, A. S.; Kapral, R. Mesoscale Modeling of Molecular Machines: Cyclic Dynamics and Hydrodynamical Fluctuations *Phys. Rev. E* **2008**, *77*, 050901 (1-4).
- [8] Golestanian, R. Synthetic Mechanochemical Molecular Swimmer *Phys. Rev. Lett.* **2010**, *105*, 018103 (1-4).
- [9] Riedel, C.; Gabizon, R.; Wilson, C. A. M.; Hamadani, K.; Tsekouras, K.; Marqusee, S.; Pressé, S.; Bustamante, C. The Heat Released during Catalytic Turnover Enhances the Diffusion of an Enzyme. *Nature* **2015**, *517*, 227–230.
- [10] Golestanian, R. Enhanced Diffusion of Enzymes That Catalyze Exothermic Reactions. *Phys. Rev. Lett.* **2015**, *115*, 108102 (1-5).
- [11] Minakami, S.; de Verdier, C.-H. Calorimetric Study on Human Erythrocyte Glycolysis. *Eur. J. Biochem.* **1976**, *65*, 451-460.
- [12] Goldberg, R. N.; Tewari, Y. B. Thermodynamics of Enzyme-Catalyzed Reactions: Part 4. Lyases. *J. Phys. Chem. Ref. Data* **1995**, *24*, 1669-1698.
- [13] Callens, M.; Kuntz, D. A.; Opperdoes, F. R. Kinetic Properties of Fructose Bisphosphate Aldolase from *Trypanosoma Brucei* Compared to Aldolase from Rabbit Muscle and *Staphylococcus Aureus*. *Mol. Biochem. Parasitol.* **1991**, *47*, 1-10.
- [14] Rose, I. A.; O'Connell, E. L. Studies on the interaction of Aldolase with Substrate Analogues *J. Biol. Chem.* **1969**, *244*, 126–134.
- [15] Wu, F.; Pelster, L. N.; Minter, S. D. Krebs Cycle Metabolon Formation: Metabolite Concentration Gradient Enhanced Compartmentation of Sequential Enzymes *Chem. Commun.* **2015**, *51*, 1244–1247.
- [16] Fromm, H. J.; Zewe, V. Kinetic Studies of Yeast Hexokinase. *J Biol Chem* **1962**, *237*, 3027–3032.
- [17] Wilkinson, K. D.; Rose, I. A. Isotope Trapping Studies of Yeast Hexokinase during Steady State Catalysis. A Combined Rapid Quench and Isotope Trapping Technique. *J. Biol. Chem.* **1979**, *254* (24), 12567–12572.

- [18] Kuser, P. R.; Krauchenco, S.; Antunes, O. A. C.; Polikarpov, I. The High Resolution Crystal Structure of Yeast Hexokinase PII with the Correct Primary Sequence Provides New Insights into Its Mechanism of Action. *J. Biol. Chem.* **2000**, *275* (27), 20814–20821.
- [19] Einstein, A. Über die von der molekularkinetischen Theorie der Wärme geforderte Bewegung von in ruhenden Flüssigkeiten suspendierten Teilchen *Ann. Phys.* **1905**, *17*, 549.
- [20] Kubo, R. The Fluctuation-dissipation Theorem *Rep. Prog. Phys.* **1966**, *29*, 255.
- [21] Kasprzak, A. A.; Koch, M. Interaction of Fructose- 1,6-Bisphosphate Aldolase with Adenine Nucleotides *Eur. J. Biochem.* **1980**, *104*, 443–450.
- [22] Hawkins, R. J.; McLeish, T. C. B. Coarse-Grained Model of Entropic Allostery *Phys. Rev. Lett.* **2004**, *93*, 7–10.
- [23] Illien, P.; Adeleke-Larodo, T.; Golestanian, R. Diffusion of an Enzyme: The Role of Fluctuation-Induced Hydrodynamic Coupling, *Eur. Phys. Lett.* **2017**, *119*, 40002.
- [24] Kardar, M.; Golestanian, R. The “Friction” of Vacuum, and Other Fluctuation-Induced Forces *Rev. Mod. Phys.* **1999**, *71*, 1233–1245.
- [25] Echeverria, C.; Togashi, Y.; Mikhailov, A. S.; Kapral, R. A Mesoscopic Model for Protein Enzymatic Dynamics in Solution *Phys. Chem. Chem. Phys.* **2011**, *13*, 10527–10537.

Chapter 3

Enzyme Chemotaxis

A part of this chapter is an adapted reproduction from *Nat. Chem.* **2018**, *10* (3), 311–317. with permission from the Springer Nature Publishing Group.

3.1 Introduction

The interaction between enzymes in living cells is an area of active research. In many instances, enzymes that participate in reaction cascades have been shown to assemble into metabolons in response to the presence of the initial substrate to facilitate substrate channeling. Inspired by these biological cascade reactions, multicatalyst nanostructures have been fabricated to carry out efficient synthesis [1-6]. The mechanism for metabolon formation and substrate channeling for some cases involves stable protein/protein interactions [7-12]. In other cases, metabolon formation through reversible and/or post-translational modifications has been suggested, but such transient complexes have eluded isolation [13,14]. Recent work, however, shows both substrate concentration-dependent enhanced diffusion, as well as preferential migration of enzymes up the substrate gradient - an example of molecular chemotaxis [15-17]. Here we present evidence that suggests that enzymes along a metabolic pathway in which the product of one is the substrate for the next tend to associate through a process of sequential, directed chemotactic movement. Such a process may contribute to the formation of metabolons in living cells colocalized around mitochondria that serve as sources of the ATP cofactor [18].

3.2 Results and discussion

This experimental study applies microfluidic and fluorescence spectroscopy techniques to study the coordinated movement of hexokinase (HK) and aldolase (Ald), the first and fourth enzymes of the glycolysis cascade, which are connected by the intermediate enzymes phosphoglucose isomerase (Iso) and phosphofruktokinase (PFK), **Figure 3-1A**. In order to monitor the movement of HK and Ald by confocal microscopy, we fluorescently labeled them with distinct amine-reactive (ex/em: 493/518) and thiol-reactive (ex/em: 638/658) Dylight dyes, respectively. The use of different dyes enables simultaneous measurement of both enzymes in microfluidic experiments. For both HK and Ald, a linear relationship was observed between fluorescence intensity and concentration **Figure 3-2**. This allowed us to estimate the amount of enzyme that migrated into a specific substrate channel.

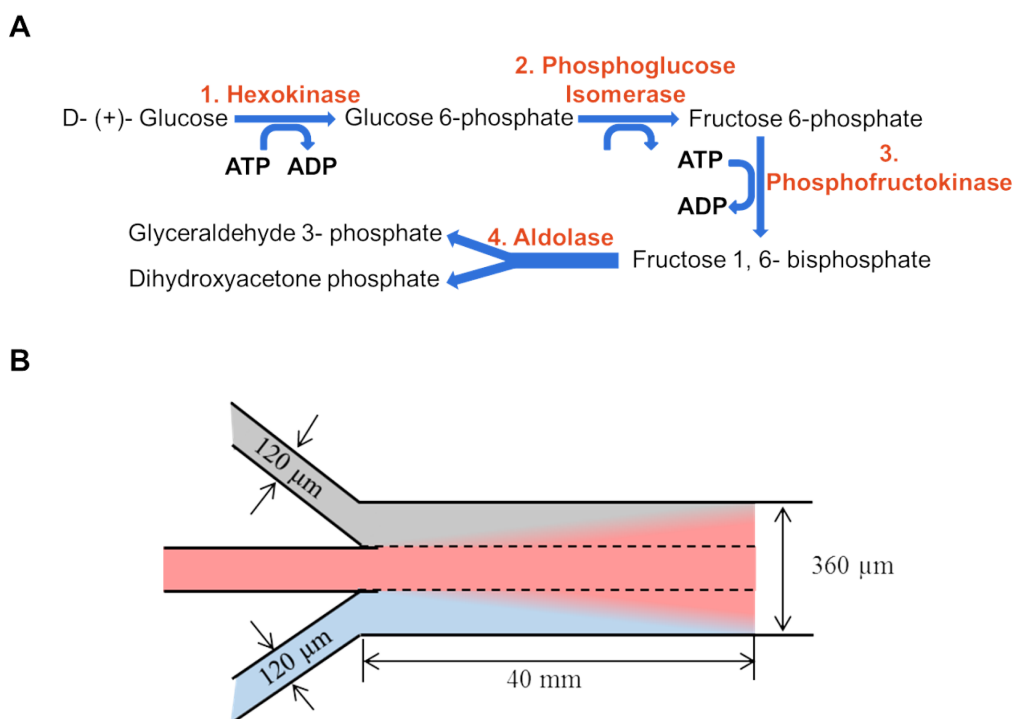


Figure 3-1. (A) The first four steps of glycolysis and their associated enzymes: hexokinase (HK), phosphoglucose isomerase (Iso), phosphofruktokinase (PFK), and aldolase (Ald). (B) Photo-lithographically fabricated flow-based microfluidic channel for studying enzyme chemotaxis. The channel is 40 mm in length, 360 μm in width, and 100 μm in depth. Due to laminar flow, the effective

width of each flow channel is 120 μm . Fluorescence intensities were analyzed along the black line shown in the figure, leaving off 20 μm next to the sidewalls. Reprinted from *Nat. Chem.* **2018**, *10* (3), 311–317. Copyright 2018.

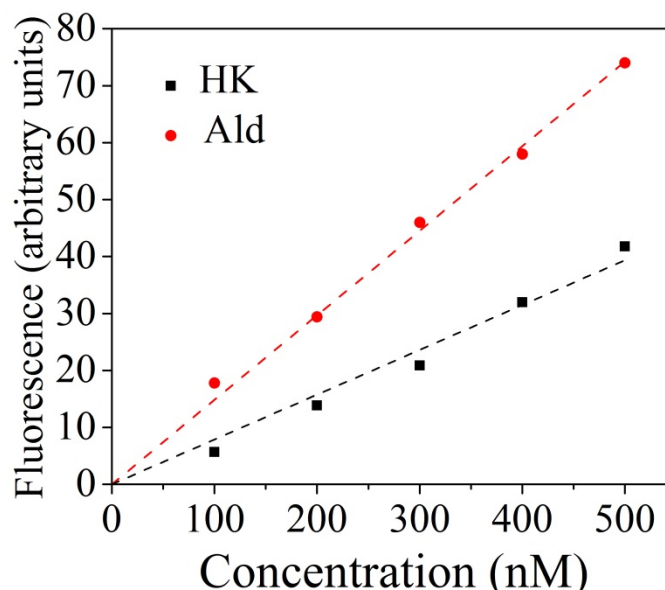


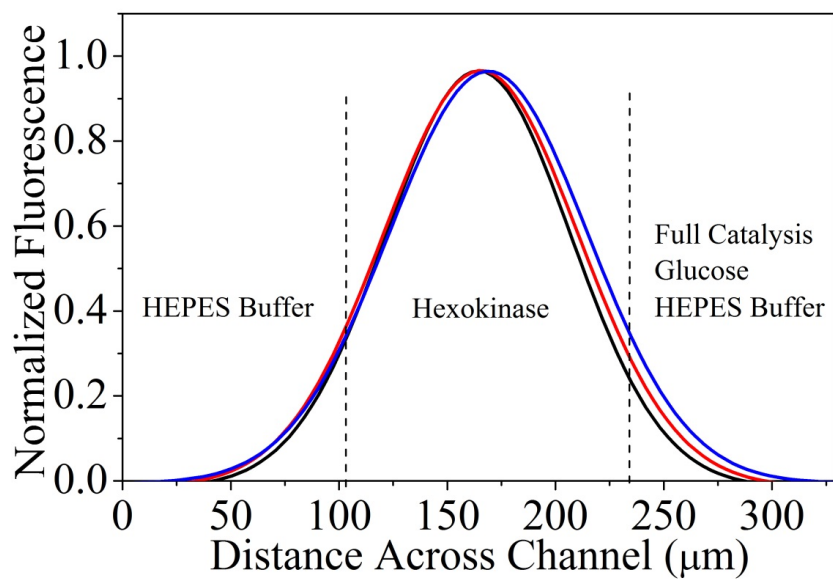
Figure 3-2. Linear relationships between fluorescence intensity (arbitrary units) and concentration for both HK and Ald. This enables directly correlating fluorescence intensity to the concentration of enzyme. Reprinted from *Nat. Chem.* **2018**, *10* (3), 311–317. Copyright 2018.

3.2.1 Hexokinase Chemotaxis

Hexokinase is an ATP dependent enzyme which can convert glucose to glucose- 6-phosphatase with Mg^{2+} as activator. When glucose binds to hexokinase, it induces a conformational change of the enzyme thus excluding water molecules and making the hydroxyl oxygen closer to the phosphate on ATP [20]. The structure of hexokinase can be refined as two lobes. Generally, the cleavage between to lobes remains open. When the enzymes bind to glucose, the two lobes will be in a closed state leading to a modified structure [21]. Hexokinase will only undergo a conformational

change by associating and disassociating to glucose when there is no ATP and Mg^{2+} to promote catalysis. The rates of association and disassociation are comparable [22]. We studied the chemotactic migration of hexokinase in the presence of an imposed gradient of substrate with and without catalysis. We used a flow-based three inlet- one outlet microfluidic channel for chemotaxis measurements as shown **Figure 3-1B**. The dimension of microfluidic channel was with 40 mm in length, 360 μm in width and 100 μm in depth. Measurements were performed under a confocal microscope setup where fluorescently labeled enzyme solution (1 μM) in 50 mM HEPES buffer was passed through the middle channel. Buffer was passed through one of the side channels continuously, while buffer solution, 1 mM glucose solution and 1 mM glucose with 1 mM ATP and 2 mM $MgCl_2$ solution was injected into the other, respectively. The flow rate was 50 $\mu\text{L/h}$ and maintained by syringe pump. At steady state, the spreading of the enzyme molecules within the glucose channel and full catalysis solution channel was recorded at 38 mm from the start of the microchannel and evaluated by measuring the fluorescent intensity profiles of the fluorescent enzyme molecules. The chemotactic migration is the difference between the distance hexokinase moved into substrate and buffer solution at the same observing position. (**Figure 3-3.**) To eliminate the background fluorescence of PDMS, the measurements were always performed on a middle plane along the depth direction and left with 15 μm from either ends close to the channel walls. As shown in **Figure 3-3**, hexokinase not only moves towards the channel containing both substrate and activator but also move towards the side with glucose only. The shift of hexokinase migrating into glucose channel was nearly 4 μm , while the shift into the full catalysis channel was around 11 μm . The results propose that catalysis is not the only reason for chemotactic shift. The conformational change of enzyme is very crucial to the collective behavior.

A



B

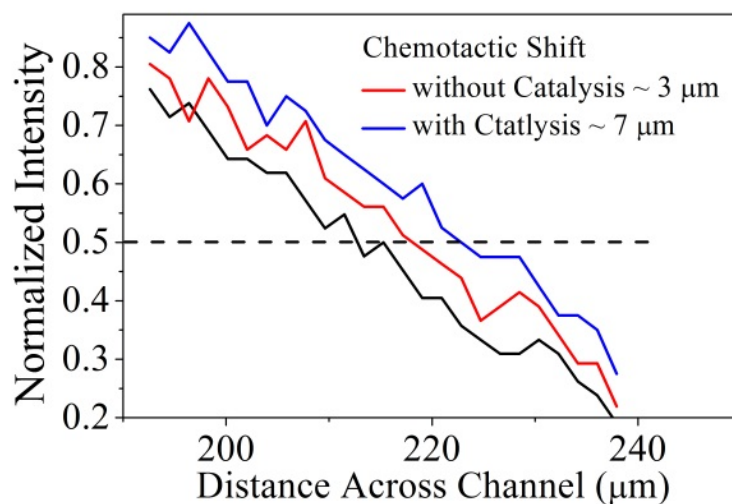


Figure 3-3. A) The chemotactic migrations of hexokinase within the channel with glucose only and within the channel with glucose, ATP and cofactor were measured at the end of microfluidic channel. The fluorescent intensity profile was smoothed by Gaussian fitting in Origin. B) an enlarged

portion of **Figure 3-3A**. When a gradient of only glucose was imposed, enzyme migrated more than in the buffer and slightly less than the migration observed during the full catalysis gradient.

To examine the chemotactic movement of enzymes in response to a substrate gradient, a three inlet and one outlet microfluidic flow device was fabricated through photolithography, **Figure 3-1B**. With known fluid flow rates and channel geometries, the distance from the input points to the measurement line can be converted into the time available for the enzymes to react and diffuse, **Table 3-1**.

Table 3- 1 Distance from the start of the microfluidic channel converted into time spent inside the channel for specified channel geometry. Reprinted from *Nat. Chem.* **2018**, *10* (3), 311–317. Copyright 2018.

Flow rate	Length	Interaction
($\mu\text{L/h}$)	(mm)	Time (s)
50	10	8.6
	20	17.3
	30	25.9
	40	34.6
30	10	14.4
	20	28.8
	30	43.2
	40	57.6

As a control experiment, HK (200 nM), D-glucose (50 mM) and $MgCl_2$ (100 mM) were passed through all three channels. Then, the solution in the central channel was changed to HK (200 nM), D-glucose (50 mM), $MgCl_2$ (100 mM), and ATP (50 mM). 150 mM NaCl was added into the two flanking channels to balance the ionic strength of the ATP disodium salt added to the center channel. As shown in **Figure 3-4**, we observed significant enzyme “focusing” in the central channel following an interaction time of 34.6 s in the microchannel, compared to when ATP was absent. The total fluorescence intensity in all the experiments was normalized to 1 for comparison and representation on a common scale. We repeated the experiment substituting mannose, another substrate with higher binding affinity to hexokinase, and found that the enzyme focused less than in the presence of D-glucose. We also repeated the experiment substituting L-glucose, the enantiomer of D-glucose but is not a substrate of hexokinase, and we observed no focusing. Similarly, the substitution of ATP by its analog, adenosine 5'-(β,γ -methylene) triphosphate (AMP-PCP) at the same concentration, in the central channel resulted in no focusing. Note that both ATP and AMP-PCP bind to HK but that the latter cannot turnover and phosphorylate glucose [23].

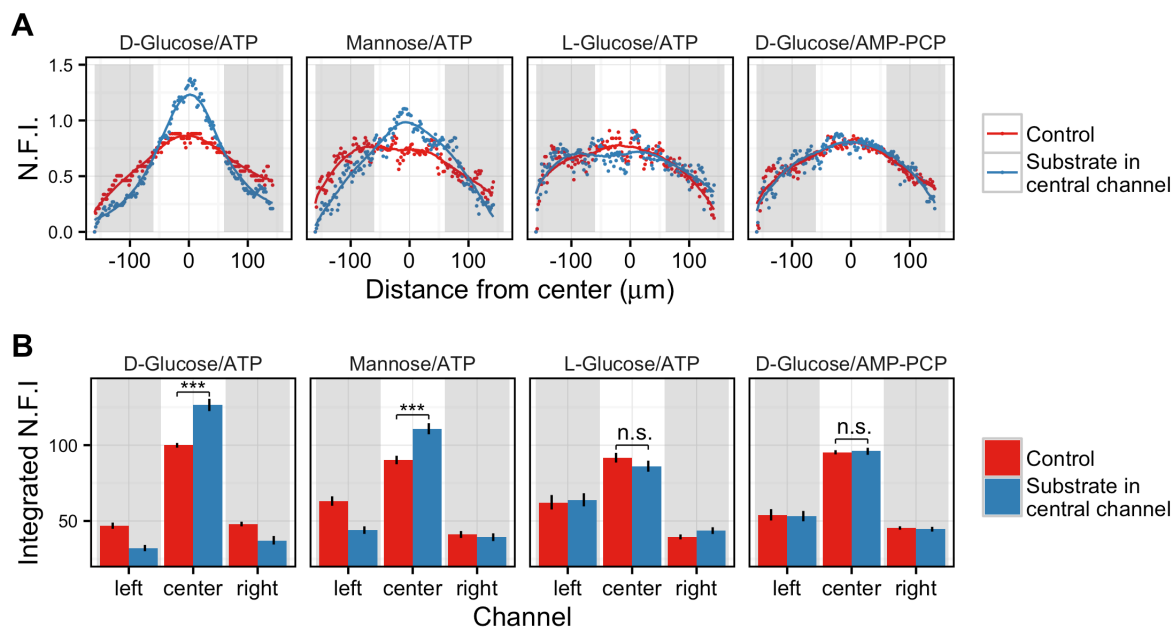


Figure 3-4. Catalysis induced enzyme focusing. A starting equilibrium distribution of HK (200 nM), D-glucose (50 mM), and MgCl₂ (100 mM) shows focusing towards the middle channel when ATP (50 mM) is introduced into it. Note that catalysis does not occur in the absence of ATP (control). Experimental conditions: Flow rate, 30 μ l/h; distance, 38 mm; interaction time, 55 s. The general concave shape of the curves is indicative of the wall effect. **(A)** N.F.I. (Normalized fluorescence intensity) as a function of distance from the center of the channel. Fluorescence intensities are normalized across all channels such that the total fluorescence intensity across all channels is fixed for all experiments, and rescaled such that the central channel for the D-Glucose control experiment sums to 100. Side channels are shaded in gray. Data points are locally fitted to a second degree polynomial. **(B)** Integrated N.F.I. per channel. Error bars are 95% confidence intervals obtained from 500 bootstrap iterations of the fitting process. A pairwise t-test with Holm adjustment was conducted to test for significant differences in the intensities across channels. ***: $p < 0.001$, n.s.: not significant. Reprinted from *Nat. Chem.* **2018**, *10* (3), 311–317. Copyright 2018.

As expected, the extent of focusing for D-glucose decreased under otherwise identical conditions when the interaction time in the middle channel was reduced, **Figure 3-5**.

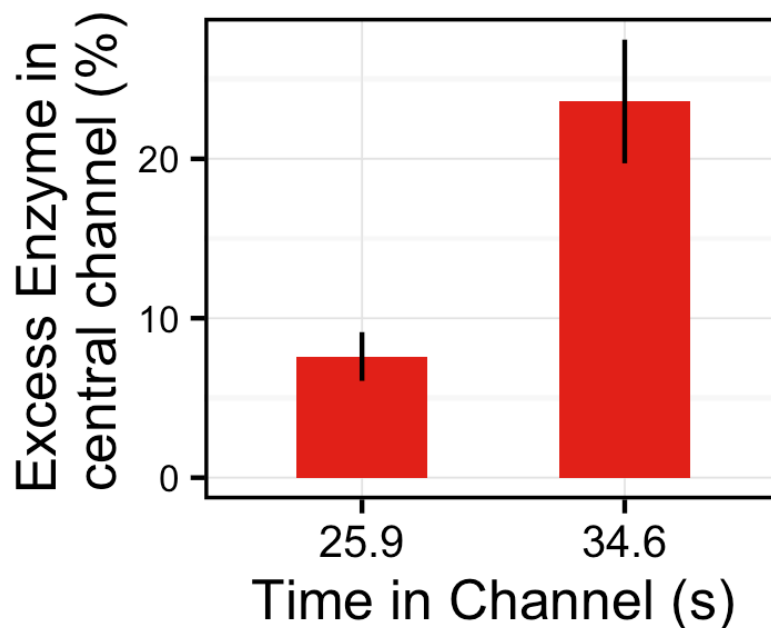


Figure 3-5. Catalysis induced enzyme focusing as a function of interaction time in the microchannel. A starting equilibrium distribution of HK (200 nM), D-glucose (50 mM), and MgCl₂ (100 mM) shows focusing towards the middle channel when ATP (50 mM) is introduced into it. Percent Excess enzyme in the middle channel = amount of enzyme in the middle channel in the experiment minus

the amount of enzyme in the middle channel in the control (no ATP) divided by the total amount of enzyme in all three channels. The error bar represents the standard deviation of three identical measurements. Reprinted from *Nat. Chem.* **2018**, *10* (3), 311–317. Copyright 2018.

3.2.2 Aldolase Chemotaxis

We also investigated the chemotactic migration of aldolase in the presence of an imposed substrate, FBP, concentration gradient. Measurements were performed under a confocal microscope setup where fluorescently labelled enzyme solution (1 μM) in 50 mM HEPES buffer was allowed to pass through the middle inlet at a flow speed of 50 $\mu\text{L}/\text{h}$ using a syringe pump. Through one of the side channels a solution of only buffer was injected and through the other a buffered solution of 10 mM FBP solution were allowed to flow through at the same speed. At steady state, the chemotactic spreading of the enzyme molecules within the substrate channel was estimated by measuring the fluorescence intensity profile of the molecules at specific positions along the length of the microchannel and comparing them with their diffusive spread within the buffer channel at the same positions. The fluorescence intensity was always measured across the channel width, leaving approximately 15 μm from either ends close to the channel walls. This was done to minimize the effect of background fluorescence of the PDMS wall on the recorded signal.

The chemotactic migration of aldolase within the substrate side were measured at 38 mm from the start of the microchannel. We measured a shift of (5.61 ± 0.51) μm in fluorescent intensity profile at this position when the substrate concentration at the inlet was 10 mM. As can be expected, the magnitude of the chemotactic shift depends on not only the strength of the substrate gradient but also on the duration of enzyme-substrate *interaction time* during the measurement, **Figure 3-6A**. For laminar flows of liquid under steady state conditions, different positions along the length of the microchannel will correspond to different interaction times for the enzyme molecules with the

imposed substrate concentration gradients. This allows us to correlate the chemotactic shift with the duration of the substrate-particle interaction. **Figure 3-6B** shows the magnitude of aldolase chemotaxis as a function of the interaction time with the substrate. This demonstrates that the extent of chemotactic migration can be controlled by changing substrate-particle interaction times in solution. As hypothesized previously, aldolase chemotaxis can still result from an enhanced diffusion mechanism although reaction enthalpy does not seem to play any role in the overall process.

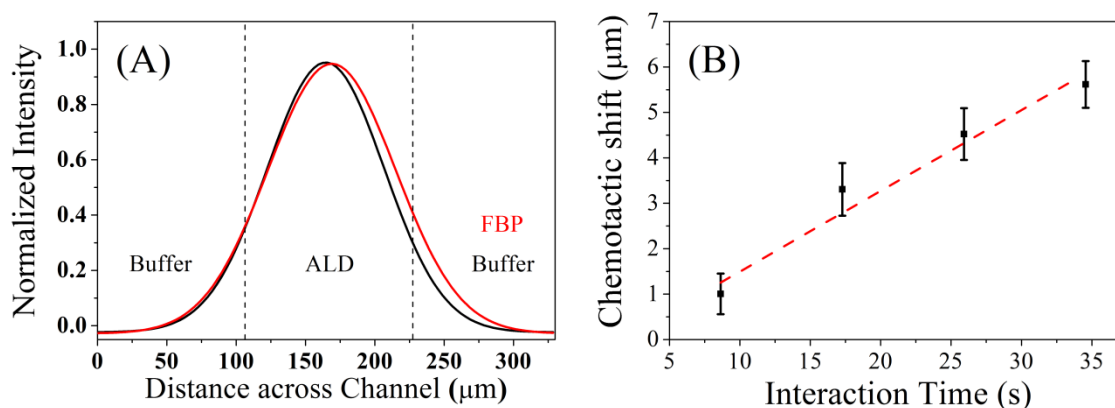
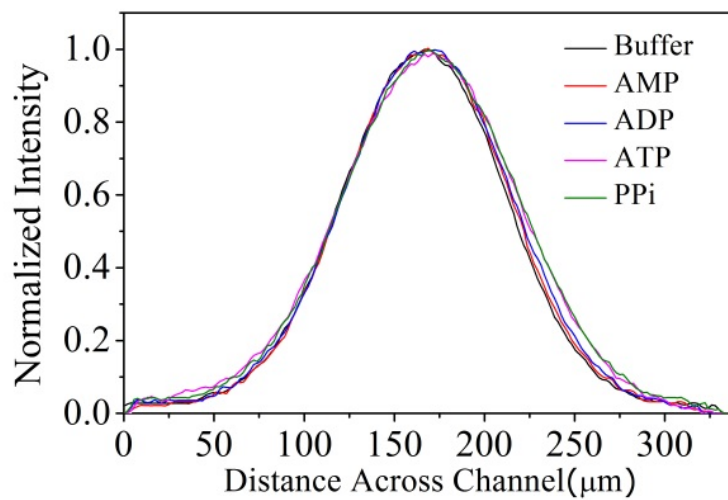


Figure 3-6. (A) Chemotactic migration of aldolase within the substrate side, measured at 38 mm from the start of the microchannel. We measured a shift of (5.61 ± 0.51) μm in fluorescent intensity profile at this position when the FBP concentration at the inlet was 10 mM. The intensity profiles were smoothed by B-spline fitting in Origin. (B) Magnitude of aldolase chemotaxis as a function of the interaction time with the substrate. The errors bars represent standard deviations calculated for three independent measurements carried out under identical conditions.

The collective behavior of aldolase was also observed in the gradient of competitive inhibitor, **Figure 3-6**. In the presence of competitive inhibitors alone, PPI, AAMP, ADP, ATP [24] only binds and unbinds to the active sites, the same place where FBP binds to aldolase. Enzymes shows more chemotactic movement towards PPI (around 7.5 μm) which has higher affinity of binding aldolase, compared to chemotactic shift towards lower affinitive inhibitor AMP (around 3.7 μm).

A



B

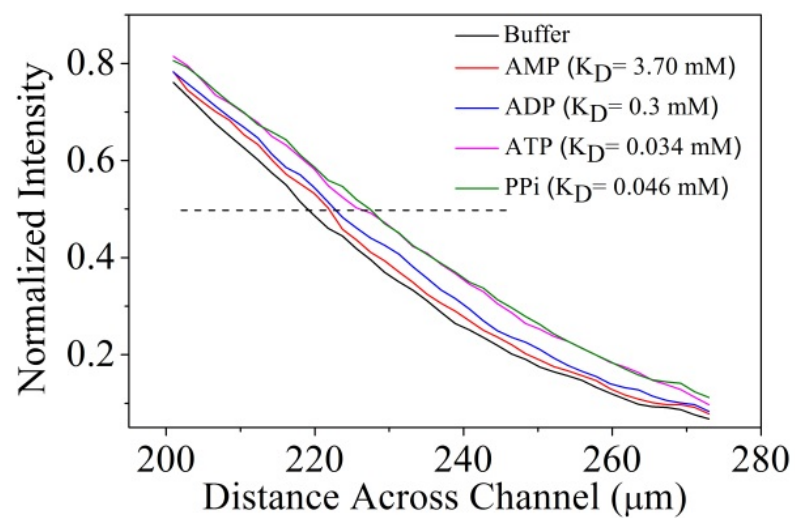


Figure 3-7. Aldolase migrated more towards where it changes conformations. The easier it is to bind with the inhibitor (with lower disassociation constant), the more chemotactic shift aldolase shows.

3.2.3 Chemotaxis as a Factor in Metabolon Formation

Having demonstrated that HK undergoes chemotaxis up its substrate gradient, we then probed the chemotactic behavior of the entire four-enzyme cascade. The first experiment was designed to examine the response of Ald towards its substrate, fructose 1,6-bisphosphate, generated from D-glucose by the successive actions of the first three enzymes. In the microfluidic device, the Ald was flowed through the middle channel. The first three enzymes, HK, Iso and PFK, with Mg^{2+} and ATP (required by the kinases) were passed through one of the flanking channels along with 10 mM D-glucose, while buffer was passed through the flanking channel on the opposite side. The volumetric flow rate per inlet was fixed at 50 $\mu\text{L}/\text{h}$ allowing for a total interaction time of 17.3 seconds in a 20 mm long channel. $11.9 \pm 3.0\%$ of the Ald moved into the channel where its substrate was being formed *in situ* (**Figure 3-8**).

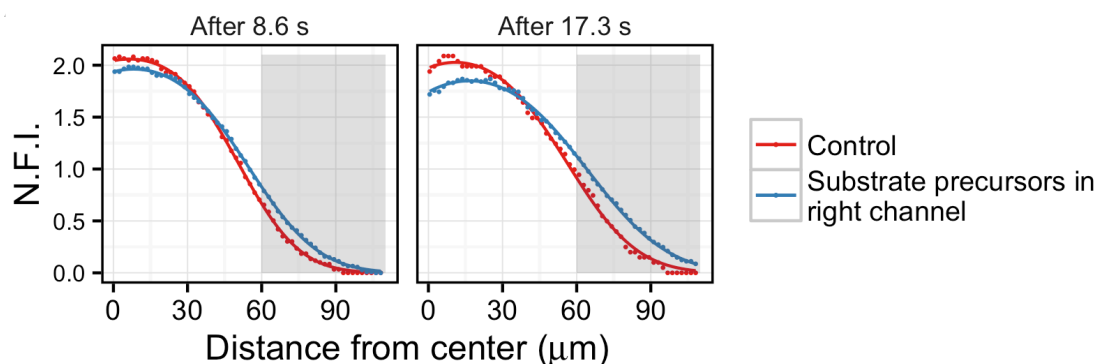


Figure 3-8. Fluorescence intensity measured across the channels are plotted against the width of the channels for center and right channels. The grey background represents the approximate right channel. When compared to the movement of Ald towards buffer, the enzyme shows enhanced migration into the channel that generates Fructose-1,6- bisphosphate *in situ*. Reprinted from *Nat. Chem.* **2018**, *10* (3), 311–317. Copyright 2018.

When the interaction time was reduced to 8.6 s, the chemotactic migration correspondingly reduced to 4.9 ± 2.4 % of the Ald. As expected, HK did not show any excess movement into the adjoining channel as compared with HK moving into a channel with buffer (**Figure 3-9A**). Additional control experiments were performed by removing either enzyme 2: Iso, enzyme 3: PFK, or D-glucose from the channel containing HK, Mg^{2+} and ATP. In each case, Ald showed no discernible chemotactic movement (**Figure 3-9B**). We then sought to examine whether there was a sequential spreading of HK and Ald when exposed to D-glucose. This is expected since D-glucose is the immediate substrate for HK, while the substrate for Ald, fructose 1,6-bisphosphate, is only formed from D-glucose through three successive enzymatic steps.

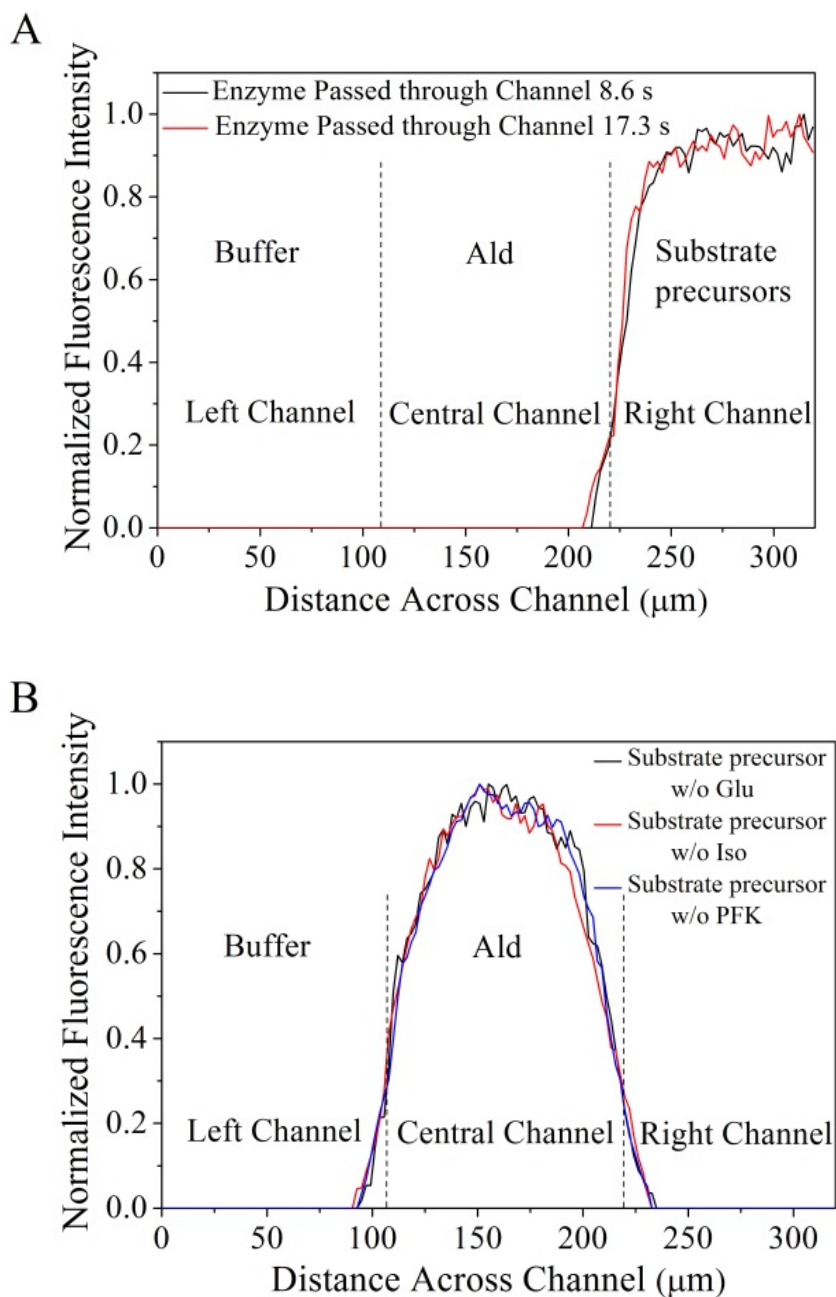


Figure 3-9. (A) While Ald chemotaxes towards its substrate gradient, HK flowing along with its substrate in its own channel shows no movement into the adjacent channel. (B) Control experiments performed for studying the chemotactic response of Ald towards its substrate precursors. Ald shows no movement towards the channel containing an incomplete mixture of the enzyme cascade. Reprinted from *Nat. Chem.* **2018**, *10* (3), 311–317. Copyright 2018.

The components of the cascade were now separated into two batches consisting of the first two and the last two enzymes, respectively. HK, ATP, Mg²⁺, and Iso were flowed through one flanking channel, while PFK, ATP, Mg²⁺, and Ald were flowed through the other flanking channel. A solution of D-glucose was passed through the middle channel. The flow rate was reduced to 30 μL/h and the channel length was increased to 40 mm allowing for a total interaction time of 57.6 s within the channel. An examination of the enzyme reaction rates confirmed that the time available within the microchannel was sufficient for the entire cascade of reactions to occur (**Figure 3-10**).

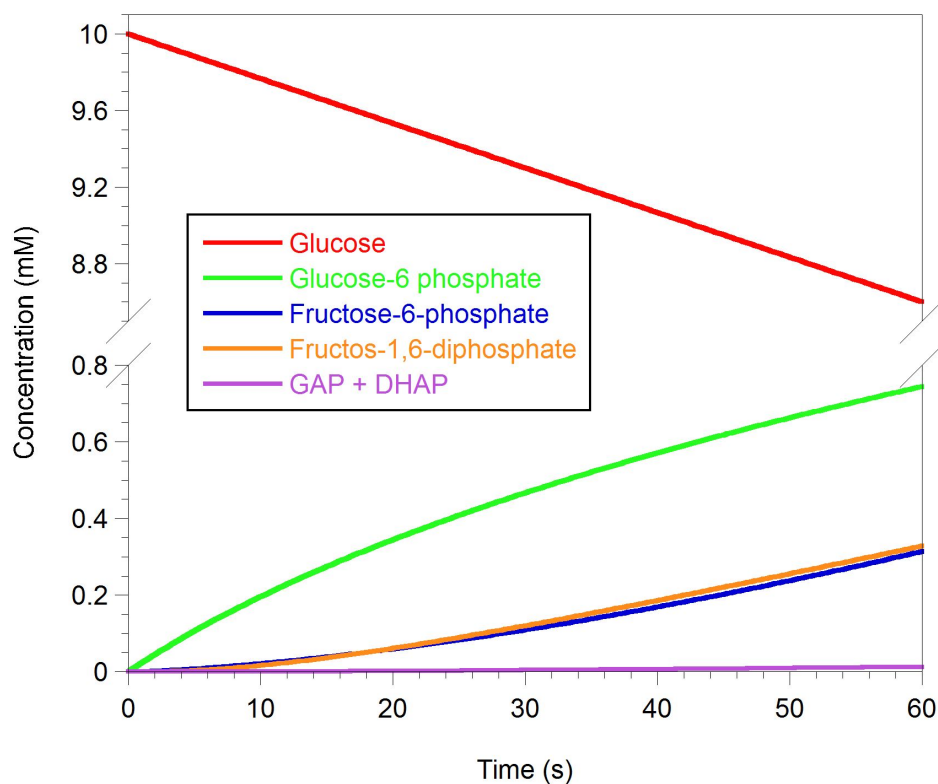
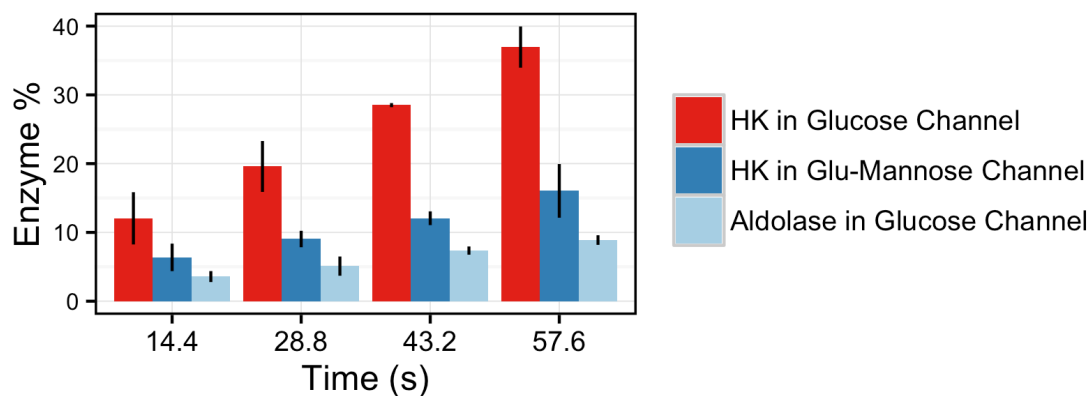


Figure 3-10 The simulated substrate and product progression curves through the first four enzymes in the glycolytic cascade. Reprinted from *Nat. Chem.* **2018**, *10* (3), 311–317. Copyright 2018.

As discussed, we hypothesized that HK should respond first to its substrate gradient by moving into the D-glucose channel, thereby producing the substrate for enzyme 2, Iso. The cascade would continue with PFK participation, finally producing fructose 1,6-bisphosphate that, in turn, should prompt Ald to chemotax towards the central channel. The fluorescence profiles for enzymes HK and Ald were noted at different interaction times, 14.4 s, 28.8 s, 43.2 s and 57.6 s, and their chemotactic behavior is summarized in **Figure 3-11A** and **Table 3-2**. For HK, our results indicate that, in 58 s, $37.0 \pm 0.3\%$ of the starting 200 nM enzyme moves into the central channel containing D-glucose (10 mM) compared to $6.7 \pm 1.3\%$ of the enzyme moving into the same channel when flowing only buffer. The corresponding numbers for Ald are $8.9 \pm 0.7\%$ and $5.9 \pm 1.0\%$, respectively. Thus, a sequential movement of HK, followed by Ald towards the central channel was observed.

A



B

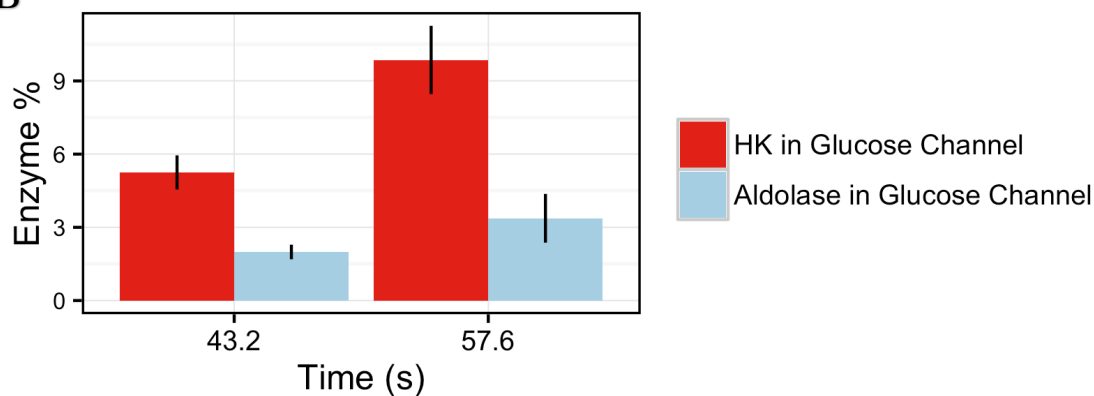


Figure 3-11 (A) Ald shows a chemotactic response compared to HK as expected based on the sequence of reactions. When 10 mM mannose is introduced along with 10 mM D-glucose, HK shows a reduced chemotaxis corresponding to the slower rate of mannose phosphorylation by HK. **(B)** D-glucose gradient-driven sequential movement of HK and Ald for the entire enzymatic reaction cascade was also observed in the presence of Ficoll PM 70 (20% w/v), an induced crowded environment mimicking cytosolic crowding conditions in a cell. Ald (blue bars) shows a chemotactic migration towards substrate channel compared to HK (red bars) corresponding to the cascade reaction sequence. Reprinted from *Nat. Chem.* **2018**, *10* (3), 311–317. Copyright 2018.

Table 3- 2 Amount of enzyme (HK or Ald) migrated into the central channel (containing either buffer only or 10 mM D-glucose and buffer) at specified time periods (see Figure 6B). The starting concentration of both enzymes is 200 nM. Reprinted from *Nat. Chem.* **2018**, *10* (3), 311–317. Copyright 2018.

Enzyme	Time (s)	Enzyme in buffer	Enzyme in glucose
		only channel (% of 200 nM)	+ buffer channel (% of 200 nM)
HK	14.4	2.6 ± 0.7	12.1 ± 3.8
	28.8	3.8 ± 1.6	19.6 ± 3.7
	43.2	5.0 ± 0.4	28.5 ± 0.3
	57.6	6.7 ± 1.3	37.0 ± 3.0
Ald	14.4	2.9 ± 0.4	3.6 ± 0.8
	28.8	3.4 ± 1.0	5.1 ± 1.4
	43.2	5.0 ± 2.0	7.4 ± 0.6
	57.6	5.9 ± 1.0	8.9 ± 0.7

Finally, in order to replicate the cytosolic crowding conditions that enzymes encounter in cells due to the presence of other macromolecules, we added 20% w/v Ficoll PM 70 to our experiments involving the entire cascade. Ficoll PM 70 is a highly branched polysaccharide polymer that serves as a synthetic crowding agent by affecting the fluidic properties of the solution, such as increasing the viscosity and osmolality [25]. As shown in **Figure 3-11B**, the presence of the crowding agent slows down but does not stop the chemotactic movement of the enzymes.

3.2.4 Chemotactic Co-localization of Hexokinase and Aldolase

With the same crowding conditions and enzymes used in the microfluidic experiments, we also observed the co-localization of HK and Ald (metabolon formation) in a sealed hybridization chamber starting with a uniform distribution of all the four enzymes in the cascade, as well as the substrates for HK (**Figure 3-12**).

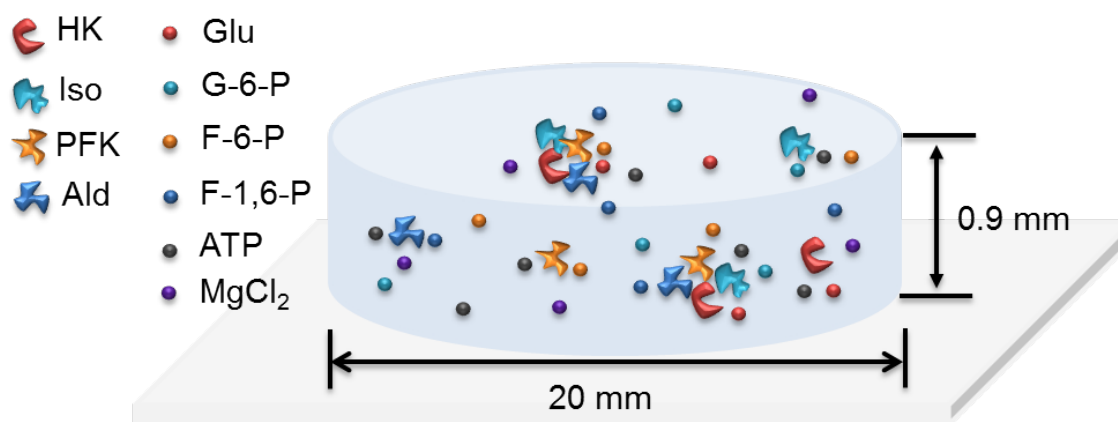


Figure 3-12. HK, Iso, PFK, Ald, D-glucose, MgCl₂ and ATP were mixed and injected into a sealed hybridization chamber. The depth of the chamber is 0.9 mm and the diameter of the chamber well is 20 mm. Conditions; 200 nM HK labeled with amine-reactive (ex/em: 493/518) Dylight dye, 200 nM Iso, 200 nM FPK, 200 nM Ald conjugated with thiol-reactive (ex/em: 638/658) Dylight dye, 10 mM

ATP, 20 mM MgCl₂, and 10 mM D-glucose in 20% w/v 70 M Ficoll was mixed and injected into a hybridization chamber, which was sealed on the surface of a glass slide. Controls were also performed either with D-glucose but no Iso and PFK present, or substituting D-glucose with L-glucose, or no glucose. Reprinted from *Nat. Chem.* **2018**, *10* (3), 311–317. Copyright 2018

In the presence of D-glucose and ATP, both the fluorescently labeled HK and Ald form bright moving spots. When the spots (with diameters ranging from 600 to 1000 nm) of HK and Ald were tracked, the trajectories of the two enzymes were found to be highly correlated, suggesting metabolon assembly during enzyme cascade reactions (**Figure 3-13**, **Table 3-3**). Similar experiments were also performed either with D-glucose but no Iso and PFK present, or substituting D-glucose with L-glucose, or with no glucose. As shown in **Table 3-3**, there were far fewer HK spots and fewer Ald trajectories that correlated with HK trajectories.

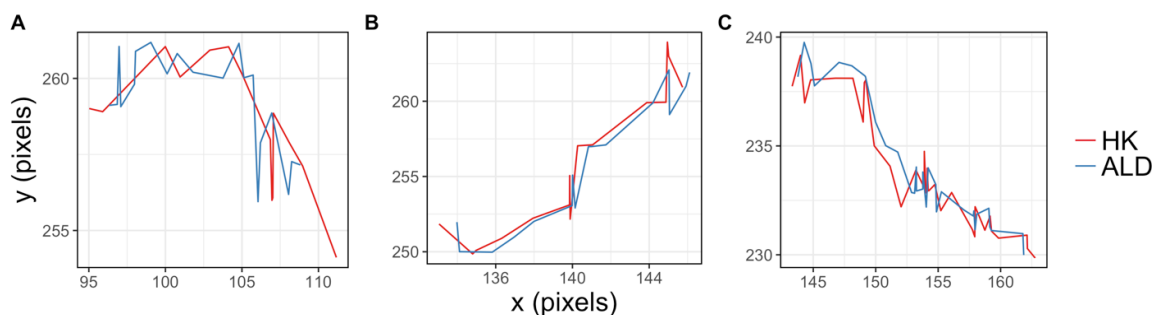


Figure 3-13. HK trajectories from three separate experiments in which D-glucose was present for which the corresponding Ald trajectory was highly correlated. Experimental conditions: 200 nM HK labeled with amine-reactive (ex/em: 493/518) Dylight dye, 200 nM Iso, 200 nM FPK, 200 nM Ald conjugated with thiol-reactive (ex/em: 638/658) Dylight dye, 10 mM ATP, 20 mM MgCl₂, and 10 mM D-glucose in 20% w/v 70 M Ficoll mixed and injected into a sealed hybridization chamber (Scheme S1). A pixel is 0.46×0.46 μm and the frame rate is 1 frame every 1.29 s. The trajectories are recorded for 10 frames, ~13 s. Reprinted from *Nat. Chem.* **2018**, *10* (3), 311–317. Copyright 2018.

Table 3- 3 Total number of detected hexokinase (HK) trajectories and total number of HK trajectories found to be correlated with an aldolase (Ald) trajectory (correlation >95%). Reprinted from *Nat. Chem.* **2018**, *10* (3), 311–317. Copyright 2018.

Experiment	Total HK trajectories	HK trajectories with high Ald correlation
D-Glucose (8 experiments)	48 ± 4	32 ± 3
D-Glucose without added Iso and PFK (3 experiments)	12 ± 4	5 ± 2
L-Glucose (3 experiments)	1	0
No Glucose (2 experiments)	1	0

3.3 Numerical Results Summary

We propose that the chemotactic aggregation of enzymes in regions of high substrate concentrations is due to cross-diffusion effects [26]. The substrate gradient-induced aggregation by cross-diffusion counteracts Fickian diffusion of enzymes, which transfers enzymes from regions with high enzyme concentration to regions with low enzyme concentration. Cross-diffusion is different from the enhanced diffusion of an enzyme in the presence of its substrate [15,16, 27, 28], which is also observed for uniform substrate concentrations and accelerates the equilibration of the enzyme concentration by Fickian diffusion.

Enzyme focusing can be theoretically described by “cross-diffusion” or “diffusiophoresis”: in a multicomponent system, the flow of one species is not only proportional to its concentration gradient (Fick’s law), but also to the concentration gradient of other species in solution. The diffusive flow for the concentration c_e of unbound enzyme E in the presence of its substrate S can then be written as:

$$J_e = -D\nabla c_e - D_{XD}\nabla c_s \quad (3-1)$$

where D is the Fick's law diffusion coefficient, D_{XD} is the “cross-diffusion” coefficient, and ∇c_e and ∇c_s are gradients in enzyme and substrate concentrations, respectively. “Cross-diffusive” effects have been experimentally measured in ternary reaction-diffusion systems [26], protein-electrolyte solutions [23], protein-polymer solutions [29], and in many other systems [30]. We followed the theory of chemotaxis originating from short-range ligand binding proposed by Schurr et al. [31] to obtain the cross diffusion coefficient, D_{XD} , as a function of the local substrate concentration, c_s , the diffusion coefficient, D , computed from the Einstein relation ($70 \mu\text{m}^2/\text{s}$ for the HK-glucose complex), and the equilibrium constant K of ATP binding to the enzyme ($5 \times 10^3 \text{ M}^{-1}$ for the binding of ATP to HK-glucose [32]):

$$D_{XD} = -Dc_e \frac{K}{1+Kc_s} \quad (3-2)$$

Inserting Equation (3-2) into Equation (3-1) shows the factors driving cross diffusion flow:

$$J_e = -D(\nabla c_e - c_e \frac{K}{1+Kc_s} \nabla c_s) \quad (3-3)$$

The first term inside the parenthesis is traditional diffusion towards lower concentrations of enzyme. The second term's sign is opposite, showing that this flow is towards *higher* concentration of substrate. In addition to the substrate gradient, this term's magnitude is determined by three factors: the diffusion coefficient D , the enzyme concentration c_e , and a factor proportional to the fraction of binding sites occupied by substrate at a given time. As with Fickian diffusion, the cross-diffusion drift arises from a thermodynamic driving force that lowers the chemical potential of the system due to favorable enzyme-substrate binding.

The system of partial differential equations corresponding to the HK-glucose catalysis reaction diffusion system has been solved numerically (see Appendix). The initial presence of ATP

in the central channel gives rise to strong ATP gradients at the boundaries between the central channel and the left and right channels. D-Glucose, present in all channels, converts HK to the HK-DG complex, which is the cross-diffusing entity described by Eq. (3-3). Without any adjustable parameters and without accounting for catalysis-induced enhanced diffusion, the model predicts focusing lower than that seen in experiments, but of the same direction and order of magnitude (**Figure 3-14**). Thus, hexokinase will chemotax up an ATP gradient due to the cross-diffusion phenomenon. One reason for the difference between experiment and theory is enhanced diffusion of the enzymes in the presence of catalysis; increased D will increase the amount of focusing, as predicted by the model. However, since there is no established theoretical framework for the determination of D as a function of position across the microfluidic channel, we have not included it in our model. We also modeled the focusing experiment in the presence of the non-hydrolyzable ATP analog, AMP-PCP, and found that the model predicts reduced focusing compared to the ATP-induced focusing (around 1% increase in the concentration in the central channel; see Appendix for details). The significantly stronger binding of AMP-PCP reduces the concentration (c_e) of unbound enzyme [33], and thereby the cross-diffusion effect. This suggests that the model is also compatible with the results for the AMP-PCP experiment in which little focusing was observed.

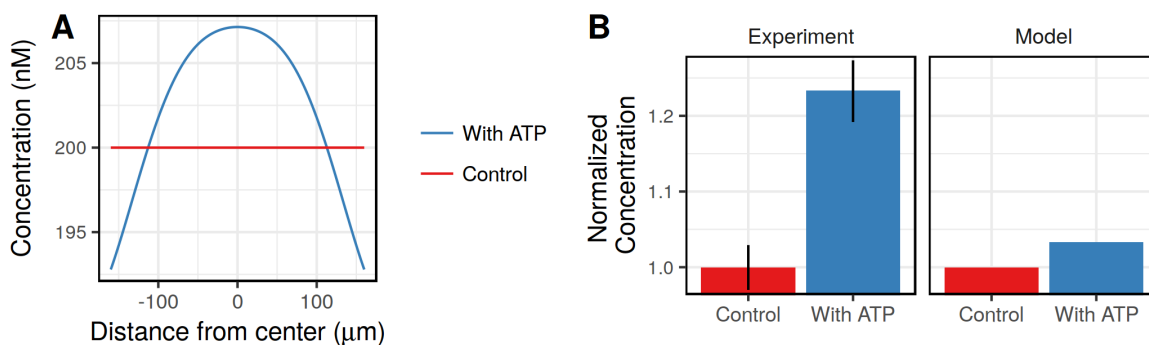


Figure 3-14. Computed profiles of the total enzyme concentration replicating experimental conditions from Figure 2 applied to catalysis-induced enzyme focusing **(A)** Modeled chemotactic response of HK in the presence of ATP. The parameters are chosen to replicate the conditions of the experiment described in Figure 2A. **(B)** Integrated N.F.I. of the enzyme in the central channel for experimental (left) and modeled (right) enzyme focusing. The experimental figure is the average of three experimental trials. Reprinted from *Nat. Chem.* **2018**, *10* (3), 311–317. Copyright 2018.

3.4 Conclusion

Our results suggest that the observed assembly of enzymes participating in a cascade in response to the presence of the initial substrate can be a result of individual enzymes undergoing chemotaxis in response to their specific substrate gradients. We identified and quantified the two major effects explaining chemotaxis: first, in the case of HK cross-diffusion up the ATP and glucose gradients is the main mechanism causing localization, and is dependent on ATP and glucose binding. Second, the magnitude of the effect is increased by the enhanced diffusion effect, which we have shown to be dependent on catalysis, for HK when both ATP and glucose are present. The extent of enzyme migration is proportional to the exposure time to the substrate gradient. The reduced chemotaxis with mannose, a less active substrate for HK, emphasizes the contribution of catalysis to the phenomenon. Significantly, the chemotactic migration of enzymes is fairly rapid even under conditions that mimic cytosolic crowding, a rate very similar to that reported for enzyme diffusion in living cells [34]. This phenomenon, chemotaxis, does not require the need for direct interaction between the enzymes to form complexes that promote substrate channeling; metabolon formation could simply be triggered by the presence of an initial substrate gradient, such as ATP gradients near mitochondria in the case of the transient metabolon, the purinosome. Furthermore, the enzymes should revert back to their equilibrium distribution once the initial substrate is completely reacted and the substrate gradients for the individual enzymes disappear. Presuming this phenomenon to be general [35], chemotaxis may be a basis for the organization of metabolic networks in the cytosol of the cell.

3.5 Experimental Details

3.5.1 Fluorescent Labeling of Hexokinase and Aldolase

Hexokinase (from *Saccharomyces cerevisiae*; Sigma-Aldrich) was tagged with an amine-reactive dye, Dylight 488 (ex/em: 493/518; Thermo Fisher Scientific). Hexokinase (44 μM) was reacted with a threefold excess of the fluorescent probe and 10 mM mannose in 50 mM Hepes (pH 7.0) at 4°C for 2–4 h on a rotator. Aldolase (from rabbit muscle; Sigma-Aldrich) was labeled with a thiol-reactive dye, Dylight 633 (ex/em: 638/658; Thermo Fisher Scientific). Labeling of Aldolase (75 μM) was carried out with a two-fold excess of the fluorescent dye and 1 mM EDTA on a rotator at 4°C for 2–3 h in 50 mM Hepes buffer (pH 7.4). The enzyme–dye conjugates were purified using a Sephadex G-25 (GE Healthcare) size exclusion column with 50 mM HEPES buffer (pH 7.4) to reduce the free-dye concentration. For FCS measurements, all enzymes were tagged with Alexa Fluor 532 dye (ex/em: 532/ 553; Thermo Fisher Scientific) by using of Alexa Fluor 532 protein labeling kit. The number of dye molecules per HK or Ald enzyme molecule was ~ 0.4 or 0.6 , respectively, as quantified using UV–vis spectroscopy. All solutions for experiments were prepared in 50 mM HEPES, pH 7.4 buffer.

3.5.2 Enzyme activity assays

Hexokinase activity before and after attachment of the fluorophore was measured spectrophotometrically by coupling with glucose-6-phosphate dehydrogenase (Sigma-Aldrich) and following the reduction of NADP^+ at 340 nm. An assay mixture, 1 mL in total volume contained 1 mM glucose, 2 mM ATP, 10 mM MgCl_2 , 50 mM HEPES (pH 7.4), 0.5 mM NADP^+ , 2 units glucose-6-phosphate dehydrogenase, and 5 nM hexokinase. All assays were performed at 25 °C. The

enzymatic activity was not significantly altered by the attachment of the fluorophore. Aldolase activity before and after attachment of the fluorophore was measured spectrophotometrically by coupling with α -glycerophosphate dehydrogenase/triosephosphate isomerase (Sigma-Aldrich) and following the oxidation of NADH at 340 nm. An assay mixture, 1 mL in total volume contained 2 mM fructose-1,6-disphosphate, 50 mM HEPES (pH 7.4), 0.1 mM NADH, 1.5 units α -glycerophosphate dehydrogenase/triosephosphate isomerase (based on GDH units), and 50 nM aldolase. All assays were performed at 25 °C. The enzymatic activity was not significantly altered by the attachment of the fluorophore.

The difference in hexokinase activity using glucose or mannose as the substrate was measured spectrophotometrically by coupling with pyruvate kinase/lactate dehydrogenase (Sigma-Aldrich) and following the oxidation of NADH at 340 nm. An assay mixture, 1 mL in total volume contained 1 mM glucose or mannose, 2 mM ATP, 10 mM MgCl₂, 3.3 mM phosphoenolpyruvate, 50 mM HEPES (pH 7.4), 0.2 mM NADH, 2 units pyruvate kinase/lactate dehydrogenase (based on PK units), and 5 nM hexokinase. All assays were performed at 25 °C. The enzymatic activity of hexokinase with mannose as the substrate was approximately half the enzymatic rate with D-glucose as the substrate under these conditions.

3.5.3 Progress Curve Simulation

The substrate depletion and product formation through the first four enzymes in the glycolytic cascade were simulated using Global Kinetic Explorer software (version 4.0, KinTek Corporation) [36]. The steady-state reaction scheme is assumed: 1) substrate binding rates are at the diffusion limit for glucose binding to hexokinase since the initial glucose concentration was sufficient to saturate the enzyme binding sites, and at k_{cat}/K_m for the subsequent enzyme reactions

because the substrates were the product of the previous enzyme reaction and their concentrations did not reach the level of saturation; 2) irreversible reaction rates fixed at k_{cat} for each enzyme since the product of each reaction would be pulled through the cascade by the presence of the downstream enzymes preventing the reverse reaction or product inhibition; and 3) that product release was not rate limiting for any individual reaction. The simulation input values were 10 mM for the starting glucose concentration; 74 nM for each starting enzyme concentration; $k_1 = 120 \mu\text{M}^{-1}\text{s}^{-1}$ and $k_{\text{cat}} = 315 \text{s}^{-1}$ for hexokinase; $k_{\text{cat}} = 408 \text{s}^{-1}$ and $K_m = 700 \mu\text{M}$ for isomerase; $k_{\text{cat}} = 113 \text{s}^{-1}$ and $K_m = 30 \mu\text{M}$ for PFK; and $k_{\text{cat}} = 5 \text{s}^{-1}$ and $K_m = 60 \mu\text{M}$ for aldolase (all values were obtained from Sigma-Aldrich Product Information sheets: cat. # H6380 for HK; cat. # P5381 for Iso; cat. # F0137 for PFK; and cat. # A2714 for Ald). The simulation assumes that all the enzymes and glucose are combined in one reaction mixture; an enzyme concentration of 74 nM was chosen because that is the amount of hexokinase determined to migrate into a channel containing 10 mM D-glucose (**Appendix Table A-1&2&3**).

3.5.4 Microfluidic Device Fabrication

The microfluidic device was cast in polydimethylsiloxane (PDMS, Sylgard 184, Dow Corning) using standard soft lithography protocols [37]. A 100- μm deep master pattern was created on a silicon wafer (Silicon Quest) using SPR-955 resist (Microposit) and deep reactive ion etching (Alcatel). The master was exposed to *1H,1H,2H,2H*-perfluorooctyl-trichlorosilane (Sigma Aldrich) to minimize adhesion of PDMS during the peeling step. After the PDMS was peeled off, the inlet and outlet regions were opened by drilling, and the device was sealed to a No. 1 glass coverslip (VWR). Fluid flow through the channel was controlled by syringe pumps (KDS 200 and 220, KD Scientific) connected by polyethylene tubing to the device.

3.5.5 Confocal Microscope Imaging

Confocal images were acquired using a Leica TCS SP5 laser scanning confocal inverted microscope (LSCM, Leica Microsystems) with a 10× objective (HCX PL APO CS, 0.70 NA) incorporated in it. The plane of interest (along the *z*-axis) for confocal imaging was chosen such that fluorescence intensity was captured from the plane that is half of the height into the channel. Videos were recorded and analyzed using Image J software. In each experiment, the mean fluorescence intensity was calculated from videos from three independent experiments. Each video is a collection of 667 images over a period of 5 min. A region of interest (ROI) was selected along the channel (as indicated by the vertical line in **Figure 3-1B**), and the stack-averaged fluorescence intensity was plotted as a function of distance along the width of the channel.

3.6 Acknowledgements

The work was supported by Penn State MRSEC funded by the National Science Foundation (DMR-1420620). Xi Zhao acknowledges Dr. Vinita Yadav, Dr. Michelle M. Spiering and Prof. Stephen J. Benkovic for enzyme tagging and activity assay experiment set-up. The author thanks Prof. Peter J. Butler for assistance with enzyme diffusion measurement and acknowledges Dr. Henri Palacci and Prof. Henry Hess for theoretical modeling.

3.7 References

- [1] Miles, E. W., Rhee, S. & Davies, D. R. The Molecular Basis of Substrate Channeling. *J. Biol. Chem.* **1999**, *274*, 12193–12196.
- [2] Wheeldon, I., Minter, S. D., Banta, S., Barton, S. C., Atanassov, P. & Sigman, M. Substrate Channeling as an Approach to Cascade Reactions. *Nat. Chem.* **2016**, *8*, 299- 309.

- [3] Lin, J.-L., Palomec, L. & Wheeldon, I. Design and Analysis of Enhanced Catalysis in Scaffolded Multienzyme cascade reactions. *ACS Catal.* **2014**, *4*, 505–511.
- [4] Yamada, Y., Tsung, C., Huang, W., Huo, Z., Habas, S. E., Soejima, T., Aliaga, C. E., Somorjai, G. A. & Yang P Nanocrystal Bilayer for Tandem Catalysis. *Nature Chem.* **2011**, *3*, 372–376.
- [5] Zhao, M., Deng, K., He, L., Liu, Y., Li, G., Zhao, H. & Tang, Core-shell Palladium Nanoparticle@metal-organic Frameworks as Multifunctional Catalysts for Cascade Reactions. *J. Am. Chem. Soc.* **2014**, *136*, 1738–1741.
- [6] Zhang, Y. H. Substrate Channeling and Enzyme Complexes for Biotechnological Applications. *Biotechnol. Adv.* **2011**, *29*, 715–725.
- [7] S. An, R. Kumar, E. D. Sheets, S. J. Benkovic, Reversible Compartmentalization of de Novo Purine Biosynthetic Complexes in Living Cells. *Science* **2008**, *320*, 103-106.
- [8] Nishi, H., Hashimoto, K. & Panchenko, A. R. Phosphorylation in Protein- protein Binding: Effect on Stability and Function. *Structure (London, England : 1993)*. **2011**, *19*, 1807-1815.
- [9] Lindbladh, C. et al. Preparation and Kinetic Characterization of a Fusion Protein of Yeast Mitochondrial Citrate Synthase and Malate-dehydrogenase. *Biochemistry* **1994**, *33*, 11692–11698.
- [10] Wu, F. & Minter, S. Krebs Cycle Metabolon: Structural Evidence of Substrate Channeling Revealed by Cross-linking and Mass Spectrometry. *Angew. Chem. Int. Ed.* **2015**, *54*, 1851–1854.
- [11] Winkel-Shirley, B. Evidence for Enzyme Complexes in the Phenylpropanoid and Flavonoid Pathways. *Physiol. Plantarum* **1999**, *107*, 142–149.
- [12] Jorgensen, K. et al. Metabolon Formation and Metabolic Channeling in the Biosynthesis of Plant Natural Products. *Curr. Opin. Plant. Biol.* **2005**, *8*, 280–291.
- [13] Graham, J. W. A., Williams, T. C. R., Morgan, M., Fernie, A. R., Ratcliffe, R. G. & Sweetlove, L. J. Glycolytic enzymes associate dynamically with mitochondria in response to respiratory demand and support substrate channeling. *The Plant Cell* **2007**, *19*, 3723–3738.
- [14] Campanella, M. E., Chu, H. & Low, P. S. Assembly and Regulation of a Glycolytic Enzyme Complex on the Human Erythrocyte Membrane. *Proc. Natl. Acad. Sci. U.S.A.* **2005**, *102*, 2402-2407.
- [15] Sengupta, S., Dey, K. K., Muddana, H. S., Tabouillot, T., Ibele, M. E., Butler, P. J. & Sen, A. Enzyme Molecules as Nanomotors. *J. Am. Chem. Soc.* **135**, 1406-1414 (2013).

- [16] Sengupta, S., Spiering, M. M., Dey, K. K., Duan, W., Patra, D., Butler, P. J., Astumian, R. D., Benkovic, S. J. & Sen, A. DNA Polymerase as a Molecular Motor and Pump. *ACS Nano* **8**, 2410-2418 (2014)
- [17] Yu, H., Jo, K., Kounovsky, K. L., Pablo, J. J., Schwartz, D. C. Molecular propulsion : chemical sensing and chemotaxis of DNA driven by RNA polymerase. *J. Am. Chem. Soc.* **131**, 5722-5723 (2009).
- [18] French, J. B., Jones, S. A., Deng, H., Pedley, A. M., Kim, D., Chan, C. Y., Hu, H., Pugh, R. J., Zhao, H., Zhang, Y., Huang, T. J., Fang, Y., Zhuang, X. & Benkovic, S. J. Spatial colocalization and functional link of purinosomes with mitochondria. *Science* **2016**, *351*, 733-737 (2016).
- [19] Menard, L., Maughan, D. & Vigoreaux, J. The Structural and Functional Coordination of Glycolytic Enzymes in Muscle: Evidence of a Metabolon *Biology* **2014**, *3*, 623–644.
- [20] Fromm, H. J.; Zewe, V. Kinetic Studies of Yeast Hexokinase. *J Biol Chem* **1962**, *237*, 3027–3032.
- [21] Wilkinson, K. D.; Rose, I. A. Isotope Trapping Studies of Yeast Hexokinase during Steady State Catalysis. A Combined Rapid Quench and Isotope Trapping Technique. *J. Biol. Chem.* **1979**, *254* (24), 12567–12572.
- [22] Kuser, P. R.; Krauchenco, S.; Antunes, O. A. C.; Polikarpov, I. The High Resolution Crystal Structure of Yeast Hexokinase PII with the Correct Primary Sequence Provides New Insights into Its Mechanism of Action. *J. Biol. Chem.* **2000**, *275* (27), 20814–20821.
- [23] Myers, T. C., Nakamura, K. & Flesher, J. W., Phosphonic acid analogs of nucleoside phosphate. I. the synthesis of 5'- adenylyl methylenediphosphate, a phosphonic acid analog of ATP *J. Am. Chem. Soc.* **1963**, *85*, 3292- 3295.
- [24] Callens, M.; Kuntz, D. A.; Opperdoes, F. R. Kinetic Properties of Fructose Bisphosphate Aldolase from *Trypanosoma Brucei* Compared to Aldolase from Rabbit Muscle and *Staphylococcus Aureus*. *Mol. Biochem. Parasitol.* **1991**, *47*, 1-10.
- [25] Vopel, T. & Makhatadze, G. I., Enzyme activity in the crowded milieu. *PLOS One* **2012**, *7*, 1-6.
- [26] Paduano, L., Sartorio, R., Errico, G. D. & Vitagliano, V. Mutual diffusion in aqueous solution of ethylene glycol oligomers at 25 degrees C. *J. Chem. Soc. Faraday T.* **1998**, *94*, 2571-2576.
- [27] Muddana, H. S., Sengupta, S., Mallouk, T. E., Sen, A. & Butler, P. J. Substrate catalysis enhance single- enzyme diffusion. *J. Am. Chem. Soc.* **2010**, *132*, 2110- 2111.

- [28] Riedel, C., Gabizon, R., Wilson, C. A. M., Hamadani, K., Tsekouras, K., Marqusee, S., Pressé, S., Bustamante, C. The heat released during catalytic turnover enhances the diffusion of an enzyme. *Nature* **2015**, *517*, 227-230.
- [29] Annunziata, O., Vergara, A., Paduano, L., Sartorio, R., Miller, D. G. & Albright, J. G. Quaternary diffusion coefficients in a protein-polymer-salt-water system determined by rayleigh interferometry. *J. Phys. Chem. B* **2009**, *113*, 13446-13453.
- [30] Vergara, A., Paduano, L. & Sartorio, R., Mechanism of protein-poly(ethylene glycol) interaction from a diffusive point of view. *Macromolecules* **2002**, *35*, 1389-1398.
- [31] Vanag, V. K. & Epstein, I. R., Cross-diffusion and pattern formation in reaction-diffusion systems. *Phys. Chem. Chem. Phys.* **2009**, *11*, 897-912.
- [32] Schurr, J. M., Fujimoto, B. S., Huynh, L., Chiu, D. T. A theory of macromolecular chemotaxis. *J. Phys. Chem. B* **2013**, *117*, 7626-7652.
- [33] Bermingham, A., Bottomley, J. R., Derrick, W. U. & Derrick, J. P., Equilibrium and kinetic studies of substrate binding to 6-hydroxymethyl-7,8-dihydropterin pyrophosphokinase from escherichia coli. *J. Biol. Chem.* **2000**, *275*, 17962–17967.
- [34] Vopel, T. & Makhatadze, G. I., Enzyme activity in the crowded milieu. *PLOS One* **2012**, *7*, 1-6.
- [35] Baum, M., Erdel, F., Wachsmuth, M. & Rippe, K. Retrieving the intracellular topology from multi-scale protein mobility mapping in living cells. *Nature Comm.* **2014**, *5*, 4494.
- [36] Johnson, K. A., Simpson, Z. B. & Blom, Global Kinetic Explorer: A New Computer Program for Dynamic Simulation and Fitting of Kinetic Data. *Anal. Biochem.* **2009**, *387*, 20-29.
- [37] Xia, Y. & Whitesides, G. M. Soft Lithography. *Annu. Rev. Mater. Sci.* **1998**, *28*, 153–184.

Chapter 4

Enhanced Diffusion of Passive Tracers in Active Enzyme Solutions

This chapter is an adapted reproduction from *Nano Lett.* **2017**, *17*, 4807–4812 with permission from the American Chemistry Society.

4.1 Introduction

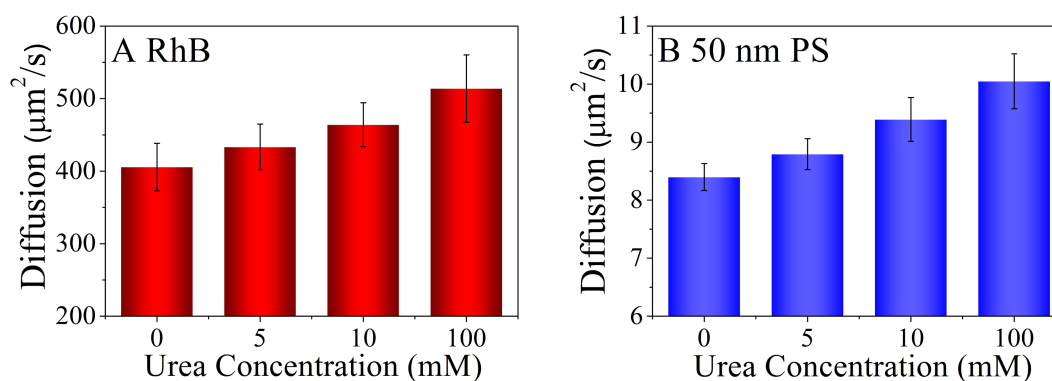
Colloidal systems driven out of equilibrium in response to periodic energy injections often display non-trivial collective dynamics and interactions [1-3]. Assemblies of active microparticles have recently been investigated as useful prototypes to understand these interactions, which require transfer of energy from the active particles to the surroundings under low Reynolds number conditions. Model systems examined include micrometer-sized bacteria [4-6], algae [7-8], and synthetic motors [9-10] that transduce chemical energy into self-propulsion under different experimental conditions. Energy transfer from the microscopic swimmers to the surroundings is usually estimated by monitoring the diffusion of passive tracers present in solution [11-12]. The measurements are carried out using swimmers and tracers suspended in quasi-two dimensional liquid films and quantifying the diffusion of tracers in the presence and absence of swimmers' activity [13-15]. The first measurements were reported by Wu and Libchaber, who investigated diffusion of large polymer particles in a bath of swimming *E. coli* [13]. They demonstrated that by increasing the population of active bacteria, effective diffusion of tracers can be made substantially higher than their normal Brownian diffusion. Miño et al. established that both bacteria and self-powered micron-sized bimetallic rods transfer their *momentum* to the surroundings, resulting in similar enhanced

diffusion of suspended tracers [9]. Although these studies were carried out with swimmers that follow very different propulsion strategies, their behavior in terms of energy transfer to the surroundings were found to be strikingly similar. This prompted us to look for a similar phenomenon at the molecular scale and investigate if mechanical energy generation by active molecules is significant enough to influence the dynamics of inert particle assemblies even at the ultralow Reynolds number regime. Among the different available self-powered systems, molecules of active enzymes arguably constitute the best prototypes, owing to their biocompatibility and specificity in operation. In addition to their primary function as catalysts in biochemical reactions, enzymes have been found to be force-generating during substrate turnover [16-18]. Using fluorescence correlation spectroscopy (FCS) and dynamic light scattering (DLS) measurements, we demonstrate that active enzymes molecules, much like their microscopic counterparts, are also able to influence significantly the dynamics of their surroundings. The diffusivity of both micro and nanoscopic tracers suspended in active enzyme solutions are enhanced as a function of total substrate concentration in the system – indicating catalysis-induced force generation and energy transfer at the molecular scale. We propose that the observed diffusion enhancement of the tracers is due to the *momentum* transferred from active enzyme molecules to the surrounding.

4.2 Results and discussion

We measured diffusion of nanoscopic tracer particles dispersed in active enzyme solutions in the presence and absence of catalysis using FCS, equipped with time-correlated single-photon counting (TCSPC) instrumentation. We used the enzyme urease as model molecular swimmer owing to its robustness, high turnover rate reported at room temperature ($k_{\text{cat}} = 2.34 \times 10^4 \text{ s}^{-1}$) [19], and generation of reaction products that are not expected to influence the measurements. The reaction

catalyzed by urease is significantly exothermic (ΔH , -102.5 kJ/mol) [20]. Experiments were carried out with molecules of Rhodamine B (RhB; hydrodynamic radius = 0.57 nm) [21] and fluorescent polymer particles (Fluoro-Max Fluorescent Polymer Microspheres, 1% solid) of diameters 50 and 100 nm respectively. The concentration of urease used was 10 nM and that of the substrate, urea was varied between 0 to 100 mM. For each measurement, a fresh 1 mL mixture of urease and urea was prepared to which 1 μ L of 50 or 100 nm tracer solution was added. From this total mixture, 50 μ L was used in the actual measurement. For molecules of RhB, the final concentration of tracer in the solution was optimized to be approximately 1-2 nM for better signal to noise ratio and reliable autocorrelation fits. **Figure 4-1** shows diffusion coefficients of tracer particles of various sizes measured in 10 nM urease solution at different concentrations of urea. For each of these tracers, the diffusion increased with increasing substrate concentration and reaction rate. The total reaction rates for the experimental enzyme and substrate concentrations were calculated and found to increase monotonically within the substrate concentration regime used, **Figure4-1D**. The maximum percentage increase in diffusion observed for RhB, 50 nm and 100 nm tracers were approximately 30.0 ± 5.5 , 19.6 ± 5.8 and 12.5 ± 3.0 , respectively. These observations suggest that the increase in tracer diffusivity is a function of the total substrate turnover rate and results from the effect of enzymes' activity in solution.



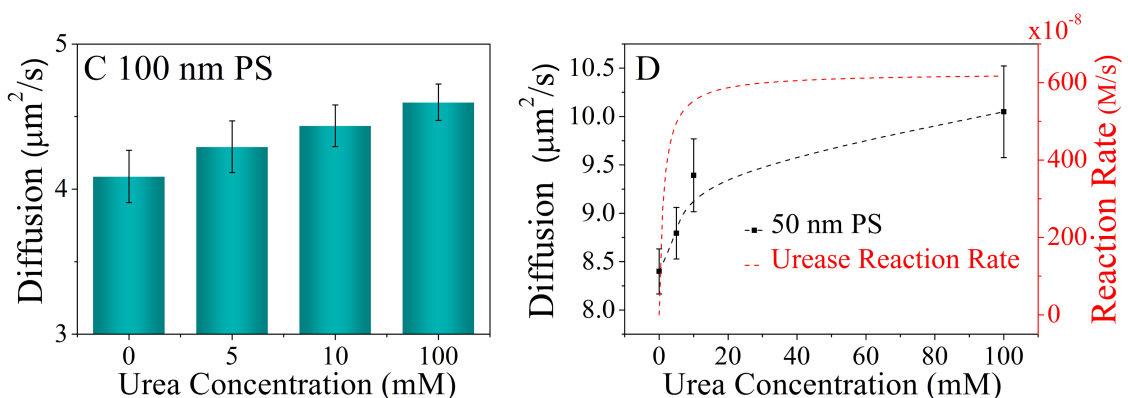
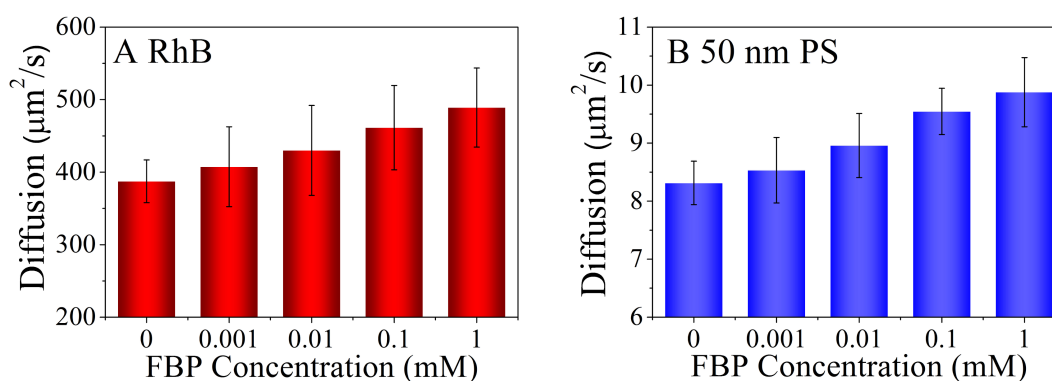


Figure 4-1. Diffusion of (A) RhB, (B) 50 nm and (C) 100 nm fluorescent polystyrene particles measured in active urease solutions (10 nM) at different concentrations of urea. The error bars represent standard deviations calculated for 20 different measurements, under identical conditions. With increasing reaction rate, the diffusion of tracers in each case was enhanced, suggesting transfer of *momentum* from the catalysts to these particles. (D) Correlation between the diffusion of 50 nm fluorescent particles and total reaction rates at various concentrations of urea. The reaction rates are calculated based on Michaelis-Menten kinetics, for 10 nM urease. Reprinted from *Nano Lett.* **2017**, *17*, 4807–4812 Copyright 2017.

To investigate the possible role of reaction-induced heat generation in the enhancement of tracer diffusion, we next considered a different catalytic system: the enzyme aldolase which catalyzes the reversible splitting of fructose 1,6-bisphosphate (FBP) into glyceraldehyde 3-phosphate and dihydroxyacetone phosphate (DHAP). The reaction is endothermic (ΔH , +30-60 kJ/mol) [22-23] and, therefore, will not result in the heating of the reaction mixture. Experimentally, we used solutions of 10 nM aldolase (from rabbit muscle, Sigma-Aldrich), and the diffusion of RhB, 50 and 100 nm polystyrene particles was measured at different concentrations of FBP. The concentration of FBP was varied between (0-1) mM and measurements were all taken at room temperature. The measurement conditions were identical to that for urease. The diffusion of each tracer particle was found to increase with substrate concentration and reaction rate. The results using an endothermic enzyme suggest that, at best, reaction-generated heat is only one of the factors influencing tracer dynamics in solution. For molecules of RhB, 50 and 100 nm tracers, the maximum percentage increase in diffusion was 26.2 ± 6.3 , 18.8 ± 4.0 and 15.7 ± 3.4 , respectively **Figure 4-2**. We also

investigated if the non-catalytic conformational change by hexokinase produces enough hydrodynamic disturbances to influence the dynamics of their surroundings. (**Figure 4-3**). The diffusion of fluorescent beads (Thermo Scientific Fluoro-Max Red Aqueous Fluorescent Particles, 1% solids) with diameter of 50 nm was also measured under FCS in the active unlabeled hexokinase suspension with various concentration of glucose. 1 μ L of fluorescent nanoparticle suspension was added in each experimental solution which contained 20 nM unlabeled active hexokinase with various concentration of glucose and was 1 mL as total volume. The positive results will help us underscore novel interaction principles in active molecular system under low Reynolds number circumstances. We executed the experiment by measuring the diffusion of microscopic fluorescent polystyrene particles in the active hexokinase and glucose solution. The diameter of the polystyrene beads was 50 nm. The diffusion of tracer increased as glucose concentration increased with $35.5 \pm 7.4\%$ augment. The result strongly suggests that, enzymes even with periodically conformational change only without catalysis are capable to transduce enough mechanical force to perturb dynamics of their surroundings.



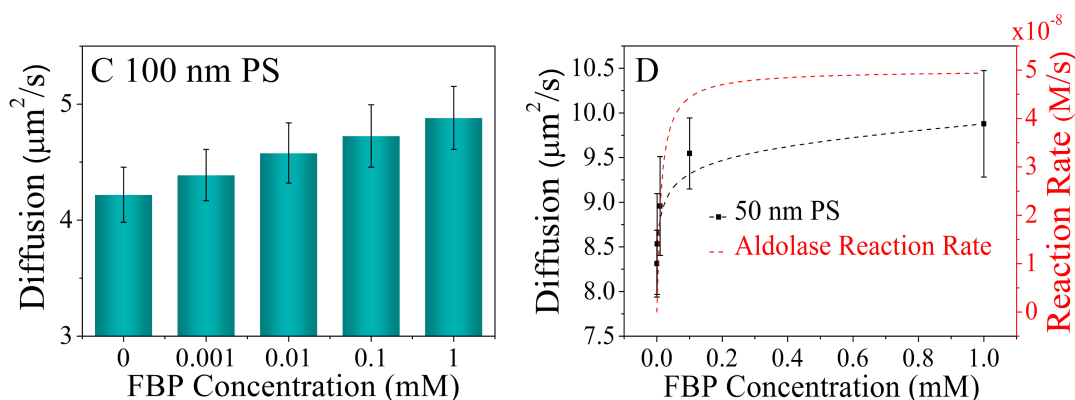


Figure 4-2. Diffusion of (A) RhB, (B) 50 nm and (C) 100 nm fluorescent polystyrene particles measured in active aldolase solutions at different concentrations of FBP. The error bars represent standard deviations calculated for 20 different measurements, under identical conditions. With increasing reaction rate, the diffusion of tracers in each case was found to enhance, suggesting transfer of *momentum* from the catalysts to these particles. (D) Correlation between the diffusion of 50 nm fluorescent particles and total reaction rates at various concentrations of FBP. The reaction rates are calculated based on Michaelis-Menten kinetics, for 10 nM aldolase. Reprinted from *Nano Lett.* **2017**, *17*, 4807–4812 Copyright 2017.

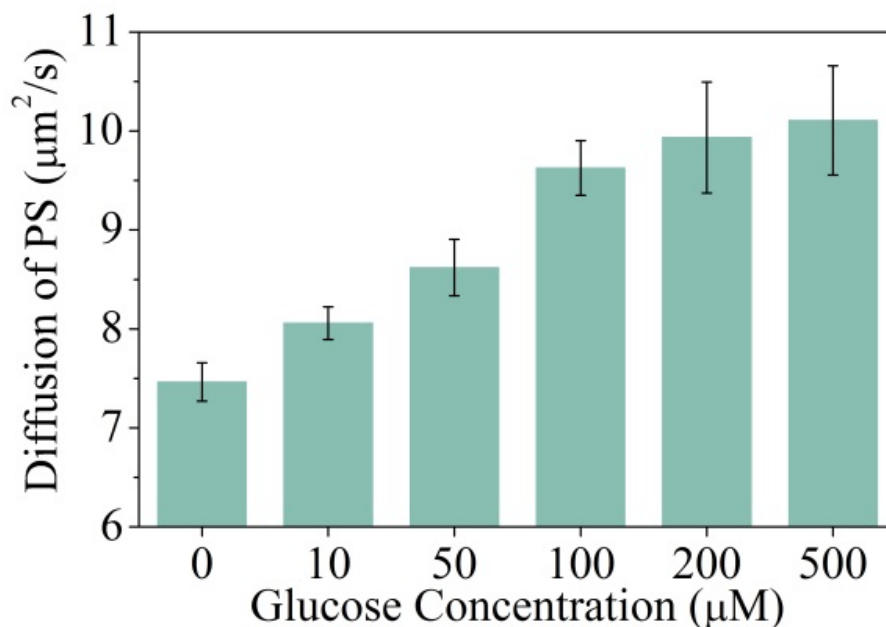


Figure 4-3. Diffusion of 50 nm fluorescent polystyrene beads measured in active hexokinase at different concentration of glucose without cofactors. The error bars represent standard deviations calculated for 10 different measurements, under identical conditions.

To confirm our FCS observations, we employed dynamic light scattering particle size analyzer to investigate *momentum* transfer from active enzymes to microscopic polymer particles in solution. For spherical particles, the time dependent fluctuation of the scattered light intensity can be fitted to estimate the *effective* diffusion coefficient (D) of the particles, which can then be related to their hydrodynamic radius (R) using Stokes-Einstein relation. For particles with constant hydrodynamic radius dispersed in an active colloid, if the temperature and the viscosity are assumed constants, any changes in diffusivity can directly be attributed to the activity of the medium. Measurements were carried out in a Malvern Zetasizer ZS instrument, which employs non-invasive backscatter optics (NIBS) to measure particle size in suspensions. Solution of Jack bean urease was prepared in deionized water and was mixed with aqueous solution of urea (Sigma- Aldrich) in calculated proportions. The final concentration of urease in the mixture was kept 10 nM and that of urea was in the range 0-10 mM. Before experiments, 2 μm polystyrene sulfate latex particles (8% w/v, Life Technologies) were passivated against enzyme adsorption by coating their surfaces with a layer of Bovine Serum Albumin (BSA) (for details, See SI). Coating the tracers with BSA does not significantly alter their hydrodynamic radii because of the negligible molecular size of BSA (3.5 nm) [24]. The experiments were all carried out at 25 $^{\circ}\text{C}$ and each measurement involved three successive runs, each run consisting of 14 scans on average. **Figure 4-4A** shows a representative example of DLS experiment involving tracer diffusion in the presence of 10 nM urease and 0.5 mM urea.

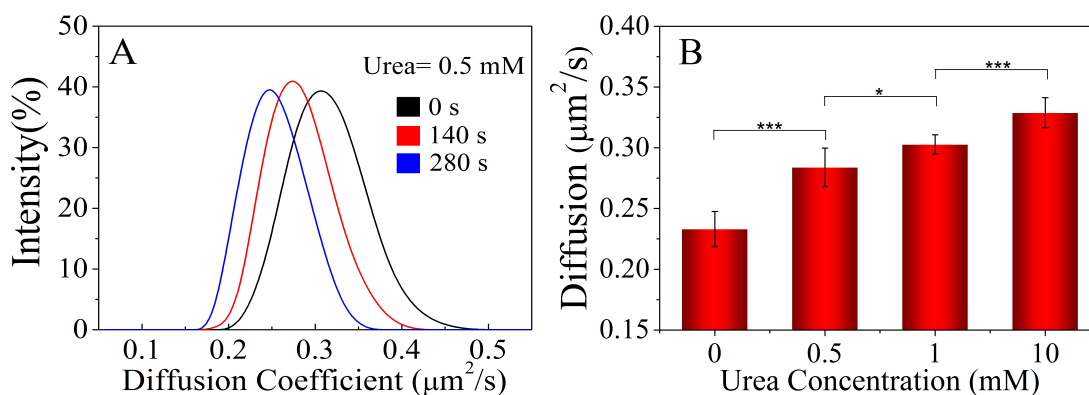


Figure 4-4. (A) Time dependent shifts in diffusion of 2 μm BSA-coated polystyrene sulfate microspheres, dispersed in 10 nM urease and 0.5 mM urea, estimated using dynamic light scattering particle size analysis. As the reaction goes to completion, the peak for the diffusion coefficient distribution profile gradually returns to the zero substrate value (from black to blue). All the curves are smoothed with B-spline fitting in Origin. (B) Tracer diffusion as a function of substrate concentration, measured using DLS. For each substrate concentration, 3 separate measurements were taken at time zero (which corresponded to the maximum changes in tracer diffusion at that substrate concentration). ***: $p < 0.001$; *: $p < 0.05$. Reprinted from *Nano Lett.* **2017**, *17*, 4807–4812 Copyright 2017.

Figure 4-4B shows diffusion coefficient distribution profiles of 2 μm BSA-coated polystyrene sulfate tracer particles dispersed in 10 nM urease solution, in the presence of various concentrations of urea. In the absence of substrate, the average of three measurements showed a distribution peak at $0.23 \pm 0.01 \mu\text{m}^2/\text{s}$, which is consistent with the value obtained in deionized water and in pure substrate solution **Figure 4-5**.

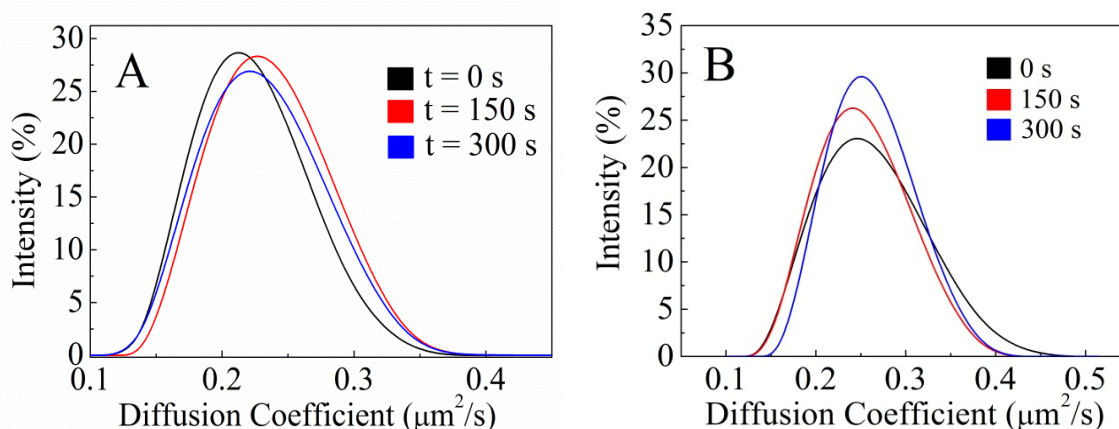


Figure 4-5. (A) Diffusion coefficient distribution of 2 μm polystyrene sulfate tracers, coated with BSA, dispersed in (A) DI Water and (B) 10 mM Urea, recorded in DLS. The measurements were taken successively at three different times. The measured diffusion of the tracers is $0.23 \pm 0.01 \mu\text{m}^2/\text{s}$ in DI water and $0.24 \pm 0.01 \mu\text{m}^2/\text{s}$ in 10 mM urea. Reprinted from *Nano Lett.* **2017**, *17*, 4807–4812 Copyright 2017.

However, in the presence of catalysis the distribution shifted to higher diffusion values, indicating enhanced motion of the tracers in the presence of enzymatic reactions. The percentage

change in diffusion was measured to be nearly 40.8 ± 1.7 , which is quite significant considering the size difference of the swimmers and the tracers. Consistent with the FCS measurements, the diffusion increased in a substrate concentration-dependent manner, suggesting higher *momentum* transferred to the tracers with increased turnover rate. For each substrate concentration, the measured distribution showed a gradual shift towards the base value, as the reaction proceeded towards completion. The maximum shift observed in the diffusion profiles of particles for various concentration of urea were used to calculate the substrate concentration-dependent diffusion enhancement (**Figure 4-4B**). To further confirm that the observed shift in diffusion distribution was due to enzymatic catalysis, experiments were repeated with molecules of inhibited urease. Urease activity was inhibited by pre-treating the enzymes with pyrocatechol [25]. Sample of 2 μM urease was prepared in 10 mM phosphate buffer and then incubated with 4 mM pyrocatechol, also prepared in buffer, for a period of 24 hr. Pyrocatechol irreversibly inhibits urease activity, without altering any other physical characteristics. The inhibited ureases were separated from unreacted pyrocatechol using membrane dialysis (10 kDa pores; Amicon ultra-4 centrifugal filter unit, Millipore). The concentration of enzymes in the purified solutions was calculated from UV-vis measurements, taking molar extinction coefficient of the enzyme at 280 nm as $75592 \text{ M}^{-1} \text{ cm}^{-1}$ [19]. The absorption spectra recorded for the inhibited enzyme in UV-vis measurements is shown below. The diffusion of inhibited urease in the presence of 10 mM urea is $0.23 \pm 0.01 \mu\text{m}^2/\text{s}$, which is similar to the diffusion of 2 μm polystyrene sulfate tracers, coated with BSA, dispersed in DI water. As mentioned before, control experiments were also performed with solution of 10 mM urea to examine the effect of only substrate on the diffusion of tracers. On both the occasions, the measured diffusion of the tracers did not show any significant shift from the base value (**Figure 4-5B and Figure 4-6B**).

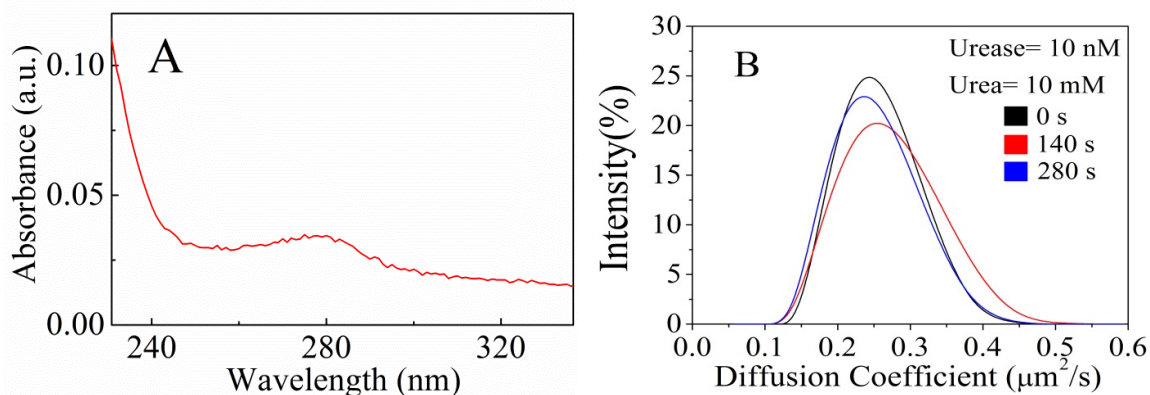


Figure 4-6. (A) Absorption spectra of urease inhibited with pyrocatechol. (B) Diffusion profile of 2 μm sulfate tracers in inhibited urease solution in the presence of substrate. Reprinted from *Nano Lett.* **2017**, *17*, 4807–4812 Copyright 2017.

We also employed dynamic light scattering particle size analyzer to investigate *momentum* transfer from the endothermic enzyme aldolase to microscopic polymer particles in solution. We repeated the DLS measurements with 2 μm BSA-coated polystyrene sulfate tracers. We prepared a 10 nM stock solution of aldolase in deionized water. Stock solution of 10 mM aqueous FBP was used as the substrate. The results are shown in **Figure 4-7**.

The diffusion of the microscopic tracer particles increased in a substrate concentration-dependent manner during aldol splitting reaction by aldolase. At maximum FBP concentration used (1 mM), the percentage increase in diffusion was nearly 35.4 ± 1.2 , while control experiments carried out with tracers dispersed in only FBP did not show any enhancement in diffusion (**Figure 4-8**), suggesting the observed momentum transfer was a consequence of catalytic turnover and reaction exothermicity is not a necessary criterion.

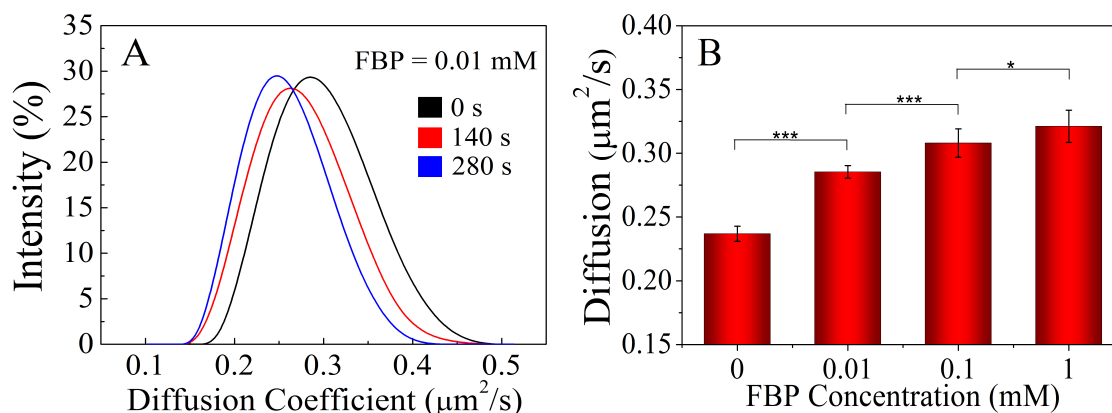


Figure 4-7. (A) Time dependent shifts in diffusion of 2 μm BSA- coated polystyrene sulfate tracers, dispersed in 10 nM aldolase and 0.01 mM FBP. As the reaction proceeds to completion, peak of the diffusion coefficient distribution profile gradually returns to the zero substrate value (from black to blue). The plots are smoothened with B-spline fitting in Origin. **(B)** Tracer diffusion as a function of substrate concentration, measured using DLS. For each substrate concentration, 3 separate measurements were taken at time zero (which corresponded to the maximum changes in tracer diffusion at that substrate concentration). ***: $p < 0.001$; *: $p < 0.05$. Reprinted from *Nano Lett.* **2017**, *17*, 4807–4812 Copyright 2017.

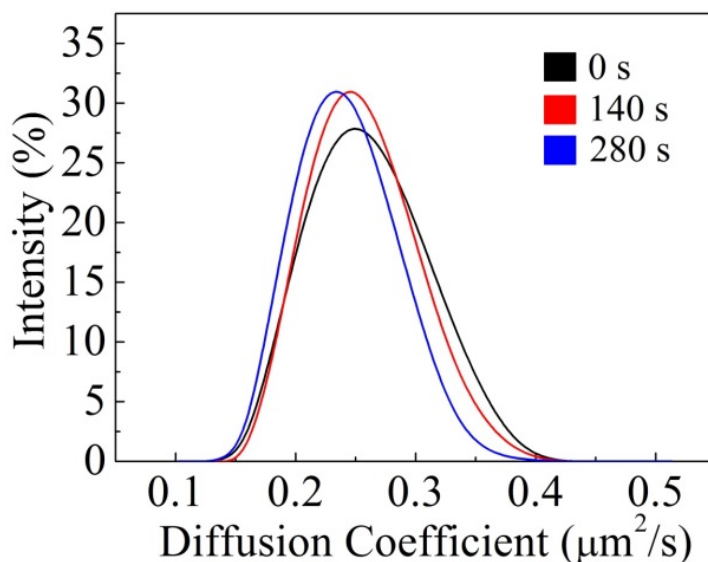
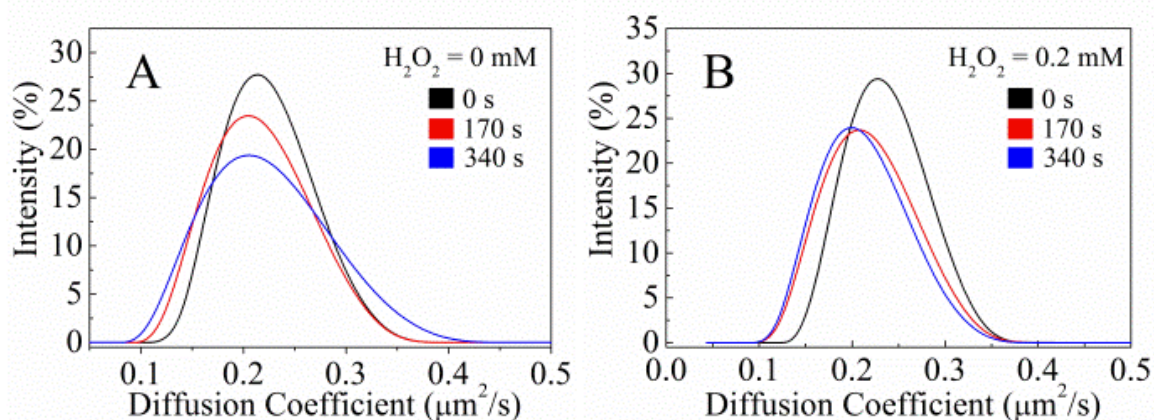


Figure 4-8. Diffusion coefficient distribution of 2 μm polystyrene sulfate tracers, coated with BSA, dispersed in 1 mM FBP only, and recorded in DLS. The measurements were taken successively at

three different times. The measured diffusion of the tracers is $0.24 \pm 0.01 \mu\text{m}^2/\text{s}$. Reprinted from *Nano Lett.* **2017**, *17*, 4807–4812 Copyright 2017.

To demonstrate that the transfer of *momentum* to the tracers during enzymatic catalysis is a generic phenomenon, we used molecules of bovine liver catalase (Sigma-Aldrich) and repeated DLS measurements with $2 \mu\text{m}$ BSA-coated polystyrene sulfate tracers. Like urease, catalase is robust and has a high turnover rate ($k_{\text{cat}} = 2.12 \times 10^5 \text{ s}^{-1}$) at room temperature [17]. We prepared a 200 nM solutions of catalase in deionized water. Stock solution of 10 mM aqueous hydrogen peroxide was used as the substrate. The experimental concentrations of catalase and peroxide solutions selected ensured no visible bubble formation within the experimental chamber during the measurements. The results are shown in **Figure 4-9**. The diffusion of the microscopic tracer particles increased in a substrate concentration-dependent manner during catalytic decomposition of H_2O_2 by catalase. At maximum H_2O_2 concentration used (1mM), the increase in diffusion was $46.0 \pm 2.5\%$, while control experiments carried out with tracers dispersed in only H_2O_2 did not show any enhancement in diffusion (**Figure 4-10**), suggesting that the observed *momentum* transfer was a consequence of catalytic turnover and is generic in nature **Figures 4-10 and 4-11**.



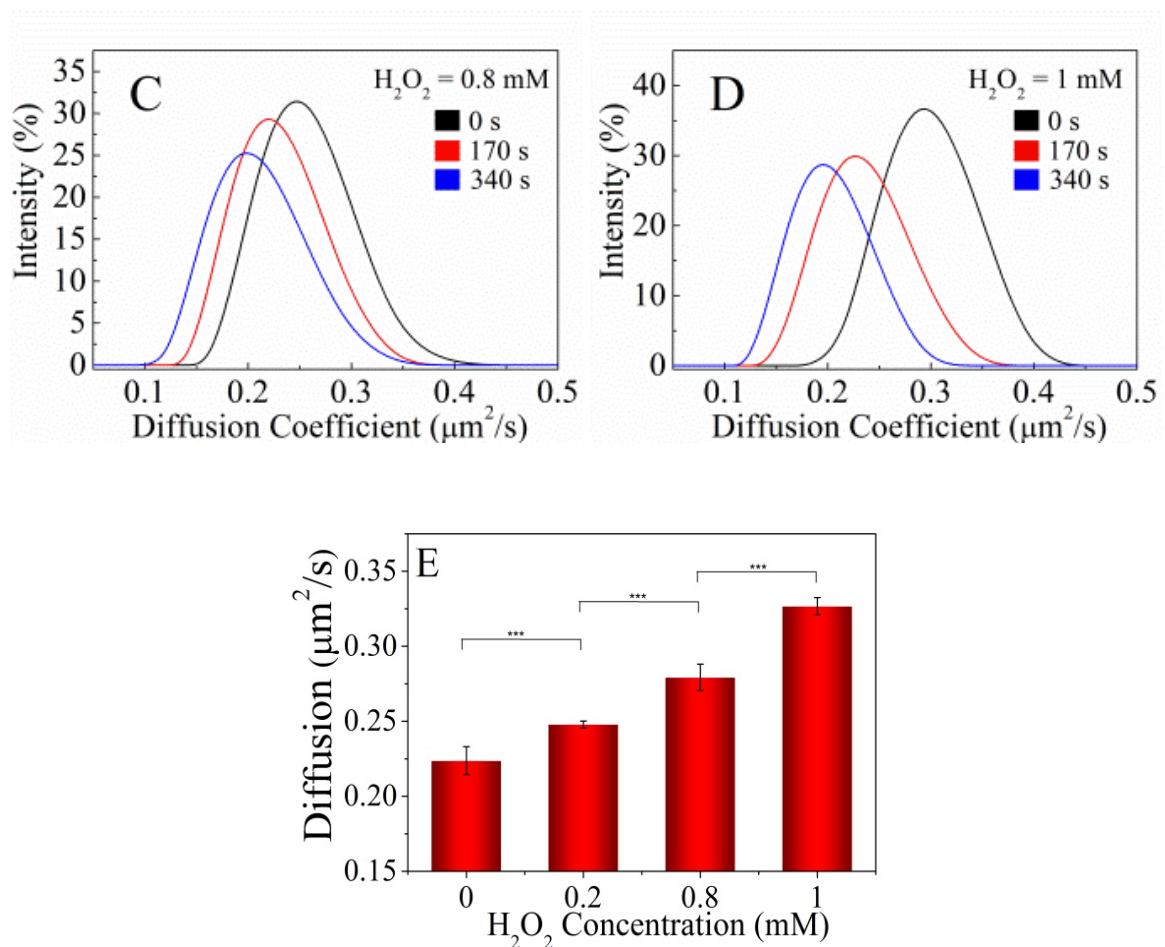


Figure 4-10. (A-D) Time dependent shifts in diffusion of 2 μm polystyrene sulfate tracers, coated with BSA, dispersed in 200 nM catalase and (0-1) mM H₂O₂ solutions. As the reaction proceeds to completion at each substrate concentration, the peak of the diffusion coefficient distribution profile gradually returns to the zero substrate value (from black to blue). The plots are smoothed with B-spline fitting in Origin. (E) Tracer diffusion in active catalase solution as a function of H₂O₂ concentration. For each substrate concentration, 3 separate measurements were taken at time zero (which corresponded to the maximum changes in tracer diffusion at that substrate concentration). ***: $p < 0.001$. Reprinted from *Nano Lett.* **2017**, *17*, 4807–4812 Copyright 2017.

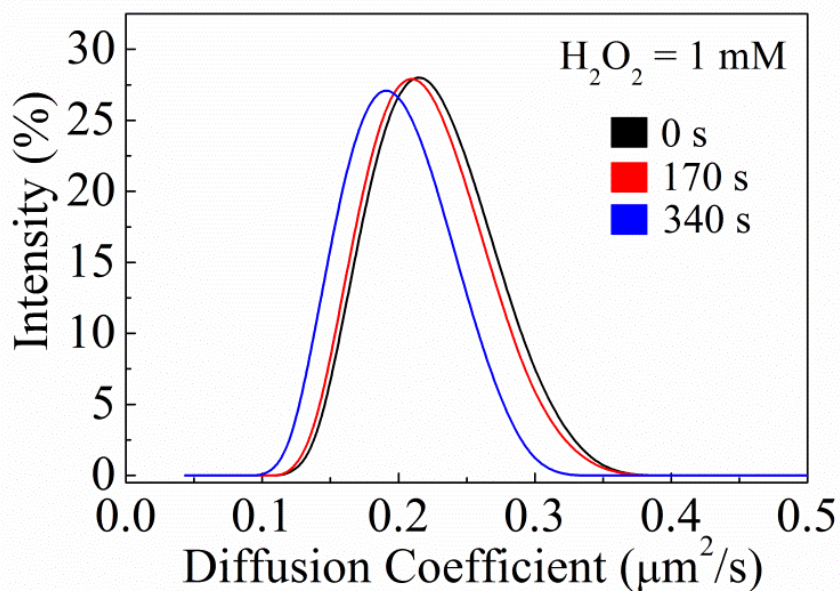


Figure 4-11. Diffusion coefficient of 2 μm polystyrene sulfate tracers, coated with BSA, in 1 mM H_2O_2 , showing no significant enhancement in diffusion. Reprinted from *Nano Lett.* **2017**, *17*, 4807–4812 Copyright 2017.

In order to check the consistency of results obtained in FCS and DLS, we measured the diffusion of the same 50 nm fluorescent polymer tracer (used in FCS experiments) in the presence of enzymatic reactions using DLS. Solutions of active urease were used and the concentrations of enzyme and substrate solutions chosen for DLS measurements were same as those used in FCS studies. During catalysis, the particles' diffusion in active solution (mixture of urea and urease) increased by $20.1 \pm 2.1\%$, which is consistent with the increase measured in FCS ($19.6 \pm 5.8\%$). The diffusion of the same particles in FBP and aldolase solutions measured by DLS increased by $20.4 \pm 2.4\%$, which is close to the value recorded in FCS ($18.8 \pm 4.0\%$) % FCS. The results of these measurements are provided in **Figure 4-12**.

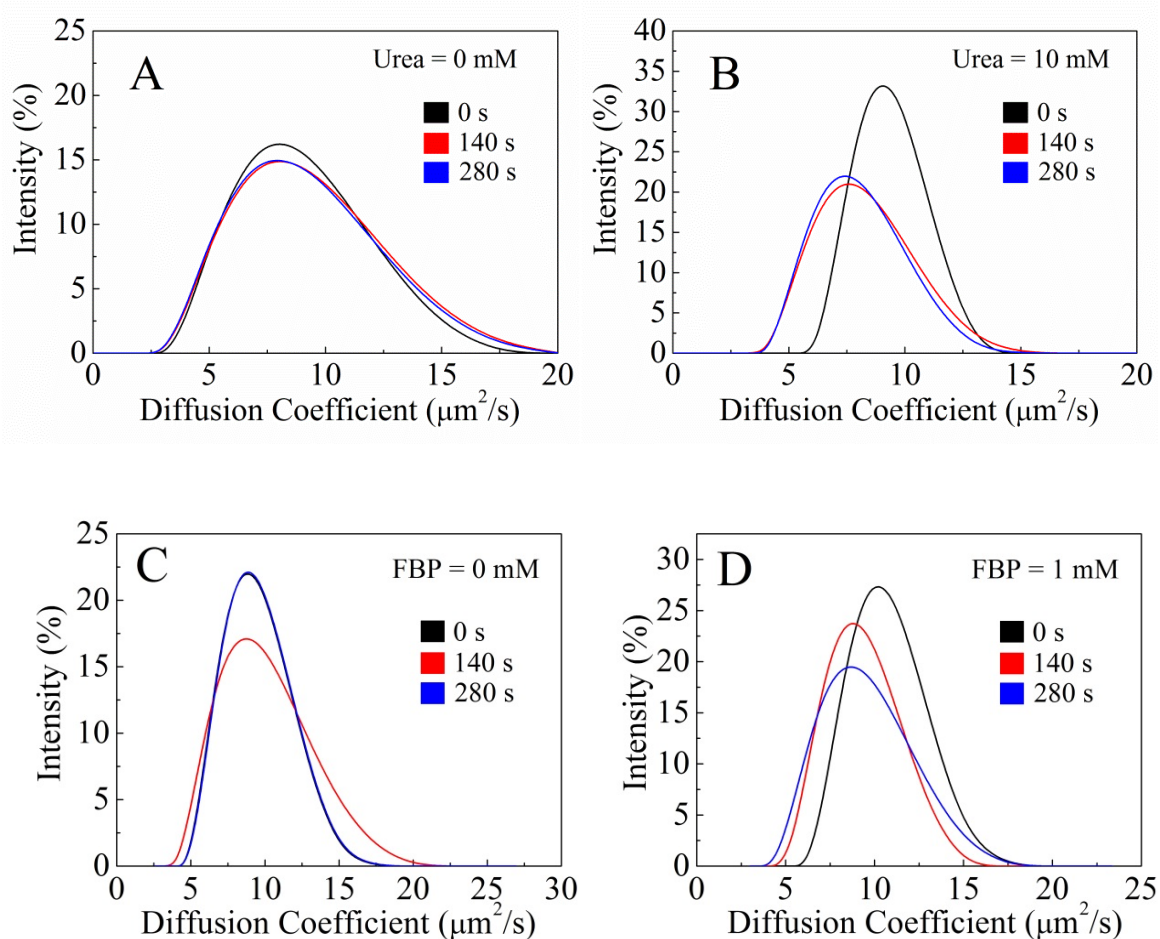


Figure 4-12. Enhanced diffusion of 50 nm polystyrene fluorescent tracers during urea hydrolysis and (C-D) FBP splitting, measured using dynamic light scattering particle size analyzer. During catalysis, the particles' diffusion in urea and urease solution increased by nearly $20.1 \pm 2.1\%$, which is consistent with the increase measured in FCS ($19.6 \pm 5.8\%$). The diffusion of the same tracer particles in FBP and aldolase solutions, measured by DLS increased by $20.4 \pm 2.4\%$, which is close to the enhancement recorded in FCS ($18.8 \pm 4.0\%$). Reprinted from *Nano Lett.* **2017**, *17*, 4807–4812 Copyright 2017.

There are several possible mechanisms that may explain the increase in tracer diffusion in the presence of active enzymes [26-28]. According to Mikhailov and Kapral, active enzymes act as stochastic oscillating force dipoles generating hydrodynamic flows and thereby collectively affecting the diffusion of passive tracers [28]. The theory, however, estimates the magnitude of such

hydrodynamic coupling for enzyme concentrations of the order of 10^{-4} M, much higher than concentrations used in our experiments (nM). Similar hydrodynamic arguments have also been put forward in support of measured enhanced diffusion of microscopic tracers in active bacterial suspensions [5, 30-33]. Protein crowding, however, can attenuate this effect. Clearly, our observations reflect the influence of active enzymes in the absence of both crowding and drift due to local gradients in enzyme concentrations. **Figure 4-13** shows that the increase in tracer diffusion correlates inversely with size ($1/R$) at the same enzyme and substrate concentrations (and therefore, at the same reaction rates), similar to the observations made in microscopic active systems [30]. The inverse radius dependence of induced diffusion of tracers in active bacterial suspensions has been proposed to be related to their hydrodynamic interaction [13] with the surroundings. But, as described recently by Burkholder and Brady [29], enhanced tracer diffusion observed in bacterial suspensions may not necessarily be a consequence of only hydrodynamic interactions. According to their proposal, active contribution to the effective tracer diffusivity depends on the dominating characteristic time scale of the process. Because of their small size, the reorientation time for the enzymes is significantly faster than either the enzyme or tracer advection, which should result in behavior similar to what we see in **Figure 4-13**. Such behavior results from collisions between the tracers and the enzymes occurring from different directions on a short timescale dominated by the reorientation time of the enzymes. This situation resembles that of Brownian motion of a colloidal particle, but here with an additional contribution from a “hot” (active) fluid. The enzyme molecules are no longer thermally equilibrated but rather at a different energy state, and a tracer particle behaves as if it is in suspension in a bath at a higher temperature. Thus, our data are consistent with the arguments proposed by Burkholder and Brady in the context of tracers dispersed in dilute suspensions of active microscopic Brownian particles. Clearly, enzymes behave analogously to these larger micron-sized active particles and, despite their small size, they can affect transport properties

of other particles in their vicinity. Our results also allow quantitative prediction of size-dependent tracer diffusion in active enzyme solutions.

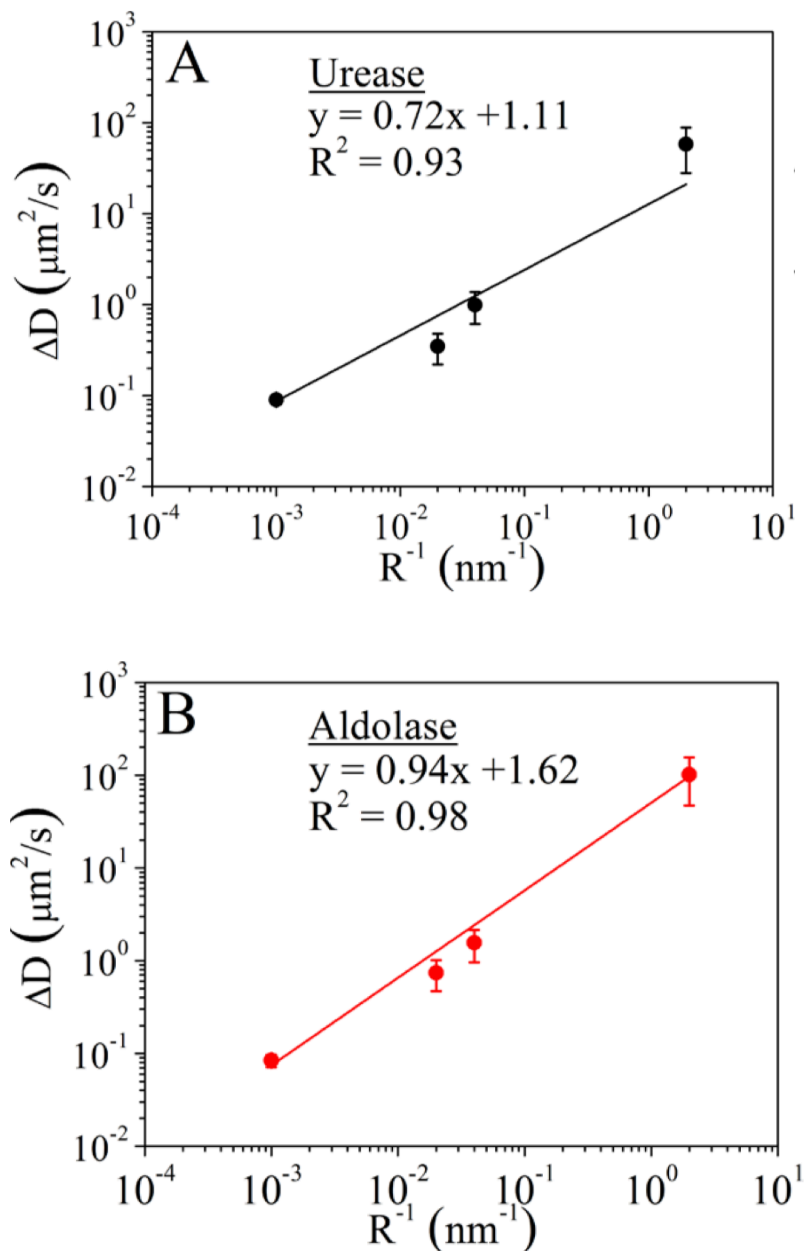


Figure 4-13. The change in tracer diffusion as a function of inverse tracer radius at the same enzyme and substrate concentrations (and therefore, at the same reaction rates). **(A)** For urease, the variation was measured for 10 nM enzyme and 10 mM urea concentration, **(B)** while for aldolase the enzyme and substrate concentrations were 10 nM and 1 mM respectively. Reprinted from *Nano Lett.* **2017**, *17*, 4807–4812 Copyright 2017.

4.3 Conclusion

In summary, active enzyme molecules have been found to influence the dynamics of their immediate surroundings significantly during catalytic reactions. Diffusion of passive tracers over a wide range of size increases in an activity dependent manner, similar to what has been reported for dilute microscopic swimmer suspensions. The enhanced diffusive transport of molecules and particles during enzymatic reactions has important scientific and technological impacts. The catalysis-induced force generation may be sufficient for the recently reported stochastic motion of the cytoplasm [30-32], cytoplasmic glass transitions, and enhanced mixing observed during metabolic transformations in bacterial cells [33]. Translocation within the cytoplasmic matrix is a fundamental requirement for proteins to be able to exert their functions in different organelles [26, 34]. *Momentum* transfer from freely diffusing active enzymes also suggests possible role of membrane-bound enzymes in exerting forces on cell-membranes, amplifying mechanically-induced signaling mechanisms [35].

4.4 Experimental Details

4.4.1 Urease Activity Assay

Activity assay of Jack bean urease was performed following the protocol reported in the literature [36, 37]. 6 mg/mL urease solution was prepared in de-ionized water and the actual concentration of urease in solution was determined by UV-vis spectroscopy. The absorbance of the solution measured at 280 nm was 0.170, which corresponded a concentration of 2.25 μ M. Phenol red was used as an indicator in activity assay, which changes color from yellow to pink with increasing pH. For the control, absorbance of 500 nM urea mixed with 28.2 μ M phenol red was measured at

560 nm. This was followed by measuring the absorbance of 1 μL of stock enzyme solution mixed with 500 nM urea and 28.2 μM phenol red in every 6 seconds. The total volume of the experimental solution was kept fixed at 1 mL. By measuring the rate of color change, we estimated the enzyme activity in solution. The rate of color change measured in our experiments is shown in the **Figure 4-14**.

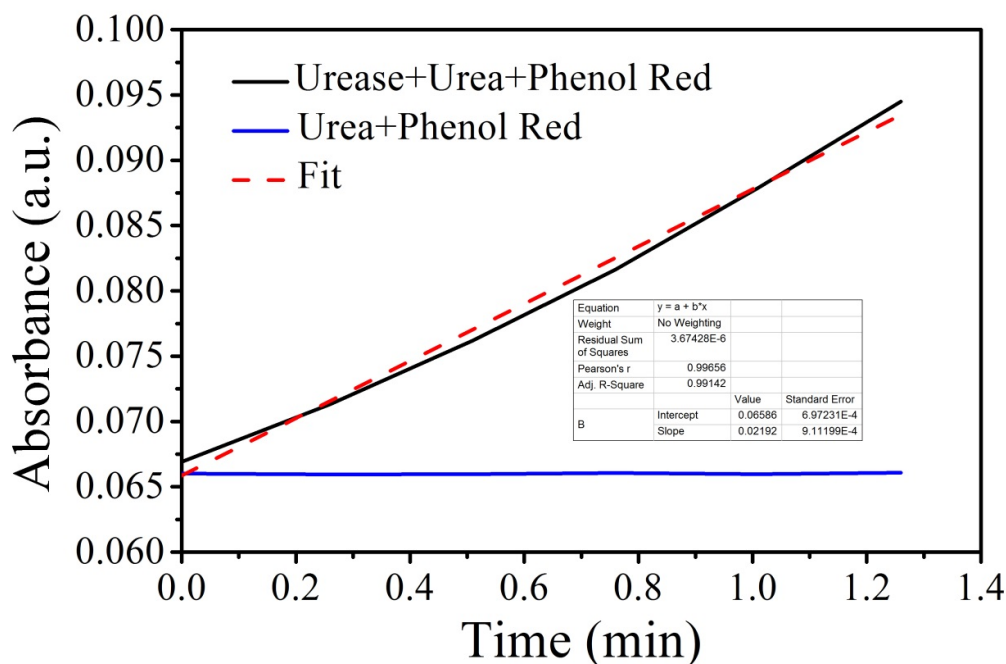


Figure 4-14. Colorimetric activity assay of urease. From the rate of change of absorbance with time, activity of the enzyme was estimated following the reference curve reported in Ref. (S1). The measured turnover number of Jack bean urease was 625/s. Reprinted from *Nano Lett.* **2017**, *17*, 4807–4812 Copyright 2017.

4.4.2 Fluorescence Correlation Spectroscopy (FCS) Measurements

We performed FCS using a custom-built microscope. Excitation light from a PicoTRAIN 532 nm, 80 MHz, 5.4 ps pulsed laser (High-Q Laser) was guided through an IX-71inverted

microscope (Olympus), with an Olympus 60×/1.2-NA water-immersion objective. Emitted fluorescent light from the sample was passed through a dichroic beam splitter, a set of high quality emission filters, and finally a polarizer fixed at an angle of 54.7° (Z520RDC-SP-POL, Chroma Technology), before focusing onto a 50 μm, 0.22-NA optical fiber (Thorlabs), which served as a confocal pinhole. The photomultiplier tube signal was routed to a preamplifier (HFAC-26), followed by a time-correlated single-photon counting (TCSPC) board (SPC-630, Becker and Hickl). The sample was positioned using a high-resolution 3D piezoelectric stage (NanoView, Mad City Laboratories). Photon arrival times were recorded on a SPC-630 module from Becker and Hickl (Berlin, Germany).

Fluorescent tracers moving in and out of the diffraction-limited observation volume induced bursts in fluorescence collected in first-in, first-out (FIFO) mode by the TCSPC board, which was incorporated in the instrument. Fluctuations in fluorescence intensity from the diffusion of particles were auto-correlated and fit by a multicomponent 3D model to determine the diffusion coefficients of the tracers. The autocorrelation of the intensity signal is defined by Eq. (4-1)

$$G(\tau) = \frac{1}{N} \left[1 + \left(\frac{\tau}{\tau_D} \right) \right]^{-1} \left[1 + \left(\frac{1}{w} \right)^2 \left(\frac{\tau}{\tau_D} \right) \right]^{-\frac{1}{2}}, \quad (4-1)$$

where

$$\tau_D = \frac{r^2}{4D} \quad (4-2)$$

Here, N is the average number of fluorescent tracers in the observation volume, τ is the autocorrelation time, w is the structure factor, which is defined as the ratio of height to width of the illumination profile ($\sim 4-8$), and τ_D is the characteristic diffusion time of the fluorescent particle with diffusion coefficient D crossing a circular area with radius r (~ 400 nm). The measurements were performed with 30.2 μW excitation power, and the optical system was calibrated before each

experiment using free 50 nm fluorescent tracers in double distilled water. Autocorrelation curves were fit to Eq. (4-1) using Levenberg–Marquardt non-linear least squares regression algorithm with Origin software to determine τ_D . The quality of the fitted curves was assessed based on chi-square (χ^2) values. The experimental solutions were prepared in deionized water instead of phosphate buffer, since in the presence of free ions the tracer particles were found to agglomerate, resulting in distortions in the recorded signal.

4.4.3 Coating Tracer Particle Surface with Bovine Serum Albumin

Polystyrene sulfate latex microspheres (8% w/v, Life Technologies) were passivated towards enzyme adsorption by coating their surfaces with Bovine Serum Albumin (BSA, Sigma-Aldrich). BSA makes polystyrene surfaces hydrophilic, which not only prevents aggregation of the tracers in solution but also minimizes adsorption of enzymes over their surfaces. Further, coating the micron scale tracer surfaces with BSA does not significantly alter their hydrodynamic radii because of the negligible molecular size of albumin (3.5 nm) [24]. For our experiments, approximately 50 μL of stock solution of tracers was mixed with 200 μL of 10 mg/mL ($\sim 150 \mu\text{M}$) BSA solution prepared in 10 mM phosphate buffer (pH=7.2). The mixture was kept undisturbed for 20 min and then centrifuged three times at 6000 rpm for 7 min to remove unreacted BSA from the suspension. The filtered microspheres were dispersed in 500 μL of fresh deionized water and used as tracers in DLS measurements.

To confirm that the BSA coating of the polymer surface minimizes enzyme adsorption, 30 μL of BSA treated particles was dispersed in 200 μL of $\sim 1 \mu\text{M}$ urease (Jack bean, Sigma-Aldrich), tagged with DyLight 550 Maleimide dye (Thermo Scientific, ex/em: 557/572). The tracers were kept in enzyme solution for 10 min and then centrifuged three times at 6000 rpm for 7 min to remove free

unreacted enzyme-dye complex. The filtered particles were dispersed in 200 μ L deionized water and were imaged under fluorescence microscope Nikon Eclipse TE300 (Nikon, Japan) with Nikon HMX-4 Mercury Lamphouse. The BSA treated particles were not found to be fluorescent, suggesting negligible amount of enzyme adsorption over their surfaces. In contrast, experiments carried out with particles not treated with BSA showed highly fluorescent beads, implying deposition of enzymes over the polymers. Similar results were obtained for beads dispersed in solution of catalase tagged with Alexa Fluor 594 dye. The results of fluorescence measurement are shown in the **Figure 4-15**. That the lack of fluorescence observed in case of BSA treated beads was due to the passivation of tracer surface and not due to the fluorescence quenching by BSA was further confirmed by measuring the fluorescence of tagged urease solution in the presence of varying concentration of BSA, **Figure 4-16**.

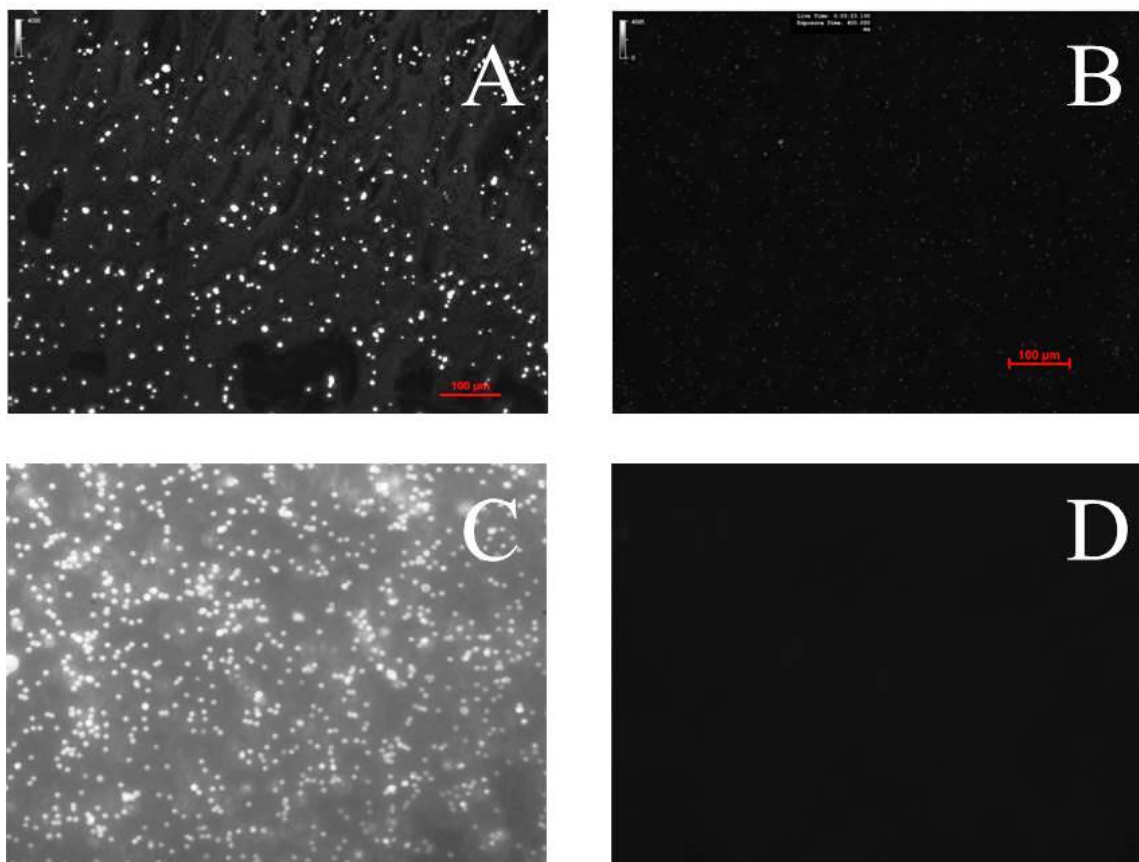


Figure 4-15. (A-B) Fluorescence images of 2 μm polystyrene sulfate tracers (A) without and (B) with BSA coatings, after treating them with DyLight 550 Maleimide dye tagged urease solution for 10 min. Images (C-D) shows similar experiments carried out with catalase tagged with Alexa Fluor 594 dyes. BSA coating significantly minimized adsorption of enzymes on the particle surface. Reprinted from *Nano Lett.* **2017**, *17*, 4807–4812 Copyright 2017.

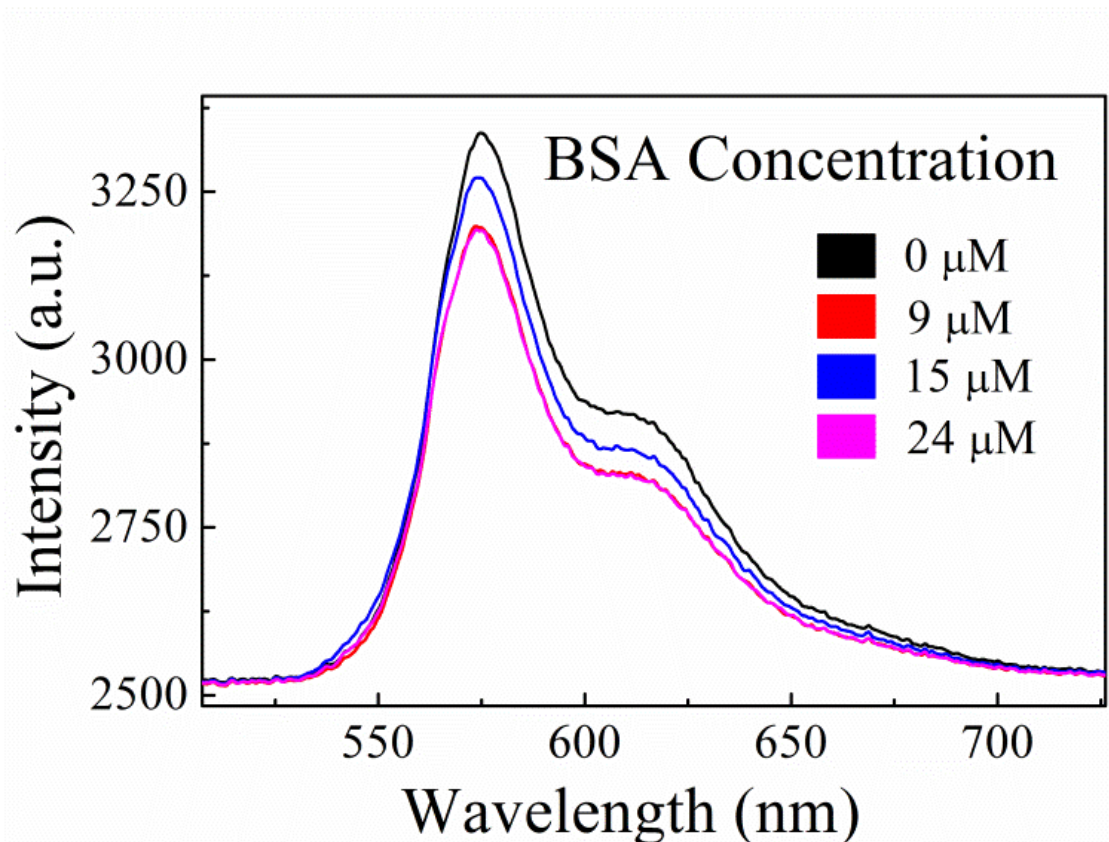


Figure 4-16. (A-B) Fluorescence images of 2 μm polystyrene sulfate tracers (A) without and (B) with BSA coatings, after treating them with DyLight 550 Maleimide dye tagged urease solution for 10 min. Images (C-D) shows similar experiments carried out with catalase tagged with Alexa Fluor 594 dyes. BSA coating significantly minimized adsorption of enzymes on the particle surface. Reprinted from *Nano Lett.* **2017**, *17*, 4807–4812 Copyright 2017.

4.4.4 DLS measurements

DLS measurements were carried out in a Malvern Zetasizer ZS instrument with 10 nM urease and varying concentrations of urea (0-10 mM). In each measurement, after preparing the mixture of urease and urea (1 mL), 10 μ L of BSA treated tracer solution was added to it. The solution was then placed inside the DLS chamber in a capped disposable cuvette and was thermally equilibrated for 2 mins before recording the particles' diffusion. Similar experiments were carried out with tracers dispersed in 10 nM aldolase and (0-1) mM FBP; 200 nM catalase and (0-1) mM H_2O_2 , prepared in de-ionized water. The measurements were all carried out at 25 $^{\circ}C$, considering the particle refractive index and absorbance to be 1.59 and 0.01 respectively **Figure 4-17**.

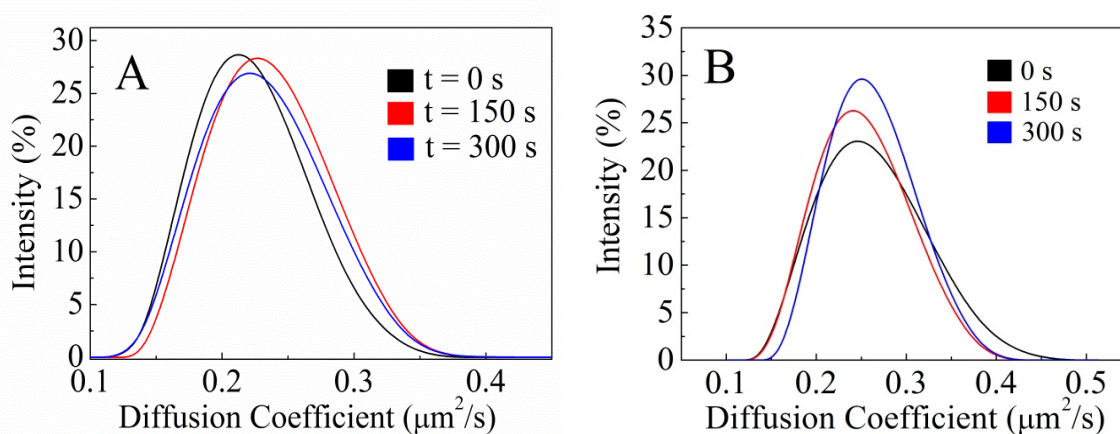


Figure 4-17. Diffusion coefficient distribution of 2 μ m polystyrene sulfate tracers, coated with BSA, dispersed in (A) DI Water and (B) 10 mM Urea, recorded in DLS. The measurements were taken successively at three different times. The measured diffusion of the tracers is $0.23 \pm 0.01 \mu\text{m}^2/\text{s}$ in DI water and $0.24 \pm 0.01 \mu\text{m}^2/\text{s}$ in 10 mM urea. Reprinted from *Nano Lett.* **2017**, *17*, 4807–4812 Copyright 2017.

4.5 Acknowledgements

Xi Zhao would like to acknowledge Penn State MRSEC under NSF grant DMR-1420620. Xi Zhao thank Penn State Materials Characterization Laboratory for providing with Dynamic Light Scattering measurement facility. The author acknowledges Dr. Peter J. Butler, Dr. Krishna Kanti Dey and Selva Jeganathan for assistance with FCS measurements, and thank Ubaldo M. Córdova-Figueroa for insightful discussions on theory part.

4.6 References

- [1] Kapral, R. Nanomotors without Moving Parts that Propel Themselves in Solution. *J. Chem. Phys.* **2013**, *138*, 020901.
- [2] Solovev, A. A.; Sanchez, S.; Schmidt, O. G. Collective Behaviour of Self-propelled Catalytic Micromotors. *Nanoscale* **2013**, *5*, 1284- 1293.
- [3] Wang, W.; Duan, W.; Ahmed, S.; Sen, A.; Mallouk, T. E. From One to Many: Dynamic Assembly and Collective Behavior of Self-Propelled Colloidal Motors. *Acc. Chem. Res.* **2015**, *48*, 1938- 1946.
- [4] Kasyap, T. V.; Koch, D. L.; Wu, M. Hydrodynamic Tracer Diffusion in Suspensions of Swimming Bacteria. *Phys. Fluid* **2014**, *26*, 081901.
- [5] Minõ, G. L.; Dunstan, J.; Rousselet, A.; Clément, E.; Soto, R. Induced Diffusion of Tracers in a Bacterial Suspension: Theory and Experiments. *J. Fluid Mech.* **2013**, *729*, 423- 444.
- [6] Peng, Y.; Lai, L.; Tai, Y.-S.; Zhang, K.; Xu, X.; Cheng, X. Diffusion of Ellipsoids in Bacterial Suspensions. *Phys. Rev. Lett.* **2016**, *116*, 06830
- [7] Leptos, K.C.; Guasto, J. S.; Gollub, J. P.; Pesci, A. I.; Goldstein, R. E. Dynamics of Enhanced Tracer Diffusion in Suspensions of Swimming Eukaryotic Microorganisms. *Phys. Rev. Lett.* **2009**, *103*, 198103.
- [8] Kurtuldu, H.; Guasto, J. S.; Johnson, K. A.; Gollub, J. P. Enhancement of Biomixing by Swimming Algal Cells in Two-dimensional Films. *Proc. Natl. Acad. Sci. U. S. A.* **2011**, *108*, 10391- 10395.

- [9] Minõ, G.; Mallouk, T. E.; Darnige, T.; Hoyos, M.; Dauchet, J.; Dunstan, J.; Soto, R.; Wang, Y.; Rousselet, A.; Clement, E. Enhanced Diffusion Due to Active Swimmers at a Solid Surface. *Phys. Rev. Lett.* **2011**, *106*, 048102.
- [10] Orozco, J.; Jurado-Sánchez, B.; Wagner, G.; Gao, W.; Vazquez-Duhalt, R.; Sattayasamitsathit, S.; Galarnyk, M.; Cortés, A.; Saintillan, D.; Wang, J. Bubble-Propelled Micromotors for Enhanced Transport of Passive Tracers. *Langmuir* **2014**, *30*, 5082- 5087.
- [11] Valeriani, C.; Li, M.; Novosel, J.; Arlt J.; Marenduzzo, D. Colloids in a Bacterial Bath: Simulations and Experiments. *Soft Matter* **2011**, *7*, 5228- 5238.
- [12] Morozov, A.; Marenduzzo, D. Enhanced Diffusion of Tracer Particles in Dilute Bacterial Suspensions. *Soft Matter* **2014**, *16*, 2748-2758.
- [13] Wu, X. L.; Libchaber, A. Particle Diffusion in a Quasi-Two-Dimensional Bacterial Bath. *Phys. Rev. Lett.* **2000**, *84*, 3017
- [14] Kim, M. J.; Breuer, K. S. Enhanced Diffusion due to Motile Bacteria. *Phys. Fluid* **2004**, *16*, L78.
- [15] Wilson, L. G.; Martinez, V. A.; Schwarz-Linek, J.; Tailleur, J.; Bryant, G.; Pusey, P. N.; Poon, W. C. K. Differential Dynamic Microscopy of Bacterial Motility. *Phys. Rev. Lett.* **2011**, *106*, 018101.
- [16] Muddana, H. S.; Sengupta, S.; Mallouk, T. E.; Sen, A.; Butler, P. J. Substrate Catalysis Enhances Single Enzyme Diffusion. *J. Am. Chem. Soc.* **2010**, *132*, 2110.
- [17] Sengupta, S.; Dey, K. K.; Muddana, H. S.; Tabouillot, T.; Ibele, M. E.; Butler, P. J.; Sen, A. Enzyme Molecules as Nanomotors. *J. Am. Chem. Soc.* **2013**, *135*, 1406.
- [18] Sengupta, S.; Spiering, M. M.; Dey, K. K.; Duan, W.; Patra, D.; Butler, P. J.; Astumian, R. D.; Benkovic, S. J.; Sen, A. DNA Polymerase as a Molecular Motor and Pump. *ACS Nano* **2014**, *8*, 2410.
- [19] Dey, K. K.; Das, S.; Poyton, M. F.; Sengupta, S.; Butler, P. J.; Cremer, P. S.; Sen, A. Chemotactic Separation of Enzymes. *ACS Nano* **2014**, *8*, 11941- 11949.
- [20] Laidler, K. J.; Hoare, J. P. The Molecular Kinetics of the Urea- Urease System. III. Heats and Entropies of Complex Formation and Reaction. *J. Am. Chem. Soc.* **1950**, *72*, 2489- 2492.
- [21] Nag, S.; Sarkar, B.; Bandyopadhyay, A.; Sahoo, B.; Sreenivasan, V. K. A.; Kombrabail, M.; Muralidharan, C.; Maiti, S. Nature of the Amyloid- β Monomer and the Monomer-oligomer Equilibrium. *J. Biol. Chem.* **2011**, *286*, 13827.
- [22] Goldberg, R. N.; Tewari, Y. B. Thermodynamics of Enzyme-Catalyzed Reactions: Part 4. Lyases. *J. Phys. Chem. Ref. Data* **1995**, *24*, 1669.

- [23] Callens, M.; Opperdoes, F. R. Kinetic Properties of Fructose Bisphosphate Aldolase from *Trypanosoma Brucei* Compared to Aldolase from Rabbit Muscle and *Staphylococcus Aureus* *Mol. Biochem. Parasitol.* **1991**, *47*, 1- 9.
- [24] Flecha, F. L. G.; Levi, V. Determination of the Molecular Size of BSA by Fluorescence Anisotropy. *Biochem. Mol. Biol. Educ.* **2003**, *31*, 319.
- [25] Kot, M.; Zaborska, W. Irreversible Inhibition of Jack Bean Urease by Pyrocatechol. *J. Enzym. Inhib. Med. Chem.* **2003**, *18*, 413.
- [26] Mikhailov, A. S.; Kapral, R. Hydrodynamic Collective Effects of Active Protein Machines in Solution and Lipid Bilayers. *Proc. Natl. Acad. Sci. U. S. A.* **2015**, *112*, E3639.
- [27] Illien, P.; Zhao, X.; Dey, K. K.; Butler, P. J.; Sen, A.; Golestanian, R. Exothermicity Is Not a Necessary Condition for Enhanced Diffusion of Enzymes. *Nano Lett.* **2017**, *17* (7), 4415–4420.
- [28] Patterson, A. E.; Gopinath, A.; Purohit, P. K.; and Arratia P. E. Particle Diffusion in Active Fluids is Non-monotonic in Size. *Soft Matter*, **2016**, *12*, 2365- 2372.
- [29] Burkholder, E. W.; Brady, J. F. Tracer Diffusion in Active Suspensions. *Phys. Rev. E*, **2017**, *95*, 052605.
- [30] Weber, S. C.; Spakowitz, A. J.; Theriot, J. A. Nonthermal ATP-dependent Fluctuations Contribute to the in vivo Motion of Chromosomal Loci. *Proc. Natl. Acad. Sci. U. S. A.* **2012**, *109*, 7338.
- [31] Guo, M.; Ehrlicher, A. J.; Jensen, M. H.; Renz, M.; Moore, J. R.; Goldman, R. D.; Lippincott-Schwartz, J.; Mackintosh, F. C.; Weitz, D. A. Probing the Stochastic, Motor-Driven Properties of the Cytoplasm Using Force Spectrum Microscopy. *Cell* **2014**, *158*, 822.
- [32] Brangwynne, C. P.; Koenderink, G. H.; MacKintosh, F. C.; Weitz, D. A. Cytoplasmic diffusion: Molecular Motors Mix it up. *J. Cell Biol.* **2008**, *183*, 583.
- [33] Parry, B. R.; Surovtsev, I. V.; Cabeen, M. T.; O'Hern, C. S.; Dufresne, E. R.; Jacobs-Wagner, C. The Bacterial Cytoplasm Has Glass-like Properties and Is Fluidized by Metabolic Activity. *Cell* **2014**, *156*, 183.
- [34] Hung, M.-C.; Link, W. Protein Localization in Disease and Therapy. *J. Cell Sci.* **2011**, *124*, 3381.
- [35] Lodish, H.; Berk, A.; Zipursky, S. L.; Matsudaira, P.; Baltimore, D.; Darnell, J. *Molecular Cell Biology*, W. H. Freeman: New York, 2000.
- [36] Okyay, T.O.; Rodrigues, D. F. High Throughput Colorimetric Assay for Rapid Urease Activity Quantification. *J. Microbiol. Meth.* **2013**, *95*, 324.

- [37] Minakami, S.; Verdier, C. Calorimetric Study on Human Erythrocyte Glycolysis: Heat Production in Various Metabolic Concdition. *Eur. J. Biochem.* **1976**, *460*, 451.

Chapter 5

Micromotors Powered by Enzyme Catalysis in the Microfluidic Channel

This chapter is an adapted reproduction from *Nano Lett.* **2015**, *15* (12), 8311–8315 with permission from the American Chemistry Society.

5.1 Introduction

Catalytically-powered synthetic motors that mimic the behavior of biomolecular motors and microorganisms have attracted considerable attention due to their possible applications in nanoscale assembly [1], micro-robotics [2-4], and chemical/biochemical sensing [5-10]. In particular, a major incentive for the use of autonomous motors for drug or cargo delivery [11-12] is that targeted motion, when compared to passive diffusion, allows for faster delivery and the use of less material [13]. Important hurdles remain, however, before practical *in vivo* applications of motors become a reality. First, the motors should move in biological fluids that typically have high ion content. This eliminates motility based on self-electrophoresis or ionic diffusiophoresis mechanisms [14]. Second, the micro-transporters must be derived from biocompatible materials and should use fuels that are also biocompatible [12, 15]. Ideally, the motors should employ enzymes as catalysts and substrates usually present in living systems [16-21]. Finally, the most “futuristic” scenario involves the design of populations of synthetic micromotors that have the ability to organize themselves, based on signals from their environment, to perform complex tasks [22]. Particularly attractive are designs that allow coordinated movement of particles with different functionalities. Here we demonstrate a general procedure for the fabrication of microparticles powered by enzymatic reactions. In addition, ensembles of active microparticles can be directed by substrate gradients, in principle allowing for

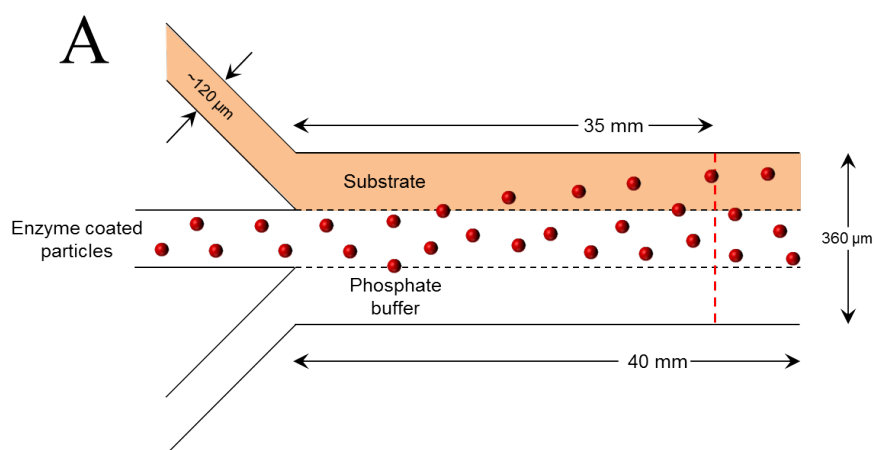
cargo delivery at specific locations. Single enzyme molecules have already been reported to undergo enhanced diffusion through substrate turnover to cause their own movement [23-25]. Furthermore, they show directional chemotaxis in the presence of a substrate gradient [24-26]. In this chapter, we therefore, sought to examine whether enzymes can impart directional drift to micron-size particles when tethered to the latter.

5.2 Results and Discussion

The observed substrate concentration-dependent enhancement in the diffusion of enzyme-powered micromotors encouraged us to investigate their behavior with respect to externally imposed substrate concentration gradients. We used fluorescent streptavidin-functionalized polystyrene particles of diameter 2 μm (Fluoresbrite® YG Microspheres, Polysciences, ex/em = 441/486), coated uniformly with biotinylated catalase and urease and allowed the particle dispersion to flow through the center of a three-inlet microfluidic architecture **Figure 5-1A**. Either buffer (control) or the appropriate substrate solution was allowed to flow through the side channels. Enhanced chemotactic shifts of the micromotors in response to substrate gradients when compared to simple diffusive spread in the buffer solution were measured at specific positions along the length of the channel. The fluorescence intensity was always measured across the channel width, leaving approximately 15 μm from either end, close to the channel walls. This was done to minimize the effect of background fluorescence of the PDMS wall on the recorded signal [27-28].

For chemotaxis of urease motors, a solution of enzyme-coated fluorescent microspheres was introduced through the center of the three-inlet device with a flow speed of 50 $\mu\text{L/h}$. Through the adjacent inlets, a solution of either 10 or 100 mM urea prepared in 10 mM phosphate buffer or simply 10 mM buffer without urea (control) was introduced at the same flow rate. After the system attained steady state, sustained concentration gradients of substrate were formed across the interface of the

laminar flows. The urease-coated particles, upon interacting with urea concentration gradients displayed chemotactic drift towards regions of higher substrate concentrations. The drift can be quantified by monitoring the normalized fluorescence intensity profile of the particles across the width of the microchannel using a confocal microscope at specific positions along the length of the microchannel. In our experiments, we usually measured and compared the shifts at 38 mm away from the start of the inlets. As shown in **Figure 5-1B**, there is a greater spreading of the particles when urea rather than buffer alone is present in both the flanking channels. When urea is introduced into one side channel and buffer only in the other, there is a clear preferential spreading of the particles towards the urea containing channel **Figure 5-1D**



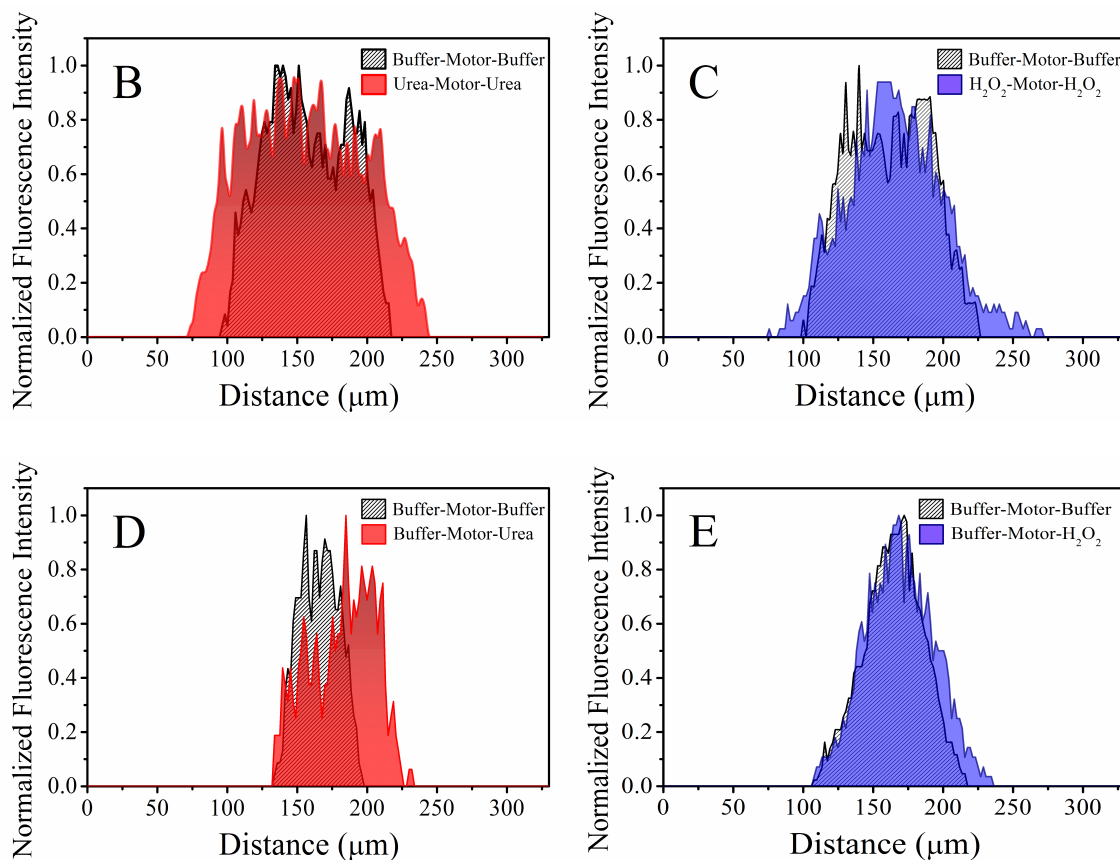


Figure 5-1. (A) Schematic of the three-inlet microfluidic set up used to observe chemotaxis of enzyme coated particles towards higher substrate concentrations. The excess migration of the functionalized particles towards the substrate side was quantified by measuring the fluorescence intensity of the polymer spheres along a straight line across the channel (shown in red) at a distance of 38 mm from the start. The figure also shows chemotactic migration of (B, D) urease and (C, E) catalase coated fluorescent microspheres in presence of imposed substrate concentration gradients, observed within three-inlet microfluidic channels. The enzyme functionalized particles are flown through the middle channel of the device, while through the side channels, either buffer alone or buffered solution of appropriate substrates are introduced at the same flow rate. Reprinted from *Nano Lett.* **2015**, *15* (12), 8311–8315. Copyright 2015.

Figure 5-1C shows greater spreading of catalase coated fluorescent microspheres in the presence of 1 mM H_2O_2 , flowing through the flanking channels compared to buffer alone. The flow speed of liquid through the inlets was maintained at 100 $\mu L/h$. Lower H_2O_2 concentration and higher

flow rate was employed to minimize the formation of oxygen bubbles within the microfluidic channel during the measurements and resulting distortion of flow profiles. Experiments performed with substrate and phosphate buffer alone flowing through the side channels simultaneously showed preferential migration of the particles towards the substrate side **Figure 5-1E**. Note that due to particle settling, the intensity profiles are different in different z-planes along the depth of the microfluidic channel. For each set of measurements, signals were recorded at the same z-plane under identical conditions.

By measuring the chemotactic shift at different positions in the microfluidic channel along its length, the magnitude of the shift as a function of time was obtained for urease-coated particles. For laminar flows of liquid under steady state conditions, different positions along the length of the microchannel will correspond to different interaction times for the enzyme coated particles with the imposed substrate concentration gradients. This allows us to correlate the chemotactic shift with the duration of the substrate-particle interaction (defined as the reaction time). As shown in **Figure 5-2A**, the chemotactic shift of particles towards the substrate side increases linearly with reaction time for constant concentration of substrate at the inlet (10 mM urea for urease coated microparticles). Also, as shown in **Figure 5-2B**, for increased concentration gradient of urea (obtained by increasing urea concentration at the inlet), the magnitude of chemotactic shifts can also be increased. These results demonstrate that substrate catalysis by enzymes anchored to a particle surface lead not only to their directional migration along the substrate gradient, but the extent of the migration can also be controlled by changing either the substrate-particle interaction times or the concentration of substrate at the inlet.

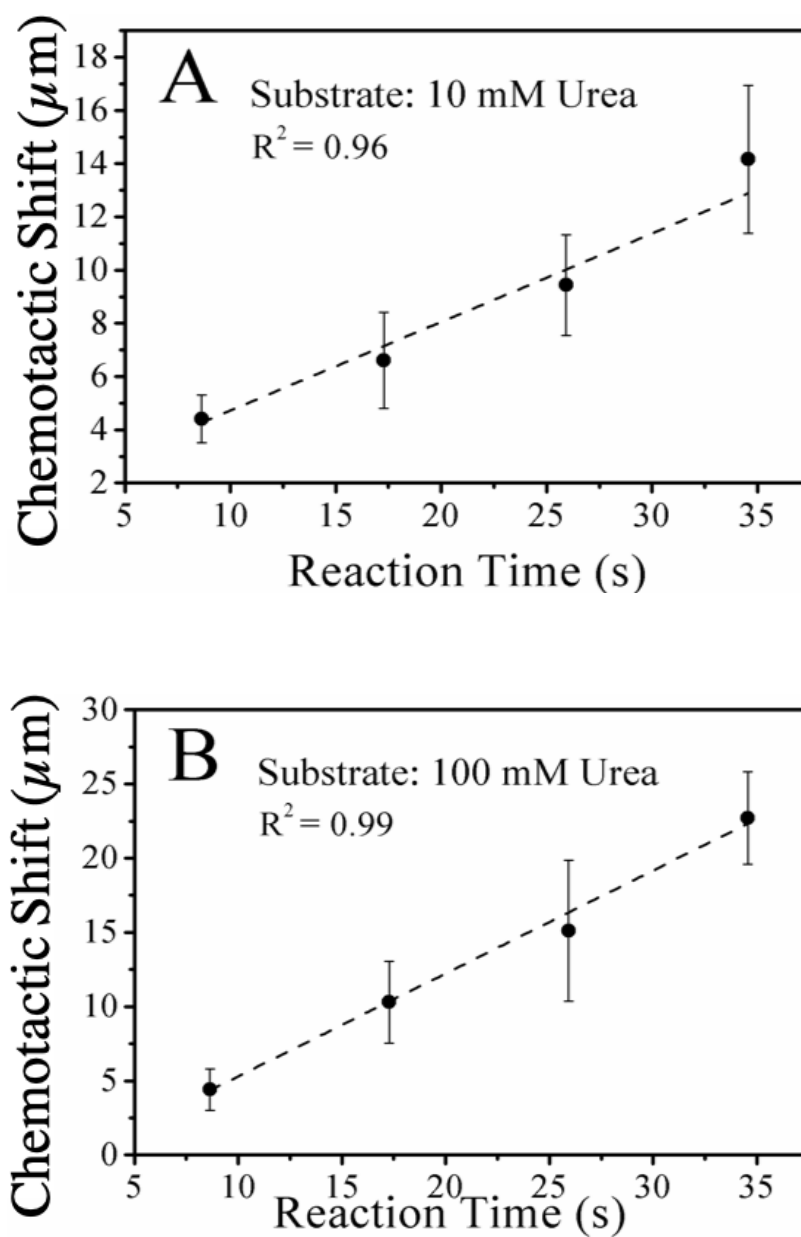


Figure 5-2. Chemotactic migrations of urease coated microparticles measured at different times (at different positions of the microfluidic channel along its length, from the start) at (A) 10 mM and (B) 100 mM urea. The error bars represent standard deviations for six independent measurements. Reprinted from *Nano Lett.* **2015**, *15* (12), 8311–8315. Copyright 2015.

5.3 Conclusion

In this work, we have demonstrated that enzymatic reactions may be utilized to power micron-sized polymer particles in solution. In addition, these hybrid micromotors can respond to specific chemical signals by moving directionally towards specific regions in space. The results constitute the first steps in the fabrication biocompatible, multifunctional hybrid motors for carrying out specific functions under physiological conditions.

5.4 Experimental Details

5.4.1 Coating of Streptavidin-functionalized Polystyrene Microspheres with Biotinylated Enzymes

To examine the chemotaxis of enzyme-coated microparticles in the presence of substrates, fluorescent streptavidin-functionalized polystyrene particles of diameter 2 μm (Fluoresbrite® YG Microspheres, Polysciences, ex/em = 441/486) were coated with catalase and urease following the same protocol, **Figure 5-3**. 2.0 μm streptavidin-functionalized polystyrene microspheres (Spherotech and Polysciences) were coated with biotinylated urease (from *Canavalia ensiformis*, Sigma-Aldrich) and catalase (from bovine liver, Sigma-Aldrich), prepared in 10 mM phosphate buffer, 7.2 pH. EZ-Link-Maleimide-PEG2-Biotin (Life Technologies) was used to tag thiol groups of urease and thereby binding the enzymes in a specific and unobtrusive manner. This reaction with EZ-Link-Maleimide-PEG2-Biotin occurs at a pH between 6.5 and 7.5. To tag catalase, EZ-Link-Sulfo-NHS-Biotin ((Life Technologies) was used. This reacts with free primary amines in the enzyme structure. The tagging was performed by mixing enzyme and biotin solutions, both diluted in 100 mM phosphate buffer.

To assure that every enzyme was tagged with biotin, a 4:1 enzyme-biotin ratio was maintained. Prior to synthesis, we estimated the concentration of enzyme required to achieve complete monolayer coverage of the microparticles. An excess of enzyme was typically employed. The enzyme-biotin solution was left for 2 hours in a mechanical shaker (speed 500 rpm) in order to allow the reaction to be completed. A calculated volume of streptavidin-functionalized polystyrene beads suspension was mixed with the enzyme-biotin solution and placed at 4°C for 30 min followed by 30 min in mechanical shaker (speed 500 rpm) at room temperature. To remove excess enzymes, the suspension of functionalized particles was centrifuged at 4500 rpm for 7 min for four successive cycles, re-dispersing the particles in 10 mM phosphate buffer after each cycle. The final solution was adjusted to approximately 500 μ L by adding fresh 10 mM buffer.

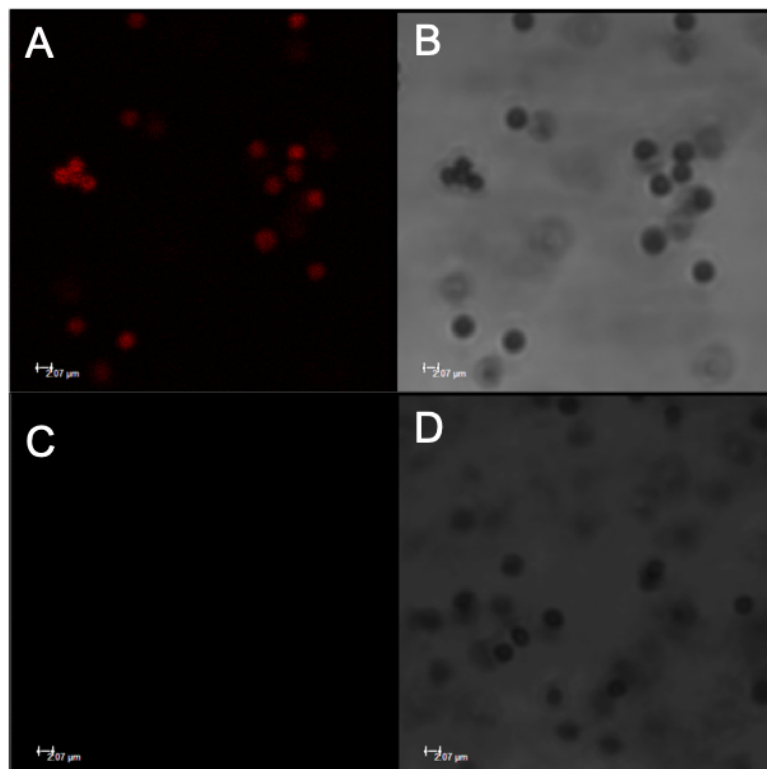


Figure 5-3. Fluorescence and optical microscopy images of (A) 2 μ m streptavidin-functionalized polystyrene particles coated with tagged biotinylated catalase and (B) uncoated 2 μ m streptavidin-

functionalized polystyrene particles. Reprinted from *Nano Lett.* **2015**, *15* (12), 8311–8315. Copyright 2015.

5.4.2 Microfluidic Channel Fabrication

Microchannel masters were fabricated over silicon wafers in the Nanofabrication Laboratory of Materials Research Institute at Penn State. Before photolithography, wafers were cleaned with acetone and then air-dried properly. These were then spin-coated with 5 mL of SPR-955 photoresist (Microposit) at 200 rpm for 10 s and then at 1000 rpm for 30 s. The coated wafers were then soft-baked over a hot plate at 100 °C for 5 min. The microchannel geometry was modelled in CAD and printed over a chrome-on-glass mask (Nanofabrication Laboratory, Materials Research Institute, Penn State). The mask was placed in contact with the photoresist over the wafers and the resist was exposed to UV radiation for 40 s in a Karl Suss MA/BA6 Contact Aligner. This was then followed by post-baking the wafer for 5 min over a hot plate at 100 °C to cross link the exposed film. To remove unexposed SPR 220 from the wafers, the mold was developed in CD26 developer for 2 min while being agitated, followed by washing thoroughly with deionized water. The wafers were then dried with a nitrogen blower followed by creation of a 100 µm deep master pattern over them using deep reactive ion etching facilities (Alcatel).

Polydimethylsiloxane (PDMS, Sylgard™ 184, Dow Corning) elastomer solution was prepared by mixing pre-polymer with a cross-linking agent in weight ratio of 10:1. To minimize adhesion of PDMS to the surface, the wafers were exposed to trichloro (1H, 1H, 2H, 2H-perfluorooctyl) silane (Sigma Aldrich) before the PDMS solution was poured over them. The PDMS solution was poured on top of the wafers to the desired thickness. They were then degassed in vacuum for about an hour to remove air bubbles from the PDMS mixture. The masters were then heated in

an oven at 60 °C for 2 h. After curing, the PDMS channels were peeled from the mold and inlets/outlets were made using a stainless steel puncher. The devices were sealed to glass coverslips (VWR) by exposing them to oxygen plasma, followed by bonding them together manually and baking them on a hot plate at 100 °C for 2 min. The PDMS channels were connected to polyethylene tubes (SPC Technology, Internal diameter 0.66 mm) and fluid flow through them was controlled using syringe pumps.

5.4.3 Confocal Set-up

Confocal images were recorded using a Leica TCS SP5 laser scanning confocal inverted microscope (LSCM, Leica Microsystems) with a 10× objective (HCX PL APO CS, 0.70 NA) incorporated in it. The plane of interest (along the *z*-axis) for confocal imaging of the fluorescence intensity was about half of the channel depth. In each experiment, videos were recorded from three experiments and the mean fluorescence intensity was determined using ImageJ software. Each video was recorded for over 5 min, resulting in a collection of 633 images. A region of interest (ROI) was selected along the channel to be at 38 μm, and the stack-averaged fluorescence intensity was plotted as a function of distance along the width of the channel.

5.5 Acknowledgements

This work was supported by Penn State MRSEC funded by the National Science Foundation (DMR-1420620). Xi Zhao would like to acknowledge Dr. Krishna Kanti Dey and Ben Tensi for their help with enzyme coated particle preparation and experimental design discussions.

5.6 References

- [1] Wang, W.; Duan, W.; Ahmed, S.; Sen, A.; Mallouk, T. E. From One to Many: Dynamic Assembly and Collective Behavior of Self-Propelled Colloidal Motors. *Acc. Chem. Res.* **2015**, *48*, 1938-1946.
- [2] Sengupta, S.; Ibele, M. E.; Sen, A. Fantastic Voyage: Designing Self-powered Nanorobots. *Angew. Chem., Int. Ed.* **2012**, *51*, 8434-8445.
- [3] Sánchez, S.; Soler, L.; Katuri, J. Chemically Powered Micro- and Nanomotors. *Angew. Chem., Int. Ed.* **2015**, *54*, 1414-1444.
- [4] Wang, H.; Pumera, M. Fabrication of Micro/Nanoscale Motors. *Chem. Rev.* **2015**, *115*, 8704-8735.
- [5] Duan, W.; Wang, W.; Das, S.; Yadav, V.; Mallouk, T. E.; Sen, A. Synthetic Nano- and Micromachines in Analytical Chemistry: Sensing, Migration, Capture, Delivery, and Separation. *Annu. Rev. Anal. Chem.* **2015**, *8*, 311-333.
- [6] Campuzano, S.; Kagan, D.; Orozco, J.; Wang, J. Motion-driven Sensing and Biosensing Using Electrochemically Propelled Nanomotors. *Analyst* **2011**, *136*, 4621-4630.
- [7] Guix, M.; Mayorga-Martinez, C. C.; Merkoçi, A. Nano/Micromotors in (Bio)chemical Science Applications. *Chem. Rev.* **2014**, *114*, 6285-6322.
- [8] Hong, Y.; Blackman, N. M. K.; Kopp, N. D.; Sen, A.; Velegol, D. Chemotaxis of Nonbiological Colloidal Rods. *Phys. Rev. Lett.* **2007**, *99*, 178103.
- [9] Baraban, L.; Harazim, S. M.; Sanchez, S.; Schmidt, O. G. Chemotactic Behavior of Catalytic Motors in Microfluidic Channels. *Angew. Chem., Int. Ed.* **2013**, *52*, 5552-5556.
- [10] Bunea, A-I.; Pavel, I-A.; David, A.; Gáspár, S. Sensing Based on the Motion of Enzyme-Modified Nanorods. *Biosens. Bioelectron.* **2015**, *67*, 42-48.
- [11] Baraban, L.; Tasinkevych, M.; Popescu, M. N.; Sanchez, S.; Dietrich S.; Schmidt, O. G. Transport of Cargo by Catalytic Janus Micro-motors. *Soft Matter* **2012**, *8*, 48-52.
- [12] Patra, D.; Sengupta, S.; Duan, W.; Zhang, H.; Pavlick, R.; Sen, A. Intelligent, Self-powered, Drug Delivery Systems. *Nanoscale* **2013**, *5*, 1273-1283.
- [13] Brangwynne, C. P.; Koenderink, G. H.; MacKintosh, F. C.; Weitz, D. A. Intracellular Transport by Active Diffusion. *Trends Cell Biol* **2009**, *19*, 423-427.
- [14] Wang, W.; Duan, W.; Ahmed, S.; Mallouk, T. E.; Sen, A. Autonomous Nano- and Micromotors Propelled by Self-generated Gradients. *Nano Today* **2013**, *8*, 531-554.

- [15] Zhang, H.; Duan, W.; Liu, L.; Sen, A. Depolymerization-Powered Autonomous Motors Using Biocompatible Fuel. *J. Am. Chem. Soc.* **2013**, *135*, 15734-15737.
- [16] Peng, F.; Tu, Y.; van Hest, J. C. M.; Wilson, D. A. Self-Guided Supramolecular Cargo-Loaded Nanomotors with Chemotactic Behavior towards Cells. *Angew. Chem., Int. Ed.* **2015**, *54*, 11662-11665.
- [17] Mano, N.; Heller, A. Bioelectrochemical Propulsion. *J. Am. Chem. Soc.* **2005**, *127*, 11574-11575.
- [18] Gáspár, S. Enzymatically Induced Motion at Nano- and Micro-scales. *Nanoscale* **2014**, *6*, 7757-7763.
- [19] Ma, X.; Jannasch, A.; Albrecht, U-R.; Hahn, K.; Miguel-López, A.; Schäffer, E.; Sánchez, S. Enzyme-Powered Hollow Mesoporous Janus Nanomotors. *Nano Lett.* **2015**, *15*, 7043-7050.
- [20] Bunea, A-I.; Pavel, I-A.; Davis, S.; Gáspár, S. Modification with Hemeproteins Increases the Diffusive Movement of Nanorods in Dilute Hydrogen Peroxide Solutions. *Chem. Commun.* **2013**, *49*, 8803-8805.
- [21] Pavel, I-A.; Bunea, A-I.; David, S.; Gáspár, S. Nanorods with Biocatalytically Induced Self-electrophoresis. *Chem. Cat. Chem.* **2014**, *6*, 866-872.
- [22] Duan, W.; Liu, R.; Sen, A. Transition between Collective Behaviors of Micromotors in Response to Different Stimuli. *J. Am. Chem. Soc.* **2013**, *135*, 1280-1283.
- [23] Muddana, H. S.; Sengupta, S.; Mallouk, T. E.; Sen, A.; Butler, P. J. Substrate Catalysis Enhances Single Enzyme Diffusion. *J. Am. Chem. Soc.* **2010**, *132*, 2110-2111.
- [24] Sengupta, S.; Dey, K. K.; Muddana, H. S.; Tabouillot, T.; Ibele, M. E.; Butler, P. J.; Sen, A. Enzyme Molecules as Nanomotors. *J. Am. Chem. Soc.* **2013**, *135*, 1406-1414.
- [25] Sengupta, S.; Spiering, M. M.; Dey, K. K.; Duan, W.; Patra, D.; Butler, P. J.; Astumian, R. D.; Benkovic, S. J.; Sen, A. DNA Polymerase as a Molecular Motor and Pump. *ACS Nano* **2014**, *8*, 2410-2418.
- [26] Dey, K. K.; Das, S.; Poyton, M. F.; Sengupta, S.; Butler, P. J.; Cremer, P. S.; Sen, A. Chemotactic Separation of Enzymes. *ACS Nano* **2014**, *8*, 11941-11949.
- [27] Robinson, T.; Schaerli, Y.; Wootton, R.; Hollfelder, F.; Dunsby, C.; Baldwin, G.; Neil, M.; French P.; deMello, A. Removal of Background Signals from Fluorescence Thermometry Measurements in PDMS Microchannels Using Fluorescence Lifetime Imaging. *Lab Chip* **2009**, *9*, 3437-3441.
- [28] Xia, Y. & Whitesides, G. M. Soft Lithography. *Annu. Rev. Mater. Sci.* **1998**, *28*, 153-184.

Concluding Remarks

In this work, I have conveyed that almost any enzyme can act as a motor protein, and a complete understanding of how enzymes convert chemical energy to mechanical force can lead us to understanding the basic principles of fabrication, development and monitoring of biological and biomimetic molecular machines. Through this work, I have addressed several questions: what leads to enzyme generated force in the presence of substrate and why when enzymes are exposed to a gradient of substrate or binding/unbinding ligands they migrate up the gradient. Also, whether enzymes transduce force to the surroundings and how we can apply the force generation of enzymes to fabricate biocompatible artificial swimmers for various biomedical uses. Through a series of experiments, we discover that increased enzyme diffusion is of relevance to binding and unbinding events between enzyme active sites to specific “ligands”. Chemotaxis of enzymes is also induced by these favorable binding interactions. The sequential chemotaxis in catalyst cascades allows time-dependent, self-assembly of specific catalyst particles participating in the cascade. This is an example of how information can arise from chemical gradients and it is tempting to suggest that similar mechanisms underlie the organization of living systems. Now, what comes next?

How do free enzymes affect cellular activities? Active free-swimming enzymes may be responsible for the organization of metabolons or other phase separated systems, like P-granular droplets. Enzyme force generation may also impact signaling transportation along pathways and the convective transport of fluid in cells. All of these require further in vivo studies.

Control and monitor enzyme powered artificial swimmers. Inspired by the features of biological motors, people develop synthetic artificial swimmers and molecular motors for various biomedical applications, such as cargo transportation, bio sensing, drug delivery and bio imaging. However, most artificial swimmers are made with inorganic materials. They either require non-biocompatible fuel like H_2O_2 and hydrazine or require high external energy and special equipment.

Therefore, exploring a biocompatible and smart power resource to propel artificial swimmers is very important. The biocompatibility of enzymes and their substrates make them ideal for applications in drug delivery, environmental sensing, and biological assays. There are multiple examples of enzymes being used as an engine to propel various materials. Despite the success of these studies, accurate monitoring of the performance of enzyme powered swimmers is still an issue that needs to be addressed.

Appendix

Supporting Information for Chapter 3:

Enzyme Chemotaxis

This chapter an adapted reproduction from *Nat. Chem.* **2018**, *10* (3), 311–317 with permission from the Springer Nature Publishing Group.

Computational modeling of cross-diffusion

We followed Wilkinson and Rose [1] for the kinetics of the reaction as follows:

Table A-1 Kinetics parameters of HK. Reprinted from *Nat. Chem.* **2018**, *10* (3), 311–317. Copyright 2018.

Reaction	Forward Kinetic Constant	Reverse Kinetic Constant
$E + G \rightleftharpoons EG$	$2 \times 10^6 \text{ M}^{-1}\text{s}^{-1}$	60 s^{-1}
$EG + A \rightleftharpoons EGA$	$1 \times 10^6 \text{ M}^{-1}\text{s}^{-1}$	200 s^{-1}
$EGA \rightleftharpoons EG6D$	8000 s^{-1}	8000 s^{-1}
$EGA \rightarrow G + EA$	1 s^{-1}	
$EG6D \rightleftharpoons EG6 + D$	400 s^{-1}	$0.2 \times 10^6 \text{ M}^{-1}\text{s}^{-1}$
$EG6 \rightleftharpoons E + G6$	$6 \times 10^3 \text{ s}^{-1}$	$2 \times 10^6 \text{ M}^{-1}\text{s}^{-1}$
$EG6D \rightarrow ED + G6$	4 s^{-1}	
$EA \rightarrow E + A$	500 s^{-1}	

$ED \rightarrow E + D$	100 s^{-1}	
------------------------	----------------------	--

where E is the Enzyme, A is ATP, G is D-glucose, G6 is glucose-6-phosphate, and D is ADP. We then modeled each reaction-diffusion equation of each component Q as follows:

$$\frac{\partial Q}{\partial t} = D_Q \nabla^2 Q + R(Q) + XD(Q, S), \quad (\text{A-1})$$

where D_Q is the diffusion coefficient of Q, $R(Q)$ are the reactions as shown above, and $XD(Q, S)$ is the cross-diffusion term of Q towards the gradient of S. We modeled the cross diffusion term following Equation 3-3:

$$XD(Q, S) = \nabla \left(C_Q \frac{K}{1+KC_S} \nabla C_S \right), \quad (\text{A-2})$$

We then obtained a set of eleven partial differential equations, for which we discretized the spatial derivatives. We then solved this system of discretized equations by numerically integrating in time using the function from the Python Scipy package [2]. The numerical scheme for discretizing in space and then numerically integrating over time is taken from reference.[3]. For the modeling of the AMP-PCP experiments, we modified the kinetic constants as follows:

Table A-2 Kinetics parameters and reaction of HK. Reprinted from *Nat. Chem.* **2018**, *10* (3), 311–317. Copyright 2018.

Reaction	Forward Kinetic Constant	Reverse Kinetic Constant
$EG + A \rightleftharpoons EGA$	$10 \times 10^6 \text{ M}^{-1}\text{s}^{-1}$	200 s^{-1}
$EGA \rightleftharpoons EG6D$	0 s^{-1}	8000 s^{-1}

This is compatible with the 10-fold reduction in dissociation constant of AMP-PCP determined previously [4], and with the absence of glucose phosphorylation. The model, using this parameters, predicted significant reduction in the amount of focusing in the central channel (1.6% for the AMP-PCP focusing).

To show that catalysis plays a crucial part in the cross-diffusion process, we modeled a simple, generic enzyme reaction as follows:

Table A-3 Glucose binding and unbinding parameters of HK. Reprinted from *Nat. Chem.* **2018**, *10* (3), 311–317. Copyright 2018.

Reaction	Forward Kinetic Constant	Reverse Kinetic Constant
$E + S \rightleftharpoons ES$	$k_{on} = 2 \times 10^6 \text{ M}^{-1}\text{s}^{-1}$	$k_{off} = 60 \text{ s}^{-1}$
$ES \rightarrow E + P$	$k_{cat} = 8000 \text{ s}^{-1}$	0

We then modeled a cross diffusion experiment with initial conditions: $[E] = 200 \text{ nM}$ in all channels, $[S] = 50 \text{ mM}$ in central channel only. The differential equations were modeled as described in the supplementary information section *Computational Modeling of Cross-Diffusion* above. We then compared the focusing amplitudes with catalysis ($k_{cat} = 8000 \text{ s}^{-1}$) and without catalysis ($k_{cat} = 0$). The results are plotted in **Fig. A-1A**: there is significant enzyme focusing towards the central channel in the case with catalysis, and almost no focusing in the case without catalysis. In the case with catalysis, ES is consumed leading to several orders of magnitude more forward binding events than in the case without catalysis (**Figure A-1B**). Indeed, in the case without catalysis, the equilibrium shifts very rapidly towards the enzyme complex ES and no more “forward” binding events are observed (**Figure A-1C** and **Figure A-1D**). After approximately twenty seconds, all the

substrate is consumed, but enzyme continues to spread diffusively, thus explaining the peak in Figure A-1A and the flattening in Figure A-1B-D. This shows that (1) the cross-diffusion phenomenon is dependent on the number of forward binding events in the region where the substrate gradient has been established and (2) the turnover induced by enzyme catalysis allows for orders of magnitude more binding events to take place. Therefore, the catalytic step is crucial in the observation of enzyme focusing.

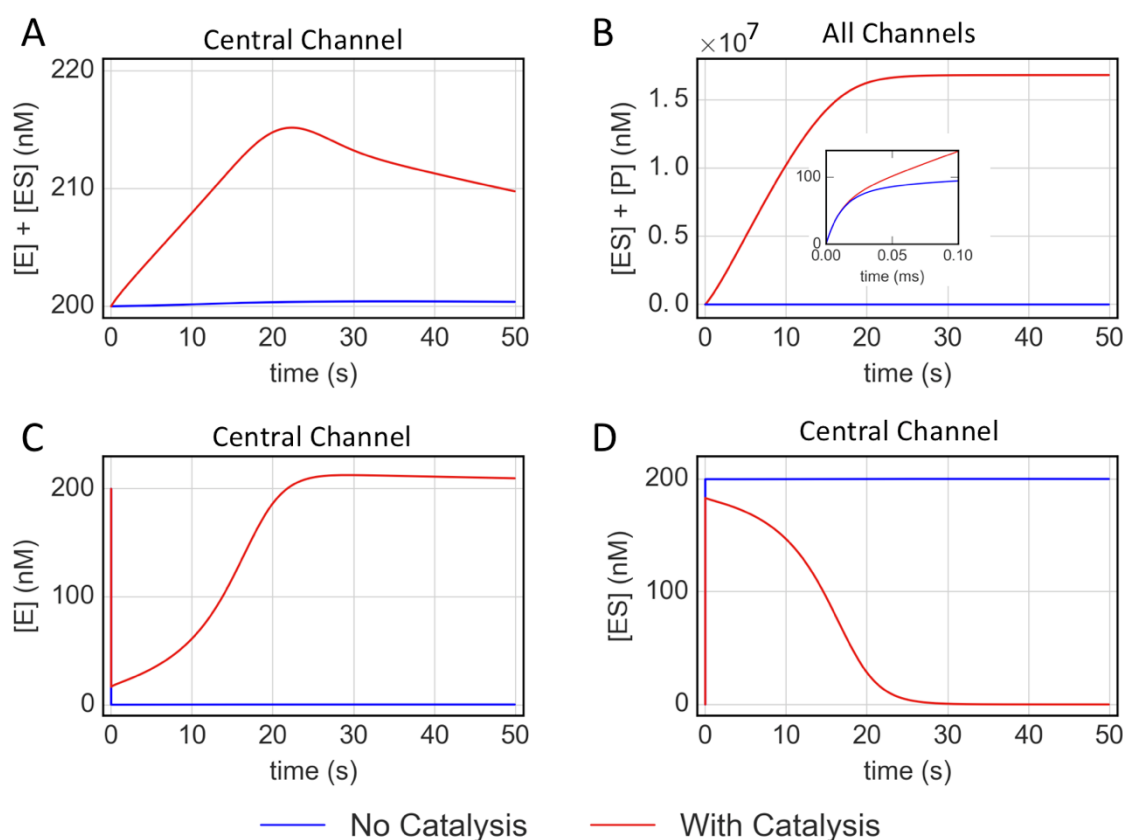


Figure A-1. Modeling results for the simplified enzyme cross diffusion. **(A)** Total enzyme concentration in central channel. With catalysis we observe significant enzyme focusing. Without catalysis, focusing is not noticeable. **(B)** The sum of product concentration and enzyme complex concentration is used to estimate the number of forward binding events. The number of binding events in the case with catalysis is several orders of magnitude greater than in the case with no catalysis due to turnover. Insert: close up of data at beginning of the reaction. **(C)** Enzyme concentration in central channel over time. Without catalysis, the enzyme-complex equilibrium shifts almost immediately towards the complex ES, and $[E]$ drops to zero. With catalysis, ES is turned over

and the equilibrium shifts towards E. **(D)** Enzyme-Substrate complex concentration in the central channel over time. Reprinted from *Nat. Chem.* **2018**, *10* (3), 311–317. Copyright 2018.

Analysis of HK and Ald Aggregates Trajectories

To test for the presence of aggregates, we ran a series of computational operations to detect punctates (with the spot diameter ranging from 600 to 1000 nm) with sub-pixel positional accuracy using a customized version of the Python package Trackpy [5]. Firstly, the parameters of the object detection algorithm were calibrated using visual inspection of two randomly chosen time points in the videos, both of the Aldolase channel and of the Hexokinase channel. The parameters chosen are shown in Table S3. The detection algorithm thresholds the image, keeping only grayscale values above an adaptively determined value. A band pass filter is applied to the Fourier-transformed grayscale image (to remove artifacts and background noise). A two-dimensional Gaussian is then fit to the brightness peaks to locate the objects. Then, the identified objects were assigned to trajectories by a linking algorithm. The linking algorithm determines potential trajectories by tracking objects from frame to frame, specifying a maximum distance the object can travel from frame to frame and a "memory" allowing the object to disappear for up to five frames. We then removed trajectories where the object was present for less than ten frames.

The parameters were calibrated very conservatively to only identify obvious trajectories. The parameters were then kept constant across all trajectories, channels, and experiments. Once the trajectories were identified, we defined a rectangular region around each HK trajectory adding a margin of 10 pixels on each side. Within this region, the closest Ald trajectory was chosen as the candidate trajectory potentially originating from the same HK-Ald aggregate as the HK trajectory (if there was no candidate trajectory, we deemed that there was no HK-Ald aggregate corresponding to this HK trajectory).

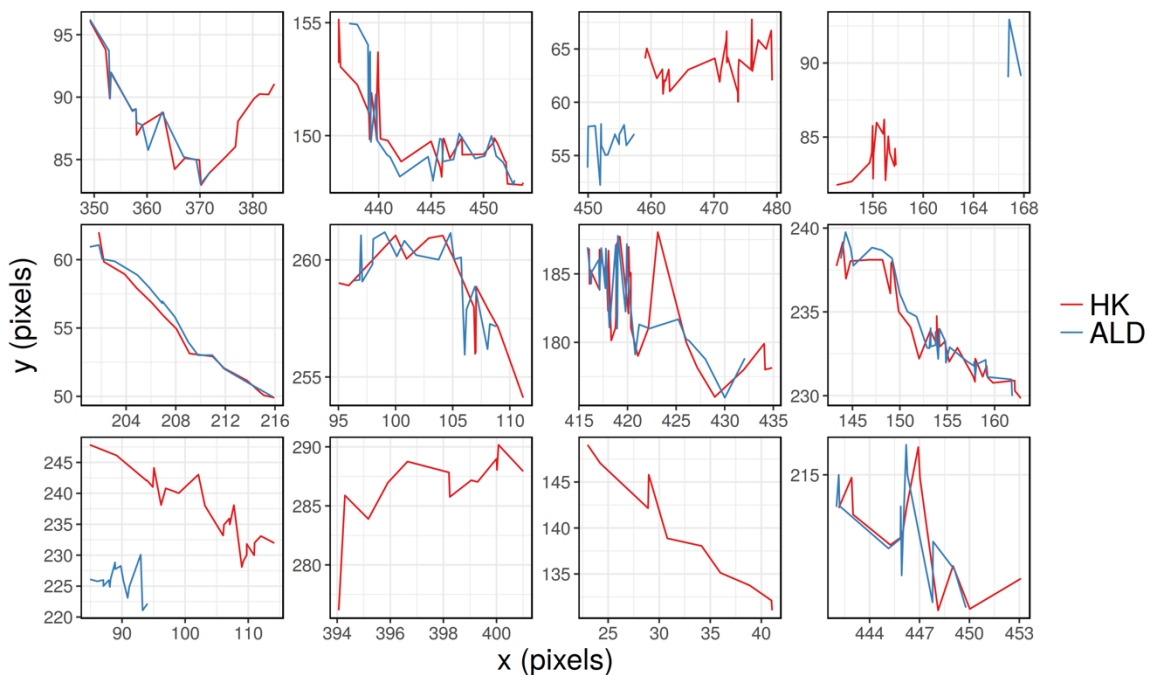


Figure A-2. Results from a confocal imaging experiment where D-Glucose and all four enzymes were present: All sample HK trajectories (red) found in the image stack, and all Ald trajectories (blue) which are identified as possible candidates for trajectories originating from the same HK-Ald aggregate. Reprinted from *Nat. Chem.* **2018**, *10* (3), 311–317. Copyright 2018.

The above analysis was run on eight experiments in which D-glucose was present (**Figure A-2.**), three experiments with D-glucose but without Iso and PFK present, three experiments with L-Glucose, and two experiments without glucose. We identified HK trajectories and Ald trajectories (punctates which persist for at least 10 frames, 13 s in total), and the subset of HK trajectories for which there is a corresponding ALD trajectory for which the spatial correlation is higher than 95%. Over half of the detected HK trajectories have an overlapping Ald trajectory. A visual representation of the HK and ALD trajectories for one experiment is shown in Figure S7. The presence of correlated HK and ALD trajectories suggests that multi-enzyme aggregates are formed. We note that although some fraction of the HK trajectories do not appear to have overlapping Ald trajectories, the quality

and duration of the overlap between the a priori independent HK and Ald trajectories provides overwhelming evidence that HK-Ald aggregation occurs.

Table A-4 Parameters used in the computational analysis. A pixel is $0.46 \times 0.46 \mu\text{m}$ and the frame rate is 1 frame every 1.29 s. Reprinted from *Nat. Chem.* **2018**, *10* (3), 311–317. Copyright 2018.

Parameter	Description	Value
Minimum Separation	Minimum distance between two aggregates	20 pixels
Minimum size	Minimum number of bright pixels	5 pixels
Buffer	Number of pixels around the HK trajectory around which we look for the Ald trajectory	10 pixels
Jump size	Maximum number of pixels we allow a particle to move between two frames	10 pixels
Memory	Number of frames we allow a particle to disappear during a trajectory	5 frames
Stub size	Number of frames a trajectory has to last to be considered	10 frames

References

- [1] Wilkinson, K. D. & Rose, I. A. Isotope Trapping Studies of Yeast Hexokinase during Steady State Catalysis. A Combined Rapid Quench and Isotope Trapping Technique. *J. Biol. Chem.* **1979**, *254*, 12567- 125672.

- [2] Jones, E., Oliphant, T. & Peterson, P. *SciPy: Open Source Scientific Tools for Python*. <http://www.scipy.org/> (2001).
- [3] Schiesser, W. E. & Griffiths, G. W. *A Compendium of Partial Differential Equation Models: Method of Lines Analysis with Matlab*. Cambridge University Press, 2009.
- [4] Bermingham, A., Bottomley, J. R., Derrick, W. U. & Derrick, J. P. Equilibrium and Kinetic Studies of Substrate Binding to 6-hydroxymethyl-7,8-dihydropterin Pyrophosphokinase from Escherichia Coli. *J. Biol. Chem.* **2000**, 275, 17962–17967.
- [5] Allan, D., Caswell, T., Keim, N., & van der Wel, C. trackpy: Trackpy v0.3.2. Zenodo (2016)

VITA

Xi Zhao

EDUCATION

DOCTOR OF PHILOSOPHY (PH.D.) IN CHEMISTRY, *The Pennsylvania State University* 2019

BACHELOR OF SCIENCE (B.SC.) IN CHEMISTRY, *Wuhan University* 2013

AWARDS AND HONORS

- Troxell Award, The Pennsylvania State University, USA, 2017
- 4th Place at PPG Poster Pitch Competition, The Pennsylvania State University, USA, 2017
- Scholl Award in Analytical Chemistry, The Pennsylvania State University, USA, 2016
- Harry and Catherine Dalalian Graduate Fellowship, The Pennsylvania State University, USA, 2016
- Selected for an oral presentation at Gordon Research Seminar, Stowe, Vermont, USA, 2016
- Braddock Robert Fellowship, The Pennsylvania State University, USA, 2013
- National Undergraduate Innovative Experimental Project Award, Wuhan University, China, 2012
- Student Scholarship (second place), Wuhan University, China, 2011 and 2012
- Recognition for excellent director, Wuhan University Student Union, China, 2011
- Excellent Student Award, Wuhan University, China, 2010, 2011
- Student Scholarship (third place), Wuhan University, China, 2010
- Incoming Student Scholarship, Wuhan University, China, 2009

PUBLICATIONS

- **Zhao, X.**; Sen, A. Chemotactic Assembly of Metabolon. *Methods in Enzymology* 2019, 617, 45-62.
- **Zhao, X.**; Gentile, K.; Mohajerani, F.; Sen, A. Powering Motion with Enzymes. *Acc. Chem. Res.* 2018, 51, 2373- 2381.
- Mohajerani, F.; **Zhao, X.**; Velegol, D.; Sen, A. A Theory of Enzyme Chemotaxis: From Experiments to Modeling. *Biochemistry* 2018, 57, 6256- 6263. (co-first author)
- **Zhao, X.**; Palacci, H.; Yadav, V.; Spiering, M.; Scott, J.; Linderberg, K.; Gilson, M. K.; Butler, P. J.; Benkovic, S. J.; Sen, A. Chemotactic Assembly in Active Enzyme Cascades. *Nat. Chem.* 2018, 10, 311-317. (co-first author)
- **Zhao, X.**; Dey, K. K.; Jeganathan, S.; Butler, P. J.; Córdova-Figueroa, U. M.; Sen, A. Enhanced Diffusion of Passive Tracers in Active Enzyme Solutions. *Nano Lett.*, 2017, 17, 4807–4812. (co-first author)
- Illien, P.; **Zhao, X.**; Dey, K.K.; Butler, P.J.; Sen, A.; Golestanian, R. Exothermicity Is Not a Necessary Condition for Enhanced Diffusion of Enzymes. *Nano Lett.*, 2017, 17 (7), 4415–4420. (co-first author)
- Dey, K. K.; **Zhao, X.**; Tansi, B. M.; Méndez-Ortiz, W. J.; Córdova-Figueroa, U. M.; Sen, A. Micromotors Powered by Enzyme Catalysis. *Nano Lett.* 2015, 11, 8311-8315.
- Zhang, H.; Duan, W.; Lu, M.; **Zhao, X.**; ShklyaeV, S.; Liu, L.; Huang, T. J.; Sen, A. Self-Powered Glucose-Responsive Micropumps. *ACS. Nano*, 2014, 8, 8537-8542
- Huang, R.; Yan, S.; Zheng, X.; Luo, F.; Deng, M.; Fu, B.; Xiao, Y.; **Zhao, X.**; Zhou, X. Development of a pH-activatable Fluorescent Probe and its Application for Visualizing Cellular pH Change. *Analyst*, 2012, 137, 4418-4420.
- Wu, J.; Huang, R.; Wang, T.; **Zhao, X.**; Weng, X.; Tian, T.; Zhou, X. Fluoride as an Inducible DNA Cross-linking Agent for New Antitumor Prodrug. *Org. Biomol. Chem.*, 2013, 11, 2365-2369.